

Fall 2019

Microcystin Exposure and Liver Injury Outcomes in NAFLD

Muayad Albadrani

Follow this and additional works at: <https://scholarcommons.sc.edu/etd>



Part of the [Environmental Health Commons](#)

Recommended Citation

Albadrani, M.(2019). *Microcystin Exposure and Liver Injury Outcomes in NAFLD*. (Doctoral dissertation). Retrieved from <https://scholarcommons.sc.edu/etd/5505>

This Open Access Dissertation is brought to you by Scholar Commons. It has been accepted for inclusion in Theses and Dissertations by an authorized administrator of Scholar Commons. For more information, please contact dillarda@mailbox.sc.edu.

MICROCYSTIN EXPOSURE AND LIVER INJURY OUTCOMES IN NAFLD

by

Muayad Albadrani

Bachelor of Medicine and Surgery
Taibah University, 2010

Master of Public Health
Tulane University, 2016

Submitted in Partial Fulfillment of the Requirements

For the Degree of Doctor of Philosophy in

Environmental Health Sciences

The Norman J. Arnold School of Public Health

University of South Carolina

2019

Accepted by:

Saurabh Chatterjee, Major Professor

Samir S. Raychoudhury, Committee Member

Geoff Scott, Committee Member

Dwayne Porter, Committee Member

Cheryl L. Addy, Vice Provost and Dean of the Graduate School

© Copyright by Muayad Albadrani, 2019
All Rights Reserved.

DEDICATION

My Doctorate effort I dedicate to my beloved parents, my wife, my adorable daughter, and my siblings . Their affection, support, love, encouragement, and sacrifices made me what I am today.

ACKNOWLEDGEMENTS

First and foremost, I would like to express and offer my sincere appreciation and gratitude to my academic advisor, Dr. Saurabh Chatterjee for his continuous support toward my Ph.D. curriculum study and related research. His guidance and wisdom helped me all through my Ph.D. dissertation.

I would also like to thank and express sincere appreciation to the rest of my Ph.D. committee members: Dr. Geoff Scott, Dr. Dwayne Porter, and Dr. Samir Raychoudhury, for their invaluable advice and critical insights.

I have been honored working with a great group of colleagues in Environmental Health & Disease Laboratory. Without their support and encouragement, this research wouldn't have been possible. Moreover, with them I have always shared knowledge, experience, and interesting discussions for research in different perspectives.

Last but not the least, I would like to thank and appreciate Taibah University at Saudi Arabia for providing me a scholarship that support me through my Ph.D. study.

ABSTRACT

Non-alcoholic fatty liver disease (NAFLD) is an emerging worldwide pandemic which is highly prevalent among obese individuals including children and adults. In a NAFLD condition, exposure to environmental contaminants or toxins can act as a second / multiple hit, which leads to the progression of simple steatosis to NASH and ultimately may result in liver cirrhosis. With climate change today, elevated levels of microcystins are an emerging problem in fresh water bodies, which are a source of drinking water. Individuals are therefore at risk of exposure to microcystin through consuming contaminated water. In the progression of NAFLD from one clinical stage to another, microcystin can play an important role. Research has proved that the main mechanism of the Microcystin-LR is to work as an exogenous Protein phosphatase 2A (PP2A) inhibitor. In this thesis we test the hypothesis that microcystin activates Kupffer cells as well as the hepatic stellate cells, which are the crucial mediators in hepatic inflammation and fibrogenesis via NOX2 dependent pathway in NAFLD condition. Results showed that microcystin exposure via intraperitoneal routes in mice that have mild steatosis will lead to advanced histopathological characteristics of NAFLD. Further, we looked at the effect of early microcystin exposure in young mice, which were then fed a high fat diet to induce obesity/NAFLD. Early exposure to microcystin resulted in exacerbation of NAFLD clinical pathology with increased expression of proinflammatory cytokines, compared to vehicle control treated mice. This process has been shown to be reduced in mice that lacked miR21, p47 phox , or NLRP3 genes. In addition, inhibition of

AKT pathway reduced microcystin -induced NOX2 activation as well as upregulation of miR21. All things considered, it was observed that microcystin exposure exacerbated NAFLD pathology via activating NOX2-dependent peroxynitrate generation by increasing miR21 levels. Moreover, early childhood exposure to microcystin will exacerbate adult hepatic injury following HFD via NLRP3 inflammasomes.

TABLE OF CONTENTS

Dedication.....	iii
Acknowledgements.....	iv
Abstract.....	v
List of Tables	viii
List of Figures.....	ix
List of Abbreviations	xi
Chapter 1 : INTRODUCTION.....	1
Chapter 2: EXOGENOUS PP2A INHIBITOR EXACERBATES THE PROGRESSION OF NONALCOHOLIC FATTY LIVER DISEASE VIA NOX2-DEPENDENT ACTIVATION OF MIR21	9
Chapter 3: EXOGENOUS PP2A INHIBITOR IN NAFLD CAN LEAD TO PYROPTOSIS AS WELL AS HEDGEHOG SIGNALING PATHWAY ACTIVATION VIA NOX2-DEPENDENT ACTIVATION OF MIR21.....	52
Chapter 4: EARLY CHILDHOOD EXPOSURE AND PRIMING TO ALGAL TOXINS INDUCE MURINE ADULT HEPATIC INJURY FOLLOWING HIGH FAT DIET FEEDING VIA NLRP3 INFLAMMASOMES	65
Chapter 5: CONCLUSION.....	95
References.....	101
Appendix A: COPYRIGHT PERMISSION FOR CHAPTERS 2.....	108

LIST OF TABLES

Table 2.1 Primer sequences for the different target genes.....	20
Table 2.2 NASH CRN (clinical research network score).....	23
Table 3.1 Primer sequences for the different target genes.....	58
Table 4.1 Primer sequences for the different target genes.....	73

LIST OF FIGURES

Figure 2.1 Exogenous protein phosphatase 2A (PP2A) inhibition in mouse liver exacerbates nonalcoholic fatty liver disease (NAFLD) pathology	37
Figure 2.2 Protein phosphatase 2A inhibition by microcystin (MC) activates Kupffer cells and hepatic stellate cells and induces an inflammatory surge in mouse liver	38
Figure 2.3 The activation of Kupffer cells, hepatic stellate cells, and an inflammatory surge in MC-exposed livers are mediated by NOX2-dependent oxidative stress	40
Figure 2.4 The protein phosphatase 2A inhibition activates NOX2-dependent oxidative stress in Kupffer cells.....	41
Figure 2.5 Protein phosphatase 2A inhibitor (MC) synergistically increases NOX2-dependent tyrosine nitration in Kupffer cells.....	42
Figure 2.6 Exogenous protein phosphatase 2A inhibitor-induced oxidative stress triggers miR21-dependent NF- κ B pathway activation in NASH	43
Figure 2.7 Exogenous protein phosphatase 2A inhibitor-induced miR21 upregulation acted downstream by modulating the p-AKT-NF- κ B signaling pathway	44
Figure 2.8 NOX2-miR21-NF- κ B signaling pathway in microcystin (MC)-exposed immortalized rat Kupffer cells	46
Figure 2.9 Exogenous protein phosphatase 2A inhibitor exposure increases M1 phenotype in Kupffer cells.....	47
Figure 2.10 Exogenous protein phosphatase 2A inhibitor exposure activates hepatic stellate cells via NOX2-miR21 axis.....	48
Figure 2.11 Exogenous protein phosphatase 2A (PP2A) inhibitor activates NOX2 via AKT pathway	49
Figure 2.12 Exogenous protein phosphatase 2A (PP2A) inhibitor-activated NOX2 generates oxidative stress via AKT pathway	50
Figure 2.13 Mechanism of protein phosphatase 2A (PP2A) inhibition-induced nonalcoholic fatty liver disease (NAFLD) pathology.....	51

Figure 3.1 Exogenous PP2A inhibitor exposure induces pyroptosis in Kupffer cells.....	63
Figure 3.2 Exogenous PP2A inhibitor exposure activates profibrogenic hedgehog signaling in hepatic stellate cells via NOX2-miR21 axis	64
Figure 4.1 Early priming with MC for two weeks in juvenile mice liver induces liver injury	83
Figure 4.2 Early exposure to MC followed by HFD will exacerbate liver injury	87
Figure 4.3 Early exposure to MC followed by HFD will induce hepatic oxidative stress	88
Figure 4.4 Early exposure to MC followed by HFD induces NLRP3 inflammasome activation.....	89
Figure 4.5 Early exposure to microcystin followed by HFD releases IL-1 β and IL-18	90
Figure 4.6 The activation of Kupffer cells, hepatic stellate cells, and an inflammatory surge in early microcystin (MC) exposure are mediated by NLRP3 inflammasome activation.....	94

LIST OF ABBREVIATIONS

AKTi	Phosphatidylinositol 3-kinase inhibitor
APO.....	Apocynin
DMPO.....	5,5 dimethyl-1- pyrroline N-oxide
FBA.....	Phenyl boronic acid
MC	Microcystin
MC-LR.....	Microcystin-LR
NAFLD	Non-alcoholic fatty liver disease
NASH.....	Non-alcoholic steatohepatitis
NOX2	NADPH oxidase 2
PP2A	Protein Phosphatase 2A enzyme

CHAPTER 1

INTRODUCTION

Nonalcoholic fatty liver disease (NAFLD) is a pathological condition mostly similar to histological features of alcoholic liver disease , but occurs without excessive consumption of alcohol [1, 2]. It includes a wide spectrum of liver stages based on different histological features ranging from simple steatosis to a complex stage of nonalcoholic steatohepatitis (NASH), which may progress to hepatic cirrhosis and hepatocellular carcinoma if it remains untreated. The main issue of the first two liver stages is that most patients are completely fine and asymptomatic at the beginning until they reach irreversible end-stage liver disease [3-5]. This silent liver disease has recently become an imperative public health concern because of its high prevalence among both adults as well as in juveniles, its high risk of progression to advanced severe liver illnesses if neglected, and its strong association with an environmental contaminant [6, 7]. Our group as well as other research studies have shown that environmental exposure to contaminants as well as toxicants and/or potentially their metabolites work as a “second and/or multiple hit” in order to exacerbate the pathophysiology of NAFLD [6, 8]. The ‘first hit’ includes metabolic changes in body system that involve leptin resistance and/or insulin resistance, which in turn result in fat accumulation in the liver (liver steatosis). The first hit can be synergized if obesity was there as it causes increase in the level of leptin. The ‘second hit’ generally involves pathological state of imbalance that includes a condition such as oxidative stress resulting in Kupffer cells activation, as well as Stellate cells activation.

These cells activation subsequently result in proinflammatory response and fibrogenesis [9-12].

Nonalcoholic fatty liver disease (NAFLD) is a clinical condition that is related to the rising levels of obesity and metabolic disorders [13].NAFLD are most predominant in adult obese individuals with high prevalence among them which is around 80-90%. Patients with metabolic disorders such as diabetes mellitus have prevalence of 30-50%. This percentage will get increased up to 90% if it is synergized with a condition like hyperlipidemia. In pediatrics epidemiology, a NAFLD condition is challenging as that children have prevalence of 3-10%. However, this percentage can get a dramatic increase to reach 70 % among obese children [14].

Obesity is a condition that is associated with different factors that promote a liver steatosis stage. For example, liver steatosis happens because of exaggerated consumption of a high fat diet and the other metabolic factors and syndromes such as NAFLD that is associated with decreased fat export in very low density lipoprotein(VLDL), increased de novo lipogenesis process, as well as decreased free fatty acid β -oxidation [10]. We can consider obesity as a pathological condition because it is associated with elevated concentrations of pro inflammatory factors such as cytokines, like Tumor necrosis factor (TNF- α), Interleukin 1 β (IL-1 β), Interleukin 6 (IL-6), and Monocyte chemoattractant protein 1 (MCP1) [15]. Moreover, hormones such as adipokines can work as proinflammatory factors in obese individuals. For example, leptin can behave as a cytokine in the body system [16]. This hormone is regularly secreted in a pulsatile phenomenon by the adipocytes and works physiologically as the satiety hormone [16, 17].

It has been already shown by our group that mice groups that were fed with a high fat diet

and had been exposed to BDCM had increased leptin concentration [6, 18]. Moreover, mice that had leptin KO gene associated with leptin deficiency showed signs of hyperphagia and mice became extremely obese as leptin is required after eating to control hunger. Also, this hormone is known to be positively associated with the body fat content. This is because the hormone specifically works to regulate and change long-term food intake as well as affecting energy expenditure in whole body systems [19].

Data from the Centers for Disease Control indicate that over a third of the entire country's population is obese. Overall, a significant portion of the adult population in the nation is affected by obesity, which is a primary risk factor in the development of many diseases. According to Ogden et al, it is estimated that 38.3 percent and 34.3 percent of women and men respectively are affected by obesity in the country [20]. Obesity as an issue tends to follow precepts of age where it progresses in severity. However, for particular races, Blacks and Hispanics, obesity is far more prevalent in youth. For instance, prevalence of obesity among participants from these races who are between 2 and 20 years of age was at about 17 percent. This is a considerable figure given the age in life and lower prevalence of risk factors, further indicating the gravity of the situation. With these statistics according to Centers for Disease Control and Prevention (CDC, 2010), 12.7 million children and adolescents are affected. Obesity is the second leading cause of preventable death in the United States after tobacco with an average toll of 300,000 annually.

Hepatocyte is one of the major elements of the liver parenchyma with multiple liver functions; one of its the important functions is to play a role in controlling carbohydrate metabolism by maintaining glucose concentrations in a normal range [21], Lipid

metabolism and its modulation are also controlled by the hepatocytes [22], etc. On the other hand, Kupffer cell, which is a specialized macrophage that resides in the liver, that liver, is situated inside the hepatic sinusoids as it shown by many researchers. It is plays a key role in the innate immunity of the liver and is also involved in different stress situations such as infection, toxins, ischemia, resection and other stresses [23] . They are representing approximately 80-90% of all tissue macrophages in the body. Stellate cells which is also known as Ito cells ,cells, are responsible for liver fibrosis as a response to different stressors [24, 25]. All above cells has shown role in advancing NAFLD progression into NASH [6, 12, 26]. For example according to Lanthier, Kupffer cells activation is considered as key element disease initiation and progression from NAFLD to NASH, while stellate cells are known to contribute to fibrosis as well as hepatocytes ballooning were found to be crucial in progression of NAFLD to NASH [27, 28].

Regarding how these environmental contaminants cause oxidative stress remains unclear. We and others have previously shown that the environmental toxin such as trihalomethane, pyrazole exacerbates NAFLD via oxidative stress induced by free radical mechanism, thus suggesting that reactive oxidative species and reactive nitrosative species play a critical role in the pathogenesis of environmental toxin induced NASH [6, 25, 29] . Previous studies have shown that the potential sources of oxidative stress includes xanthine oxidase (XDH) [30], electron transport chain enzymes, liver cytochrome P450-2E1 (CYP2E1) [31], and catalytic subunit of nicotinamide adenine dinucleotide phosphate-oxidase (NADPH oxidase or NOX) [32]. NADPH oxidase is a membrane bound oxidoreductase enzyme complex with a membranous subunit and cytoplasmic subunit. The dormant NOX complex is activated to assemble in the membrane and produce superoxide

radicals in a respiratory burst or environmental toxin [33]. Both the expression and activity of the NOX2 (NOX isoforms) is increased in the NAFLD liver and, importantly, increased expression correlates well with NAFLD severity [34].

The proliferation and expansion of harmful algal blooms (HABs) or toxic cyanobacterial blooms are an important consequence of climate change [35]. These HAB contain cyanobacteria which produce toxic metabolites and these often end up in drinking water for humans and livestock [36]. According to WHO guidelines, the amount of MC-LR in drinking water should not exceed $1\mu\text{g/L}$ [37]. However, MC-LR was found to occur in very high concentrations in several water bodies, which are a source of drinking water to both livestock and human [38]. For instance, Poyang Lake (largest fresh water lake in China) and Hoan Kiem Lake of northern Vietnam recorded $7.97\ \mu\text{g/L}$ and $46\ \mu\text{g/L}$ respectively [38]. There are different routes for exposure to the microcystin; drinking water is considered the most common route. There are other routes such as ingestion of contaminated food, by inhalation and dermal contact during bathing or showering, and during recreational activities [39, 40]. Inhalation exposure also has been reported as another route for microcystin exposure [41].

Among other cyanotoxins (saxitoxin, anatoxin, cylindrospermopsin), microcystin have been the most studied cyanotoxin so far [37]. Microcystin-LR is known to be a potent toxin that can cause damage to different organs and body systems [42]. The liver is considered to be an important target because of its toxicity and because it is known to be a potent hepatotoxin. Regarding its chemistry, it has a heptapeptide structure and has a molecular weight that varies between 900 and 1,100 Daltons. Based on the changes on amino acid position, it will have different Congener within X and Y direction. Microcystin-

LR, which has leucine (L) and arginine (R) in the X and Y, is considered the most important one because it's potent toxicity and most encountered variant Congener with different exposure routes among the microcystin family [43].

More than one species of cyanobacteria can synthesize the cyanotoxin [43]. Microcystin is an example of cyanotoxins produced by cyanobacteria *Microcystis aeruginosa* in HAB [44]. Microcystin as well as other toxins remain preserved inside the cyanobacteria cell structure until unusual conditions happen that favor cell wall lysis. So, the cyanotoxin gets out of the cyanobacteria, called blue-green algae, contaminating the fresh water as it is predominant in eutrophic (nutrient-rich) water bodies [45].

(WHO) set a guideline for MC-LR in drinking water which is $1\mu\text{g/L}$ [37]. However, MC-LR was found to be more than the recommended guideline in many water bodies [38]. For instance, Poyang Lake (largest fresh water lake in China) and Hoan Kiem Lake of northern Vietnam recorded $7.97\mu\text{g/L}$ and $46\mu\text{g/L}$ respectively [38].

MC-LR is chemically stable, resistant to gastro-intestinal digestion and transported to the liver via active transport system. In addition, it shows toxic effects to liver cells. Microcystin needs a facilitated transport system in order to get inside the cell using receptors which is the organic acid transporter polypeptide (OATp) family [46-48]. This is because microcystin has molecular weight that is very high, preventing it from passing to the cells via simple diffusion [49].

Microcystin-LR down regulates with serine/ threonine protein phosphatases (protein phosphatases) such as Protein phosphatase 2A (PP2A) after cell being exposed to microcystin [50]. Most of the mechanistic actions regarding microcystin effect have been

shown by hyperphosphorylation of the proteins by decreased dephosphorylation process by a phosphatase enzyme as it is known to be a potent inhibitor of PP2A [51].

Nicotinamide adenine dinucleotide phosphate (NADPH) oxidase (NOX) has different isoforms such as NOX1-5 and Doux1-2. NOX2, which is one of the isoforms and can be considered as an important cellular source for reactive oxygen species(ROS) [52]. NOX2 has been proven to be expressed in the hepatocyte as well as has been proven in several studies that its expression in different cell types such as smooth muscle cells, Kupffer cells and hepatic stellate cells [53-55]. NOX2, in order to be activated, has six different subunits and it needs two subunits of the six, (α subunit, and β subunit) depending on tissue or cell type, to interact together in order to form an active enzyme complex [55]. Then, when it is activated, it will result in generating superoxide anion and reactive oxygen species (ROS) [56]. For example, during activation of Kupffer cells, P47 Phox subunit will be translocated to the cell membranes to bind GP91 Phox subunit. We have shown this activation via translocation by showing significant increase in the protein colocalization events by using dual staining using immunofluorescence microscopy [55, 57].

MicroRNAs (miRs) are very small noncoding RNAs that control both mRNA and target gene protein expression, leading to changes in mRNA stability or inhibition of translation depending on MicroRNA itself. For example, MicroRNAs are about 22 nucleotides, that is the reason for considering them small noncoding RNAs . One aspect related to them is that miRNAs form mRNA silencing complexes in cytoplasm that can regulate as well as control mRNA expression at transcription stage [58]. Downregulation or upregulation of miRNAs can determine the pathway of the cellular mechanism. For example, activation of leptin-mediated NADPH oxidase was positively associated with

higher levels of miR21 expression in NASH condition. MicroRNA 21 among all miRNAs, has been discovered as an important player in NASH pathophysiology [59, 60].

In this dissertation, I inspect cues in mechanism pathways of microcystin exposure in liver in Non-alcoholic fatty liver disease (NAFLD) causing Nonalcoholic steatohepatitis (NASH) and liver injury. One of these mechanisms is that microcystins can exacerbates NAFLD pathophysiology via generation of peroxynitrite that is NOX2-dependent , via increasing pathology caused by miR21. Moreover, early exposure to microcystins following diet induced obesity will result in liver injury via activation of inflammasome.

CHAPTER 2
EXOGENOUS PP2A INHIBITOR EXACERBATES THE
PROGRESSION OF NONALCOHOLIC FATTY LIVER DISEASE VIA
NOX2-DEPENDENT ACTIVATION OF MIR21¹

¹ Albadrani M, Seth RK, Sarkar S, Kimono D, Mondal A, Bose D, Porter DE, Scott GI, Brooks B, Raychoudhury S, Nagarkatti M, Nagarkatti P, Jule Y, Diehl AM, Chatterjee S. Exogenous PP2A inhibitor exacerbates the progression of nonalcoholic fatty liver disease via NOX2-dependent activation of miR21. *Am J Physiol Gastrointest Liver Physiol* 317: G408 –G428, 2019.
Reprinted here with the permission of the publisher.

Running title: Progression of NAFLD Via NOX2-Dependent Activation Of miR21

Key words: leptin; microcystin; miR21; NADPH; NAFLD; NOX-2; oxidative stress; PP2A inhibitor; siRNA

Author for correspondence:

*Dr. Saurabh Chatterjee, Ph.D. Environmental Health and Disease Laboratory,
Department of Environmental Health Sciences, University of South Carolina, Columbia
29208 USA. Email: schatt@mailbox.sc.edu; Tel: 803-777-8120; Fax: 803-777-3391.

Grant Support: This work has been supported by National Institutes of Health Awards 2-P20-GM-103641-06, 1-P01-ES-028942-01, and P01-AT-003961 to S. Chatterjee; 1-P01-ES-028942-01 to D. Porter and G. I. Scott; and P01-AT-003961, P20-GM-103641, R01-AT-006888, R01-ES-019313, R01-MH-094755, and Veterans Association Merit Award BX001357 to M. Nagarkatti and P. S. Nagarkatti.

Abstract:

Nonalcoholic fatty liver disease (NAFLD) is an emerging global pandemic. Though significant progress has been made in unraveling the pathophysiology of the disease, the role of protein phosphatase 2A (PP2A) and its subsequent inhibition by environmental and genetic factors in NAFLD pathophysiology remains unclear. The present report tests the hypothesis that an exogenous PP2A inhibitor leads to hepatic inflammation and fibrogenesis via an NADPH oxidase 2 (NOX2)-dependent pathway in NAFLD. Results showed that microcystin (MC) administration, a potent PP2A inhibitor found in environmental exposure, led to an exacerbation of NAFLD pathology with increased CD68

immunoreactivity, the release of proinflammatory cytokines, and stellate cell activation, a process that was attenuated in mice that lacked the p47phox gene and miR21 knockout mice. Mechanistically, leptin-primed immortalized Kupffer cells (a mimicked model for an NAFLD condition) treated with apocynin or nitron spin trap 5,5 dimethyl-1-pyrroline N-oxide (DMPO) had significantly decreased CD68 and decreased miR21 and α -smooth muscle actin levels, suggesting the role of NOX2-dependent reactive oxygen species in miR21-induced Kupffer cell activation and stellate cell pathology. Furthermore, NOX2-dependent peroxynitrite generation was primarily responsible for cellular events observed following MC exposure since incubation with phenylboronic acid attenuated miR21 levels, Kupffer cell activation, and inflammatory cytokine release. Furthermore, blocking of the AKT pathway attenuated PP2A inhibitor-induced NOX2 activation and miR21 upregulation. Taken together, we show that PP2A may have protective roles, and its inhibition exacerbates NAFLD pathology via activating NOX2-dependent peroxynitrite generation, thus increasing miR21-induced pathology. NEW & NOTEWORTHY Protein phosphatase 2A inhibition causes nonalcoholic steatohepatitis (NASH) progression via NADPH oxidase 2. In addition to a novel mechanism of action, we describe a new tool to describe NASH histopathology.

2.1 INTRODUCTION

Nonalcoholic Fatty liver disease (NAFLD), a silent liver disease, has recently become an imperative public health concern because of its high prevalence, high risk of progression to severe liver illnesses, and strong association with environmental and genetic factors [6, 61]. Nonalcoholic steatohepatitis (NASH) progression is believed to be governed by a multihit paradigm. Earlier studies have shown that oxidative stress resulting

from exposure to environmental contaminants and/or their metabolites act as a “second hit” or “multiple hits” to exacerbate NAFLD to NASH pathophysiology [6, 8]. The “first hit” includes leptin resistance or insulin resistance, which might stimulate fat accumulation in the liver (steatosis). The second hit generally involves oxidative stress and/or cytokines that result in Kupffer cell and stellate cell activation, proinflammatory response, and fibrogenesis.

Environmental contaminants have been shown to act as a second hit in NAFLD for its progression to NASH and liver fibrosis. Recent incidences of higher cyanobacterial blooms that have been shown to release and concomitantly expose individuals to protein phosphatase 2A (PP2A) inhibitors like microcystin (MC) can be a significant threat to NAFLD patients of all ages. MC exposure through these cyanobacterial blooms can act as a second hit or may combine with other underlying factors such as insulin and leptin resistance and lipotoxicity, as found in morbid obesity to advance into severe liver disease from a primarily benign steatotic condition. MC is an emerging drinking water contaminant and imposes global health concern [62]. Preventing MC-induced liver injury is crucial to understand the molecular mechanism behind the toxicity of MC [63]. Recent studies largely focus on MC-induced oxidative stress, apoptosis, and oncotic necrosis as a cause of liver injury [63-66]. MC exposure also has been associated with increased incidences of liver cancer [67]. Though the environmental impact of MC remains alarming, it is too early to predict that exposures from such PP2A inhibitors might be one of the causes for NAFLD progression to NASH. PP2A consists of a large family of Ser/Thr phosphatases, consisting of a catalytic C subunit and a structural A subunit that is widely bound to a regulatory B-type subunit [37]. The B-type subunits determine the function and modulation of PP2A

trimers, but despite their importance in physiology, their roles in controlling vital pathology processes in the liver remain under investigated [37]. Conditional knockouts (KOs) of this gene, specifically in the liver in the C57BL6 background, result in less lipid deposition in the liver (decreased steatosis) [68]. The role of steatosis in NAFLD pathology remains an area of intense scrutiny. With PP2A inhibition leading to less steatosis, previous studies concerning loss of liver fat and its association with inflammation in the liver might provide some insight into the role of PP2A in NAFLD, especially if it is inhibited by an environmental factor like MC. Earlier studies, including ours, have shown that the potential sources of oxidative stress include xanthine oxidase (XDH) [30], electron transport chain enzymes, liver cytochrome P450-2E1 (CYP2E1) [31], and catalytic subunit of NADPH oxidase (or NOX) [32]. We and others have previously shown that NADPH oxidase 2 (NOX2)-induced peroxynitrite produces a stable nitrated tyrosine residue on proteins [3-nitrotyrosine (3NT)] in NAFLD. Indeed, 3NT is being considered as an established biomarker of oxidative stress in both an in vitro and an in vivo model of oxidative stress [69]. Even though peroxynitrite was discovered decades ago, the mechanism of reactive oxygen species (ROS) signaling in progressive NAFLD remains unclear, especially the route of its activation by exogenous triggers and its downstream signaling that links inflammatory pathways.

NOX2- mediated redox signaling can activate micro RNAs. Previous studies have shown the role of microRNAs (miR21) in disease pathology over the past decade. miRNAs are small (18~25 nucleotides long), endogenous, noncoding RNA molecules that regulate gene expression at the transcriptional level [70, 71]. Most recently we and several research groups have shown that microRNA 21 (miR21) is one of the most upregulated microRNAs

in NAFLD and NAFLD-associated kidney inflammation [57, 72, 73]. miR21 was shown to regulate the SMAD pathway in NAFLD fibrogenesis [57]. Since both ROS and miR21 are dysregulated in progressive NAFLD, it is important to understand the crosstalk between the external triggers and upstream and downstream pathways of NOX2-induced miR21 activation. Justifiably, since numerous studies have shown that NOX2 activation is regulated by environmental triggers which act as second hits, mechanistically, we chose to investigate whether MC, a toxin produced from cyanobacteria in harmful algal blooms and a known PP2A inhibitor [51], activated an NOX2-miR21 signaling pathway and exacerbated NASH pathogenesis.

2.2 MATERIALS AND METHODS

Materials:

All other chemicals were of analytical grade and were purchased from Sigma Chemical Company unless otherwise specified. MC-LR was purchased from Cayman (Ann Arbor, MI); leptin was purchased from BioVision (Milpitas, CA); LB-100, the PP2A inhibitor, was purchased from MedKoo; and wild-type and gene-specific KO mice, including P47 phox KO and miR21 KO mice, were purchased from Jackson Laboratories (Bar Harbor, ME). Animal diets were purchased from Research Diets (New Brunswick, NJ). Anti-3NT, anti-CD68, anti-GP91 phox, anti-P47 phox, and anti- α -smooth muscle actin (SMA) primary antibodies were purchased from Abcam (Cambridge, MA). Anti-P65 and anti-p-AKT were purchased from Santa Cruz Biotechnology (Dallas, TX). Species-specific biotinylated-conjugated secondary antibody and streptavidin-horseradish peroxidase were purchased from Vector Laboratories (Vectastain Elite ABC kit,

Burlingame, CA). Fluorescence-conjugated (Alexa Fluor) secondary antibodies and ProLong Gold antifade mounting media with DAPI were bought from Thermo Fisher Scientific (Waltham, MA).

Mouse Model:

Diet-induced NAFLD model:

Pathogen-free adult male mice with C57BL/6J background (Jackson Laboratories) were used in the study. They were fed with a high-fat (60% kcal) supplemented methionine-choline-deficient (MCD-HFD) diet, (Research Diets) for 8 wk to induce NAFLD, whereas mice kept on a normal chow diet were used as a lean control. Mice that contained the disrupted P47 phox gene (B6(cg)-Ncf1M1J/J(JAC004742) and disrupted miR21 gene (B6.129S6-Mir21tm1 Yoli/J) (Jackson Laboratories) were also fed an MCD-HFD and were treated identically to the NAFLD mouse model. All mice were housed with 3–5 mice/cage at 23°C–24°C on a 12:12-h light-dark cycle with ad libitum access to food and water. All animals were treated in strict accordance with the National Institutes of Health Guide for the Care and Use of Laboratory Animals, and the experiments were approved by the institutional review board at the University of South Carolina at Columbia.

Induction of liver injury and exposure to environmental toxin MC:

Wild-type, as well as gene-specific KO mice, at 6 wk were administered with vehicle (ethanol in PBS), MC-LR (MC-LR) (10 µg/kg, 5 dosages/wk), through the intraperitoneal route for 2 wk. A set of MCD-HFD-fed mice (NAFLD model) was not injected with MC-LR in this study. On completion of treatment, mice were euthanized, and serum or liver tissue was collected for further processing.

Kupffer Cell Culture and Treatments:

Immortalized rat Kupffer cell line (SV40) was grown and maintained in complete DMEM. The media was supplemented with 10% FBS (Atlanta Biologicals; Norcross, GA), 2 mM glutamine, 100 U/mL penicillin, and 100 µg/mL streptomycin (Gibco; Grand Island, NY) at 37°C in a humidified atmosphere of 5% CO₂. Cells were serum starved (DMEM with 1% FBS) overnight before cells were given any treatment. The cells were then treated with vehicle (control) or 100 ng/mL leptin (BioVision), MC-LR (20 µM), or PP2A inhibitor (5 µM). Other groups of cells were incubated with leptin, MC, or PP2A inhibitor in combination with 100 µM apocynin (Apo) (Sigma-Aldrich), an inhibitor of NADPH oxidase activity, and thus preventing production of superoxide, 100 µM phenyl boronic acid (FBA), was used as a scavenger for 100 mM peroxyxynitrite, the spin trap DMPO (Alexis Biochemical, San Diego, CA), 20 µM miR21 inhibitor (Qiagen; Valencia, CA), and AKTi [50 µM phosphatidylinositol 3-kinase inhibitor (LY294002) (AKTi)]. The cells were then lysed in TRIzol (Invitrogen; Grand Island, NY) for mRNA as well miRNA extraction or plated on coverslips (MatTek; Ashland, MA) for immunofluorescence staining after completion of the treatment.

Stellate Cell Culture and Treatments:

An immortalized rat hepatic stellate cell line (8B), kindly provided to us by Dr. Anna Mae Diehl (Duke-Gastroenterology), was maintained in high-glucose DMEM (Corning, Tewksbury, MA) supplemented with 10% FBS (Atlanta Biologicals), 2 mM glutamine, 100 U/mL penicillin, and 100 µg/mL streptomycin (Gibco) at 37°C in a humidified atmosphere of 5% CO₂. The cells were then treated as Kupffer cells (see *Kupffer Cell Culture and Treatments*). After treatments, the cells were lysed in TRIzol

(Invitrogen) for mRNA or plated on coverslips (MatTek Corp) for immunofluorescence staining after completion of the treatment.

Histopathology and Digital Imaging Analysis of NAFLD:

Sections of liver tissue from each mouse were collected and fixed in 10% neutral buffered formalin. These formalin-fixed, paraffin-embedded tissues were cut into 5- μm thick sections. For histological examinations, formalin-fixed liver sections were stained with hematoxylin-eosin by the Instrumentation Resource Facility, University of South Carolina School of Medicine, and observed under the light microscope. For the quantitative analysis of NAFLD, liver slices were scanned at $\times 20$ using a NanoZoomer-SQ (Hamamatsu Corporation, Hamamatsu, Japan), and digital images of entire liver sections were captured at $\times 20\times$ (pixel size: 0.452 μm) using NDPview 2 software (Hamamatsu, Japan). Steatosis, fibrosis, and liver tissue density were automatically assessed from the same entire liver sections stained with picosirius red, using Biocellvia's image processing software program. The liver steatosis was defined by the steatosis area index, which corresponds, for a liver section, to the ratio of the total surface of vesicles (diameter >5 μm) versus the total surface of the liver section, expressed in percent. The liver fibrosis was defined, for a liver section, as the ratio of the area of stained collagen fibers versus the total area of the liver section, expressed in percent. The liver tissue density was assessed automatically from the mean density value of thousands of microtiles overlaying the entire liver sections and previously detailed for the pulmonary tissue density [74].

Immunohistochemistry:

The liver sections were deparaffinized using a standard protocol. Briefly, sections were incubated with xylene twice for 3 min, washed with xylene-ethanol (1:1) for 3 min,

rehydrated through a series of ethanol (twice with 100%, 95%, 70%, and 50%) twice with distilled water, and finally rinsed twice with PBS (Sigma-Aldrich). Antigen epitope retrieval of the deparaffinized sections was performed using epitope retrieval solution and steamer (IHC World, Woodstock, MD) for 45 min. H₂O₂ (3%) was used for 5 min to block the endogenous peroxidases. The primary antibody for *CD68* (1:300, ab125212, Abcam), α -SMA (1:250, ab32575, Abcam), 3NT (1:250, ab110282, Abcam), P-65 (1:300, SC-8008, Santa Cruz Biotechnology), and p-AKT (1:300, SC-293125, Santa Cruz Biotechnology) were used overnight in recommended dilutions. Species-specific biotinylated-conjugated secondary antibody and streptavidin conjugated with horseradish peroxidase were used to perform antigen-specific immunohistochemistry according to the manufacturer's standard protocols. 3,3' diaminobenzidine (Sigma-Aldrich) was used as a chromogenic substrate. Tissue sections were counterstained with Mayer's hematoxylin (Sigma-Aldrich). Phosphate-buffered saline was used for washing three times between the steps. Sections were finally mounted in Simpo mount (GBI Laboratories, Mukilteo, WA) and observed under a $\times 20$ objective using an Olympus BX51 microscope (Olympus, America). Morphometric analysis was done using CellSens Software from Olympus America (Center Valley, PA).

Immunofluorescence Microscopy:

In vivo, formalin-fixed, paraffin-embedded liver tissue sections were subjected to deparaffinization according to standard instructions. Epitope retrieval of the deparaffinized sections was done with an epitope retrieval solution and steamer (IHC World) according to the manufacturer's protocol. The primary antibodies anti-GP-91 phox (SC-5827) and anti-p47 phox (SC-17845) were used at recommended dilutions at 1:300. Species-specific

anti-IgG secondary antibodies conjugated with Alexa Fluor 633 or 488 (Invitrogen) were used. The sections were mounted in a ProLong Gold antifade reagent with DAPI (Life Technologies, Carlsbad, CA). Images were taken under $\times 20$, $\times 40$, and $\times 60$ magnification with an Olympus BX51 microscope.

In vitro, after completion of the treatments under serum-starved conditions as in cell culture, cells attached on coverslips were fixed with 10% neutral buffered saline. After the cells were washed with PBS containing 0.1% Triton X (Sigma), they were blocked with 3% BSA, 0.2% Tween (Fisher), and 10% FBS in PBS. Cells were incubated with primary antibodies, anti- α -SMA (ab32575) and anti-3NT (ab110282) (Abcam), and were used at 1:250 dilution, followed by species-specific secondary antibody conjugated with Alexa Fluor 633 or 488. The stained cells attached on the coverslips were mounted on slides with ProLong Gold antifade reagent with DAPI (Life Technologies) and viewed under $\times 40$ and $\times 60$ magnification with an Olympus BX51 microscope.

Serum Alanine Aminotransferase:

Serum alanine aminotransferase (ALT) levels were quantified using an automated analyzer at the University of Georgia Clinical pathology core facility.

Quantitative Real-Time Polymerase Chain Reaction:

Gene expression (mRNA and miRNA) levels from mice liver tissue and the immortalized rat hepatic stellate cell line (8B) were measured by quantitative real-time reverse transcription-polymerase chain reaction (qRT-PCR) by following our routine laboratory protocol. The primers used for RT-PCR in 5' to 3' orientations are provided in Table 2.1.

Table 2.1. Primer sequences for the different target genes.

<i>Gene</i>	<i>Primer sequence</i>
CD68 (Mouse)	Forward: GCTACATGGCGGTGGAGTACAA Reverse: ATGATGAGAGGCAGCAAGATGG
MCP-1 (Mouse)	Forward: CACAGTTGCCGGCTGGAGCAT Reverse: GTAGCAGCAGGTGAGTGGGGC
TNF- α (Mouse)	Sense: CAACGCCCTCCTGGCCAACG Antisense: TCGGGGCAGCCTTGTCCTT
IL-1 β (Mouse)	Sense: CCTCGGCCAAGACAGGTCGC Antisense: TGCCATCAGAGGCAAGGAGGA
p47 phox (Mouse)	Sense: GGTCGACCATCCGCAACGCA Antisense: TGTGCCATCCGTGCTCAGCG
RelA (Mouse)	Sense: TAGGTCCTTTTGCCTTCTC Antisense: GCTCCTGTTCGAGTCTCCAT
P65 (Mouse)	Sense: CAAGTGCCTTAATAGCAGGGCAA Antisense: AGAGCTAGAAAGAGCAAGAGTCCAAT
NFk β 1_P105 (Mouse)	Sense: GAACGATAACCTTTGCAGGC Antisense: ATTCGATTCCGCTATGTGTG
PP2AR1 (Mouse)	Sense: CAACCTGGATTGTGTGAACG Antisense: AATTCCACACCAAGCTGTCC
PP2AC1 (Mouse)	Sense: TACTCCGAGGGAATCACGAG Antisense: TCGGATGTGATCCAGTGTGT

PP2AR5D (Human)	Sense: CCCCAGATTGTCAAGAAGGA Antisense: CTGAGTGGGTCTGACACGAA
PP2ACB (Human)	Sense: CCCTGGATCGTTTACAGGAA Antisense: TGGGTGCACTGAAAATGGTA

Western Blot Analysis:

Each liver protein lysate (25 µg each) was resolved on 4%–12% bis-Tris gradient gel (Invitrogen). Resolved protein bands were transferred (semidry) to nitrocellulose membrane using the Trans-Blot Turbo transfer system (Bio-Rad Laboratories, Hercules, CA). Primary antibodies P65 (SC-8008, Santa Cruz Biotechnology), AKT and p-AKT (9272 and 4060, respectively, Cell Signaling Technology), and PP2A (ab32065, Abcam) were used at recommended dilutions (1:500), as well as β-actin used at 1:1,000, and compatible horseradish peroxidase-conjugated species-specific secondary antibodies were used at 1:5,000 dilutions. Pierce ECL Western Blotting Substrate (Thermo Fisher Scientific, Rockford, IL) was used for detection. The blot was imaged using G:BoxChemi XX6 (Syngene Imaging Systems) and subjected to densitometry analysis using Image J.

Estimation of Nitric Oxide:

Nitric oxide (NO) was estimated by measuring total nitrite formation in freshly harvested cell culture fluids using the Griess Reagent system (Promega, Madison, WI) according to the manufacturer's standard protocols.

Statistical Analyses

All in vivo experiments were repeated three times with at least 3 mice per group ($n = 3$; data from each group of 3 mice were pooled). All in vitro experiments were repeated at least 3 times ($n = 3$). The statistical analysis was carried out by unpaired t -test and ANOVA. For all analyses, $P < 0.05$ was considered statistically significant.

2.3 RESULTS

Exogenous PP2A inhibitor exacerbates NAFLD pathology

We and others have shown that environmental contaminants and their metabolites act as a second hit to exacerbate NAFLD pathophysiology [6, 8]. To study the role of MC-LR, an exogenous PP2A inhibitor in exacerbating NASH, we used MCD-HFD-fed mice to induce NAFLD, followed by a low, chronic dose of MC (NAFLD + MC). The NAFLD + MC mice showed a marked increase in NASH pathophysiology, as shown by increased infiltrating immune cells (inflammation), hepatocytes with bipolar nuclei, and ballooning when compared with NAFLD control mice alone or lean mice exposed to MC (lean + MC) (Fig.2.1 A). Liver tissues were analyzed next for steatosis and fibrosis status by picrosirius red staining. NAFLD + MC liver showed significantly increased sinusoidal and bridging fibrosis as compared with NAFLD, lean, or lean + MC mice ($P < 0.001$) (Fig.2.1, B and F). NAFLD + MC mice also showed decreased total steatosis area (Fig.2. 1D) and mean vesicle size (Fig.2.1E) when compared with NAFLD mice ($P < 0.001$). However, the tissue density of NAFLD + MC mice liver was improved when compared with NAFLD mice alone ($P < 0.001$) (Fig.2.1G). In addition, the NAFLD + MC mice group showed increased NASH CRN score with increased lobular inflammation, hepatocyte ballooning, and

fibrosis when compared with both NAFLD control mice and lean + MC mice (Table 2.2). Serum ALT levels were increased in both lean and NAFLD mice exposed to MC as compared with either lean mice or NAFLD control mice, respectively (Fig.2.1C). We analyzed the mRNA expression of the two subunits of PP2A, namely PP2AR and PP2AC, in the murine liver. We observed that there was a significant increase in the PP2AR and PP2AC subunits in the NAFLD + MC group compared with the lean or lean + MC group in the mouse liver (*P < 0.05) (Fig.2.1, J and K). A similar significant increase in PP2AR and PP2AC was observed in the human NASH liver compared with the human control liver (*P < 0.05) (Fig.2.1, N and O). We used Western blot analysis to analyze the protein levels of PP2A, and our results showed an increased expression of PP2A in the NAFLD and NAFLD + MC (*P < 0.05) groups compared with the lean mouse control (Fig.2.1, H and I), though there was a decrease in the PP2A protein expression in the NASH group compared with the control group in human (Fig.2. 1, L and M). These results clearly showed that the exposure to exogenous PP2A inhibitor was significantly affecting the activity rather than the levels in the mouse liver.

Table 2.2. NASH CRN (clinical research network score)

Characteristics	Lean Control	Lean Control +MC	NAFLD	NAFLD+ MC
Steatosis	0	0	3	2
Lobular inflammation	0	1	1	2
Hepatocyte Ballooning	0	0	1	2
Stage of fibrosis	0	1A	1C	2

Activation of Kupffer cells and hepatic stellate cells in an underlying NAFLD condition by exogenous PP2A inhibitor MC.

Liver inflammation and fibrosis are the two major stages of NASH pathogenesis [75]. These two stages are regulated by liver-specific cell types such as resident macrophages or Kupffer cells and hepatic stellate cells. To investigate whether MC activated both Kupffer cells and hepatic stellate cells, immunoreactivities of Kupffer cell activation marker CD68, CD11b, and hepatic stellate cell activation marker α -SMA were analyzed in liver slices. Results showed that there was a significant increase in CD68 as well as CD11b immunoreactivity in NAFLD + MC mice as compared with NAFLD alone or lean + MC groups of mice ($P < 0.001$) (Fig.2.2, A, C, D, and F). Similarly, α -SMA immunoreactivity, a hallmark of stellate cell activation, was significantly increased in NAFLD + MC mice groups when compared with NAFLD mice or the lean + MC mice group ($P < 0.001$) (Fig.2.2, B and E). These results were further confirmed at mRNA level. CD68 mRNA expression was significantly increased in NAFLD + MC groups when compared with NAFLD mice or lean + MC mice alone ($P = 0.018$ and $P = 0.012$, respectively) (Fig.2.2, I). The above results suggested that in an underlying condition of NAFLD, exposure to an exogenous PP2A inhibitor activated Kupffer cells and hepatic stellate cells, and the resultant activation of these cell types could generate a proinflammatory and fibrotic phenotype. To assess that the Kupffer cell activation participated in a proinflammatory phenotype, mRNA expression of proinflammatory cytokines such as monocyte-chemoattractant protein-1 (MCP-1, CCL2) and tumor necrosis factor- α (TNF- α) were examined. The result showed that there was a significant increase in both CCL2 and TNF- α mRNA expression in NAFLD + MC mice when compared with

NAFLD and lean + MC mice ($P < 0.001$) (Fig.2.2, G and H). The above results thus suggested that an exogenous PP2A inhibitor exposure in NAFLD induced proinflammatory responses via CCL2 and TNF- α .

Exogenous PP2A inhibitor MC induces NOX2-dependent oxidative stress in NASH pathogenesis.

To study whether MC synergized NOX2 activation in NASH progression, immunostaining of both the membrane subunit (GP91 phox) and cytoplasmic subunit (p47 phox) of NOX2 was performed. Results showed that the colocalization events of both subunits were significantly increased in NAFLD + MC mice as compared with NAFLD mice or lean + MC mice alone ($P = 0.015$ and $P < 0.001$, respectively) (Fig.2. 3, A and C). The mRNA expression of p47 phox was significantly increased in NAFLD + MC mice as compared with NAFLD mice or lean + MC mice alone (Fig.2.3,D). Interestingly, lean mice exposed with MC (lean + MC) showed a significant increase in p47 phox mRNA expression as compared with lean mice alone ($P < 0.001$) (Fig.2.3, D) but did not show significant increase in GP91 phox-p47 phox colocalization events (Fig.2.3, A and C). There are significant colocalization events for CD68 and GP91 phox subunits in NAFLD + MC mice when compared with the NAFLD group as well as the other groups (Fig.2.3, B). CD68 is the marker for the activated Kupffer cells in the liver, and colocalization of GP91 phox with CD68 suggests that NOX2 is activated in the Kupffer cells. The result suggested that MC exacerbated NOX2 activation in an underlying condition of NAFLD. Furthermore, to investigate the role NOX2 in peroxynitrite generation and subsequent NASH progression, we used P47 phox gene-deleted mice (P47phox KO) fed with an MCD-HFD and exposed them to the exogenous PP2A inhibitor. The

immunohistochemistry of 3NT, a marker of peroxynitrite-induced oxidative stress, Kupffer cell activation marker CD68, CD11b, and stellate cell activation marker (α -SMA) was performed. Results showed that there was an increased immunoreactivity of 3NT in NAFLD + MC mice when compared with NAFLD mice alone, whereas there was a significant decrease in p47 phox KO mice groups exposed with MC ($P = 0.013$) (Fig.2.3, E and I). These results suggested that the peroxynitrite-induced oxidative stress as a result of PP2A inhibition exacerbated NASH and was NOX2 dependent. Results also showed increased immunoreactivity of CD68, CD11b, and α -SMA in NAFLD + MC mice groups as compared with NAFLD alone, whereas there was a significant decrease in P47 phox KO mice groups ($P < 0.001$) (Fig.2.3, F–H and J–L). The mRNA expression of proinflammatory cytokines CD68, CCL2, and TNF- α showed a significant increase in NAFLD + MC mice groups, whereas a decrease in P47 phox KO mice was observed (Fig.2.3, M). The data suggested that the exogenous PP2A inhibitor activated Kupffer and stellate cells, increased inflammation, and were primarily NOX2 dependent.

Exogenous PP2A inhibitor MC synergistically increases NOX2 activation and tyrosine nitration in Kupffer cells.

Recent studies have shown that activated NOX2 generates ROS in microglia and macrophages in traumatic brain injury [76] and is the primary source of oxidative stress in macrophages [77, 78]. To study whether MC generated NOX2-dependent oxidative stress via a free radical mechanism in hepatic resident macrophages, leptin-primed Kupffer cells (leptin resistance condition of NAFLD) were exposed to MC. Results showed a significant increase in GP91 phox-p47 phox colocalization events in leptin + MC-exposed Kupffer cells as compared with vehicle control (control) or leptin-primed control cells (leptin) or

MC-treated cells ($P < 0.001$, $P = 0.04$, and $P = 0.018$, respectively) (Fig.2.4, A, i–v and 2.4, B). However, leptin-primed cells treated with Apo (a nonspecific inhibitor of NADPH oxidase) and exposed to MC showed a significant decrease in GP91 phox-p47 phox colocalization events as compared with leptin + MC group cells ($P < 0.001$) (Fig.2.4, A,iv and v, and 2.4, B). Interestingly, leptin-primed Kupffer cells exposed with MC showed a significant increase in 3NT immunoreactivity when compared with either vehicle control (control), leptin-primed, or MC-treated cells. In addition, leptin-primed cells exposed to MC and either Apo, DMPO (free radical spin trap), or FBA (peroxynitrite scavenger) showed a significant decrease in 3NT immunoreactivity (Fig.2.5, A and B). The above data suggested that in exogenous PP2A inhibitor-induced NASH, Kupffer cells might be the major cellular site for NOX2-dependent ROS generation.

Exogenous PP2A inhibitor-induced NOX2 triggers miR21-dependent NF- κ B pathway activation in NASH.

NOX2 plays a significant role in regulating noncoding, small miRNAs. We and others have shown previously that NOX2 positively regulates miR21 in renal inflammation and lung cancer [72, 79]. To study whether NOX2-mediated oxidative stress triggered by a prior expression of an exogenous PP2A inhibitor can activate an miR21 signaling pathway in progressive NASH, its expression was analyzed by qRT-PCR in liver tissue. Results showed that there was a significant increase in miR21 expression in NAFLD + MC mice as compared with NAFLD control mice ($P < 0.001$) (Fig.2.6, A). However, P47 phox KO mice exposed with MC showed a significant decrease in miR21 expression in liver tissue ($P = 0.04$) (Fig.2.6, A). The data clearly suggested that miR21 expression was NOX2 dependent in MC-triggered NASH pathology. Furthermore, we studied the role of

miR21 in NASH pathogenesis. We used miR21 gene-deleted mice (miR21 KO) exposed to MC followed by the analysis of Kupffer cell pathology, stellate cell activation, and proinflammatory cytokine expression. Results showed a significant increase in CD68, CCL2, and TNF- α mRNA expression ($P > 0.01$) (Fig.2.6, B). Interestingly, miR21 KO mice showed a significant decrease in CD68, CCL2, and TNF- α ($P < 0.001$) (Fig.2. 6, B). Results showed that there was a significant increase in CD68, CD11b ($P = 0.002$ and $P = 0.003$, respectively) (Fig.2.6, C, E, F, and H) and α -SMA ($P < 0.001$) (Fig.2. 6, D and G) in NAFLD + MC mice when compared with NAFLD control mice alone. Interestingly, miR21 KO mice exposed with MC showed a significant decrease in CD68, CD11b, and α -SMA immunoreactivity ($P < 0.001$) (Fig.2.6, C–H) as compared with NAFLD + MC mice. The above data suggested that NOX2-induced miR21 plays a significant role in Kupffer cells and stellate cell activation leading to a proinflammatory phenotype in NASH.

To study whether miR21 acted downstream by modulating the p-AKT-NF- κ B signaling pathway, we analyzed the immunoreactivity as well as protein expression levels by Western blot analysis technique of the various components of the above pathway. Results showed that there was a significantly increased immunoreactivity of p-AKT and the p65 subunit of NF- κ B in NAFLD + MC mice liver when compared with the NAFLD-only liver ($P = 0.002$ and $P = 0.005$, respectively) (Fig.2.7, A–D) as well as in the Western blot analysis ($P < 0.001$ and $P < 0.001$, respectively) (Fig.2.7, F–H). miR21 KO mice exposed to MC showed a significant decrease in p-AKT and p65 immunoreactivity ($P < 0.001$ and $P = 0.002$, respectively) (Fig.2.7, A–D) as well as in the Western blot analysis ($P < 0.001$ and $P = 0.005$, respectively) (Fig.2.7, F–H). We also conducted mRNA

expression of the NF- κ B subfamily gene such as RelA, p65, and NF- κ B1 (P105). Results showed that mRNA expression of RelA and P65 were significantly increased in these genes in NAFLD + MC mice ($P < 0.001$ and $P < 0.001$, respectively), whereas miR21 KO mice showed decreased expression of P65 gene in comparison with NAFLD only ($P < 0.001$) (Fig.2.7, E). NF- κ B-p105 subfamily showed similar increased expression patterns in the NAFLD + MC group and a subsequently decreased expression in miR21 KO mice, but the change was not significant (Fig.2.7, E). The above data suggested that miR21 not only increased the activity of NF- κ B but also increased transcription of NF- κ B family genes.

To reconfirm the mechanisms in vitro, NOX2-miR21-NF- κ B signaling pathway was examined in immortalized rat Kupffer cells. The Kupffer cells were primed with leptin and exposed to MC alone or together with NOX2 inhibitor, DMPO (free radical scavenger), FBA (peroxynitrite inhibitor), and miR21 inhibitor (miR21 inh). The results showed a significant increase in miR21 expression in leptin-primed Kupffer cells exposed with MC (leptin + MC) when compared with leptin alone, MC alone, or vehicle control ($P < 0.05$) (Fig.2.8, A). Leptin-primed cells coexposed with MC and either Apo or FBA showed a significant decrease in miR21 expression ($P < 0.05$) (Fig.2.8, A). These data showed that miR21 expression was mediated by NOX2-dependent oxidative stress and was primarily in Kupffer cells. We used immunofluorescence staining to understand whether this NOX2-mediated miR21 expression caused Kupffer cell activation. Results showed that there was a significant increase in the immunoreactivity of CD68 in the leptin-primed cells exposed with MC as compared with vehicle control, leptin-, or MC-treated cells (Fig.2.8,B, i–iv, 2.8, C, iii–iv, and 2.8, D). Interestingly, leptin-primed cells cotreated with MC and Apo,

DMPO, FBA, and miR21 inh showed a significant decrease in CD68 immunoreactivity (Fig.2.8, B, v–viii and 2.8, D). The above results suggested a strong role of NOX2-miR21-NF- κ B pathway in the activation of Kupffer cells.

Exogenous PP2A inhibitor MC increases M1 phenotype in Kupffer cells via NOX2-miR21-dependent pathway.

Kupffer cells (resident liver macrophages) play a significant role in liver immunology. M1 phenotype of Kupffer cells is characterized by the release of high levels of proinflammatory cytokines [80], adaptation to an elongated morphology [81], activation of inducible nitric oxide synthase (iNOS), and release of NO [82]. We performed immunofluorescence imaging of β -tubulin for assessment of altered morphology, iNOS, and measured the NO release from Kupffer cells. Leptin-primed Kupffer cells exposed with MC showed an elongated morphology (Fig.2.9, A, iii), increased iNOS expression (Fig.2.9, B, iii), and NO release (Fig.2.9, C) as compared with control, leptin, or MC exposed alone. However, Kupffer cells coexposed with Apo, DMPO, miR21 inhibitor, or FBA showed normal cell morphology (Fig.2.9, A, v–viii), decreased iNOS expression (Fig.2.9, B, v–viii), and NO release ($P < 0.05$) (Fig.2.9, C). The above results suggested that MC-mediated NOX2-miR21 axis modulated the M1 phenotype of Kupffer cells and generated subsequent proinflammatory response.

Exogenous PP2A inhibitor-induced NOX2 and ROS activates hepatic stellate cells.

To show the exogenous PP2A inhibitor-induced profibrogenic signaling in NAFLD, we studied the hedgehog signaling mechanisms in an in vitro setup. Leptin-primed and MC-treated hepatic stellate cells were coexposed with Apo, DMPO, miR21 inhibitor, and FBA to test the role of NOX2 mediators or miR21 in liver fibrosis.

Immunofluorescence images of α -SMA (stellate cell activation marker) showed a significant increase in leptin-primed stellate cells exposed with MC when compared with control, leptin, and MC alone groups ($P < 0.001$) (Fig.2.10, A, i–iv and 2.10, B). Interestingly, the cells coexposed with Apo, DMPO, FBA, and miR21 inh showed significant decreases in α -SMA immunoreactivity as compared with leptin-primed cells exposed with MC ($P < 0.001$) (Fig.2.10, A, iv–viii and 2.10, B). Results also suggested that activation of stellate cells were mediated by MC-induced NOX2 and oxidative stress instead of the NOX2-miR21 axis.

Exogenous PP2A inhibitor MC activates NOX2 via AKT pathway.

To show the mechanistic link between the exogenous PP2A inhibitor and its subsequent activation of NOX2 both in vivo and in vitro, we conducted experiments in immortalized Kupffer cells. Leptin-primed cells were incubated with either MC, a standard PP2A inhibitor, or an AKT inhibitor. Results showed that MC alone or leptin-primed MC groups had a significant increase in NOX2 activation ($P < 0.05$) (Fig.2.11, A–D). A standard PP2A inhibitor also mimicked the results obtained by MC. Interestingly, AKT inhibitor treatment in both leptin-primed MC or PP2A inhibitor groups showed a significant decrease in the NOX2 activation, suggesting that NOX2 activation was primarily due to the AKT pathway ($P < 0.05$) (Fig.2.11, A–D). Since NOX2-derived peroxynitrite was paramount to the NASH pathology caused by exogenous PP2A inhibitor, we analyzed whether the AKT pathway was important for the generation of NOX2-induced ROS. Results showed that MC alone or leptin-primed MC groups had a significant increase in peroxynitrite generation as exhibited by 3NT levels ($P < 0.05$) (Fig.2.12, A–D). A standard PP2A inhibitor also mimicked the results obtained by MC. Interestingly, AKT

inhibitor treatment in both leptin-primed MC or PP2A inhibitor groups showed a significant decrease in the 3NT levels, suggesting that NOX2 activation-induced peroxynitrite generation was primarily due to the AKT pathway ($P < 0.05$) (Fig.2.12, A–D). A mechanistic summary of the study has been provided in (Fig.2.13).

2.4 DISCUSSION

Our studies indicate for the first time, to the best of our knowledge, the role of exogenous PP2A inhibitors in exacerbating NAFLD pathology and provide a mechanistic basis of advancing the progression of NAFLD via NOX2-mediated miR21 (Fig.2.13). The results reported herein show that the administration of MC-LR, a proven environmental hepatotoxin and a PP2A inhibitor, caused increased inflammation, increased activation of stellate cells, and advanced fibrotic lesions in NAFLD. Furthermore, the results showed a decreased hepatic steatosis concomitant to the progression of liver injury as indicated by increased serum ALT levels. Our novel histological assessment tool developed by our collaborators at Biocellvia also showed a significant increase in fibrosis area in the liver, which was subjected to exogenous PP2A inhibitor administration.

We and others have shown previously that NOX2 plays a significant role in promoting NASH and its fibrotic pattern. To understand the role of exogenous PP2A inhibition and its relationship with NASH pathogenesis, we studied the activation of NOX2. Our results of increased NOX2 activation following inhibition of PP2A and subsequent increases in protein levels of macrophage activation marker CD68 and stellate cell activation marker α -SMA while attenuation of all the above markers in p47 phox KO mice suggested that PP2A inhibition induced a strong NOX2 activation both in vivo and in vitro. Strikingly, PP2A-induced NOX2 activation and its downstream association with

inflammation and extracellular matrix deposition were also associated with increased levels of miR21. Interestingly our results showed an increase in PP2A protein levels following MC administration in mice, whereas human NASH samples showed a decrease in the same protein. Since PP2A inhibition is an enzymatic process, it is clear from our results that the activity of the protein is more relevant for the pathology rather than the levels of the same protein in the liver.

Studies show that miR21 has a prominent role in NAFLD fibrosis, and NOX2-induced downstream signaling through peroxynitrite generation can induce miR21 expression [57]. Our results of increased levels of miR21 both in vivo and in vitro and its restricted levels in the presence of either a gene deletion of NOX2 cytoplasmic subunit (p47 phox KO mice) or Apo confirmed such a hypothesis. In addition, in vitro results using peroxynitrite scavenger FBA showed a decrease in miR21 levels, suggesting strongly that NOX2-derived peroxynitrite was responsible for the induction of higher miR21 levels in the liver. The higher miR21 increased liver inflammation via the phosphorylation of AKT and subsequent activation of NF- κ B, a proven pathway for inflammation in the liver and other organs.

It is widely accepted that liver injury in progressive NAFLD is accompanied by a parallel decrease in steatosis, and simple hepatic steatosis might be a benign process in the majority of patients, thus signifying that NASH can be a separate disease with different pathogenesis [12]. Our report confirms the previous findings by showing a decrease in mean vesicle size, which is correlative of a subsequent decrease in steatosis area. Studies show that free fatty acid delivery to the liver and triglyceride accumulation is a prime cause in liver fat accumulation, and together they may exert protective functions [12]. The above

fact may be supported by studies that show inhibition of diacyl glycerol acyltransferases 1/2, principal enzymes in triglyceride synthesis in the liver, leads to increased liver injury, whereas overexpression protects the liver from macrophage activation and their accumulation in the liver lobule [83, 84]. Interestingly, PP2A plays a significant role in promoting hepatic steatosis. It does so via positively regulating SREBP1-C, a prime mediator of hepatic lipogenesis [85]. Thus, inhibiting PP2A in our studies rightly resulted in decreased steatosis area and the mean vesicle size that correlated strongly with increased inflammation and fibrosis in an underlying condition of NAFLD. It is also striking that p47 phox-deficient mice and miR21 KO mice in which liver was minimal had higher steatosis as shown by decreased lipid droplets/vesicle size. The results in these KO mice are very significant since NASH-associated inflammation has been shown to decrease steatosis, and both of these genes may represent a yet unidentified metabolic switch that can lead to reprogramming of liver metabolism in NASH.

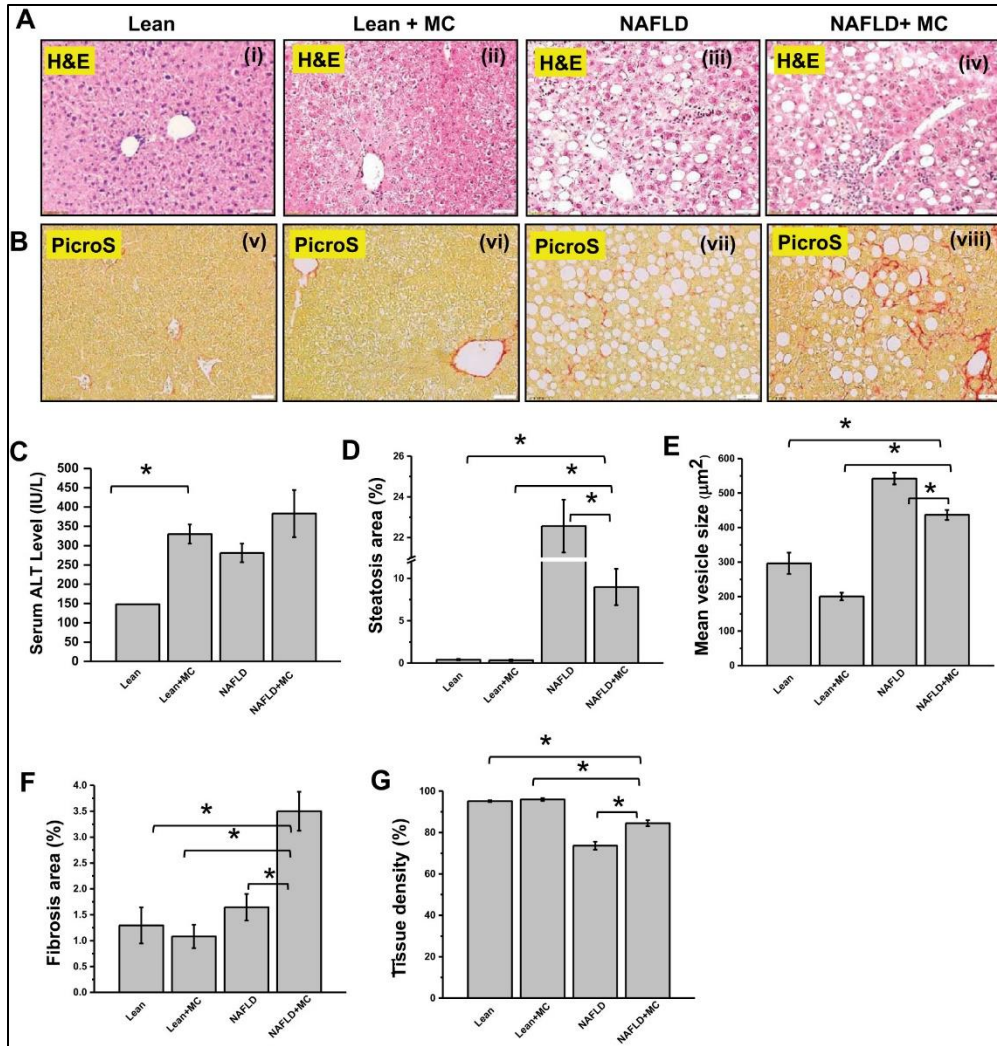
Subsequent to miR21-induced inflammation, the said pathway also was instrumental in causing increased α -SMA levels, a marker for stellate cell activation. Interestingly, all these downstream events of liver injury associated with progressive phases of NAFLD were inhibited using NOX2 inhibitors. Furthermore, our studies also showed a distinct mechanism of PP2A-induced NOX2 activation. Use of AKT inhibitor in Kupffer cells primed with leptin failed to either induce NOX2 activation or generation of peroxynitrite, suggesting that PP2A might be activating NOX2 via AKT. The above results may be a significant finding to advance our understanding of upstream modulation of NOX2 via inhibition of PP2A. Furthermore, protein phosphatases may be negatively

regulating the redox pathways in NAFLD, thus exerting a positive role in the prevention of NAFLD progression to a more progressive phenotype.

In summary, the results assume tremendous significance in NASH pathogenesis since PP2A inhibition both via endogenous and exogenous routes can be a cause of concern in the overall scenario of NAFLD incidences around the globe. NAFLD progression to NASH, though, is restricted only to a small percentage of patients with NAFLD; it is likely that the “multiple hit paradigm” may be in play. Furthermore, our studies of PP2A inhibition leading to increased fibrotic lesions in NAFLD thus also might be useful in dealing with the exogenous threats from the environment as posed by increased incidences of harmful algal blooms worldwide.

Acknowledgements:

The authors acknowledge the services offered by Charles J. Tucker and Erica Scappini at The Fluorescence Microscopy and Imaging Center, National Institute of Environmental Health Sciences (NIEHS), National Institutes of Health (NIH). We also appreciate the NIEHS, the NIH, and the Instrumentation Resource Facility at the University of South Carolina School of Medicine for equipment usage and consulting services.



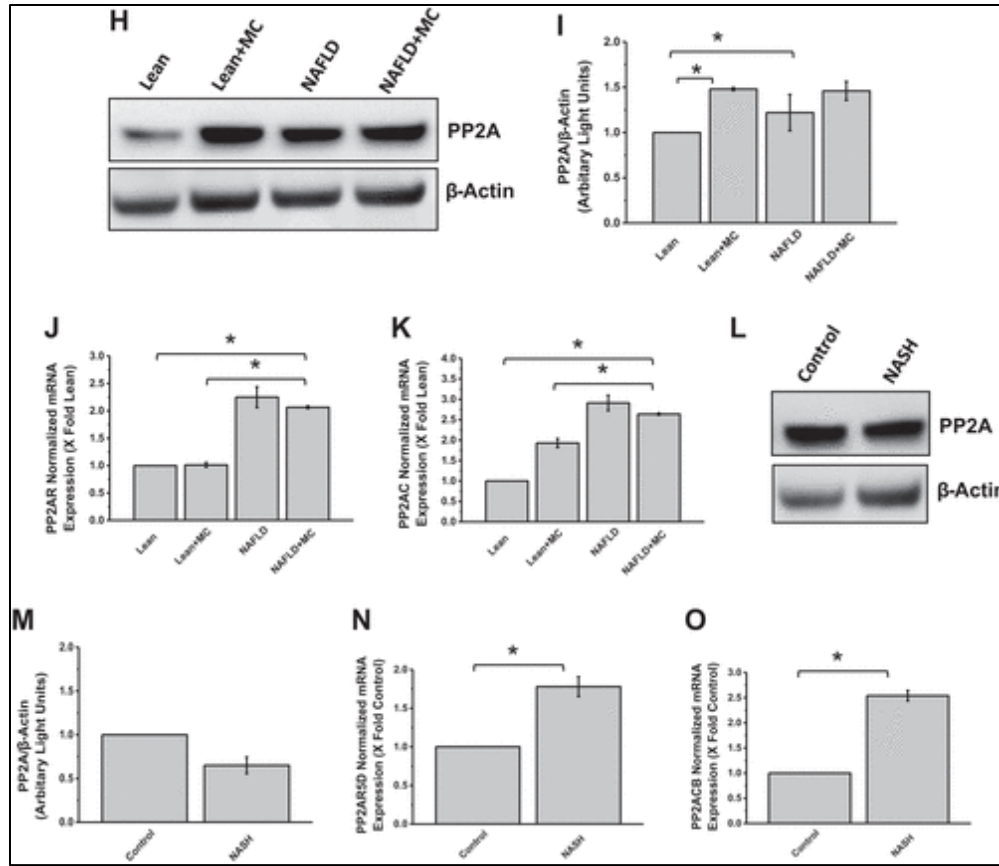


Figure 2.1 Exogenous protein phosphatase 2A (PP2A) inhibition in mouse liver exacerbates nonalcoholic fatty liver disease (NAFLD) pathology. Qualitative and quantitative image analysis of microcystin (MC) effects on liver steatosis and fibrosis induced in an NAFLD mouse model. A: representative histological images of liver sections stained with hematoxylin-eosin (H&E), from lean mouse control and lean mouse + MC (n = 3), wild-type mouse NAFLD, and NAFLD + MC (n = 3). B: representative histological images of the same groups of mice stained with picosirius red (PicroS). Images were taken at $\times 20$ magnification. C: quantification of serum alanine aminotransferase (ALT) level and comparison between control (lean and NAFLD) and MC-tested groups. Automatic digital-imaging quantification of steatosis area (%) (D), mean vesicle size (μm^2) (E), fibrosis area (%) (F), and liver tissue density (%) (G) in lean and NAFLD groups. H: Western blot analysis of β -actin and PP2A protein levels in the liver homogenates of control (lean and NAFLD) and MC-tested groups. I: morphometric band analysis of PP2A normalized against β -actin. The y-axis depicts the PP2A to β -actin ratio. J: quantitative RT-PCR (qRT-PCR) analysis of mRNA expression of PP2AR subunit in liver. K: qRT-PCR analysis of mRNA expression of PP2AC subunit in the liver for control (lean and NAFLD) and MC-tested groups. L: Western blot analysis of β -actin and PP2A protein levels in the human liver homogenates comparing control with nonalcoholic steatohepatitis (NASH). M: morphometric band analysis of PP2A normalized against β -actin. The y-axis depicts the PP2A-to- β -actin ratio. N: qRT-PCR analysis of mRNA expression of PP2AR5D subunit in liver. O: qRT-PCR analysis of

mRNA expression of PP2ACB subunit in liver comparing control with NASH. *P < 0.05. Results were expressed as means ± SE.

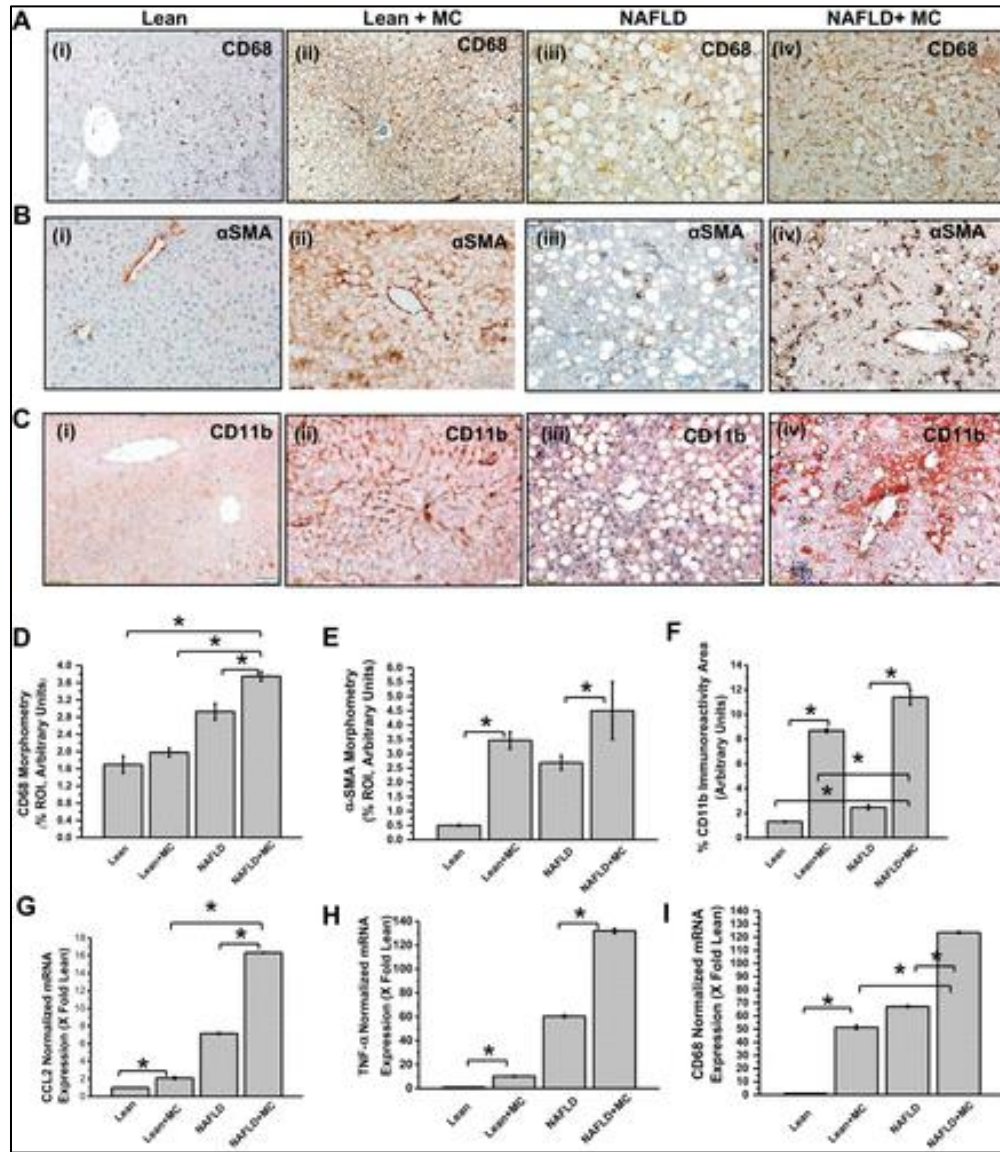
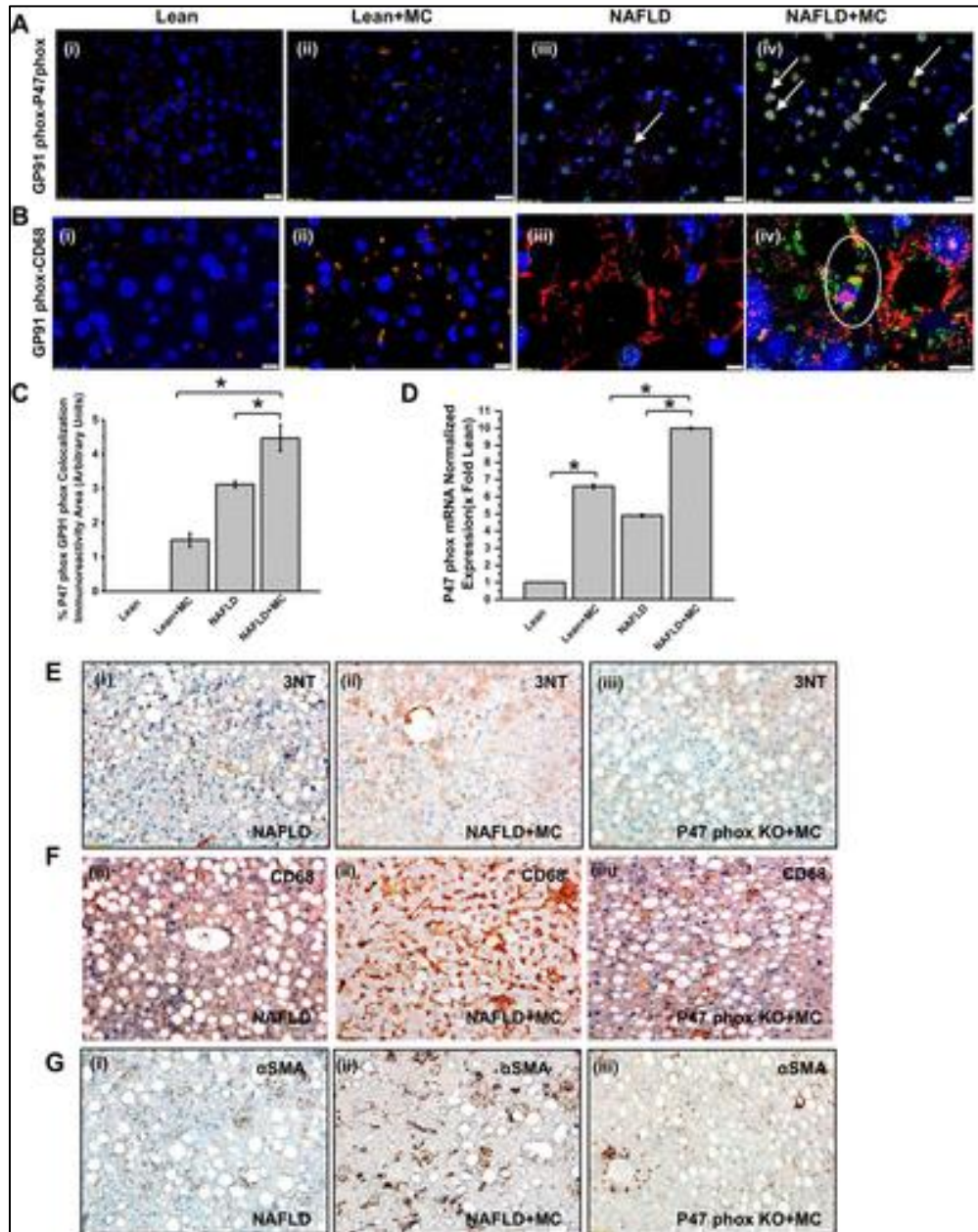


Figure 2.2. Protein phosphatase 2A inhibition by microcystin (MC) activates Kupffer cells and hepatic stellate cells and induces an inflammatory surge in mouse liver. Representative histological images of liver sections immunostained with CD68 (A), α -smooth muscle actin (SMA) (B), and CD11b (C) from lean mouse, lean mouse + MC, nonalcoholic fatty liver disease (NAFLD), and NAFLD + MC (n = 3/group). Images were taken at $\times 20$ magnification. Morphometric analysis of CD68 (D), α -SMA (E), and CD11b (F) in lean, lean + MC, NAFLD, and NAFLD + MC groups (n = 3/group). Morphometric analysis was expressed in percentage of positive immunoreactive area per regions of interest (ROIs) (3 ROIs/liver section). Quantitative RT-PCR analysis of mRNA expression of CCL2 (G), TNF- α (H), and CD68 (I), in lean, lean + MC, NAFLD, and NAFLD + MC livers. The

mRNA expressions were normalized with 18s and presented as fold change of lean group.
 *P < 0.05. Results were expressed as means ± SE.



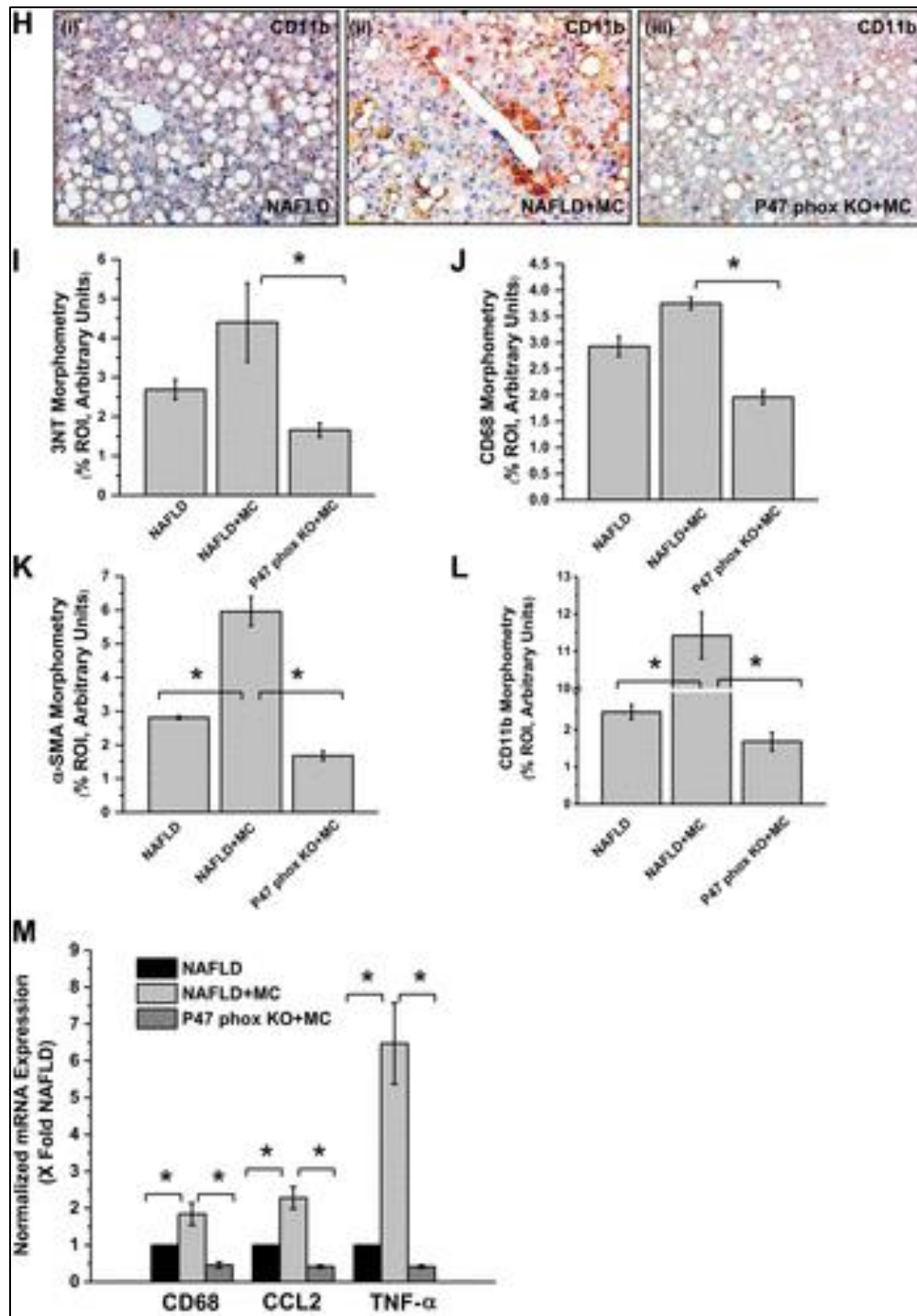


Figure 2.3. The activation of Kupffer cells, hepatic stellate cells, and an inflammatory surge in microcystin (MC)-exposed livers are mediated by NADPH oxidase 2-dependent oxidative stress. A: representative images of P47 phox (red) and GP91phox (green) immunofluorescence counterstained with DAPI (blue); colocalization indicated by arrows. Images were taken at $\times 40$ magnification. B: representative images of CD68 (red) and GP91 phox (green) immunofluorescence counterstained with DAPI (blue), from lean, lean + MC,

nonalcoholic fatty liver disease (NAFLD), and NAFLD + MC (n = 3/group). Colocalization was indicated by a circle. Images were taken at $\times 60$ magnification. C: morphometric analysis of P47 phox (red) and GP91 phox (green) colocalization expressed in percentage of positive colocalized immunoreactive area per region of interest (ROI) (3 ROIs/liver section, n = 3 each group). D: quantitative RT-PCR (qRT-PCR) analysis of mRNA expression of P47 phoxin lean and NAFLD groups treated with MC, expressed as fold change of lean control group. Representative immunohistochemistry images depicting 3-nitrotyrosine (3NT) (E), CD68 (F), α -smooth muscle actin (SMA) (G), and CD11b (H) expression in NAFLD, NAFLD + MC, and P47 phox knockout (KO) groups treated with MC. All immunohistochemistry images were taken at $\times 20$. Morphometric analysis of 3NT (I), CD68 (J), α -SMA (K), and CD11b (L) immunoreactivity in NAFLD, NAFLD + MC, and P47 KO mice treated with MC, expressed in percentage of positive immunoreactive area per ROIs (n = 3/group, 3 ROIs/liver section). qRT-PCR analysis of mRNA expression of CD68, CCL2 and TNF- α in NAFLD and P47 KO mice treated with MC, expressed as fold change of NAFLD control group (M). *P < 0.05. Results were expressed as means \pm SE.

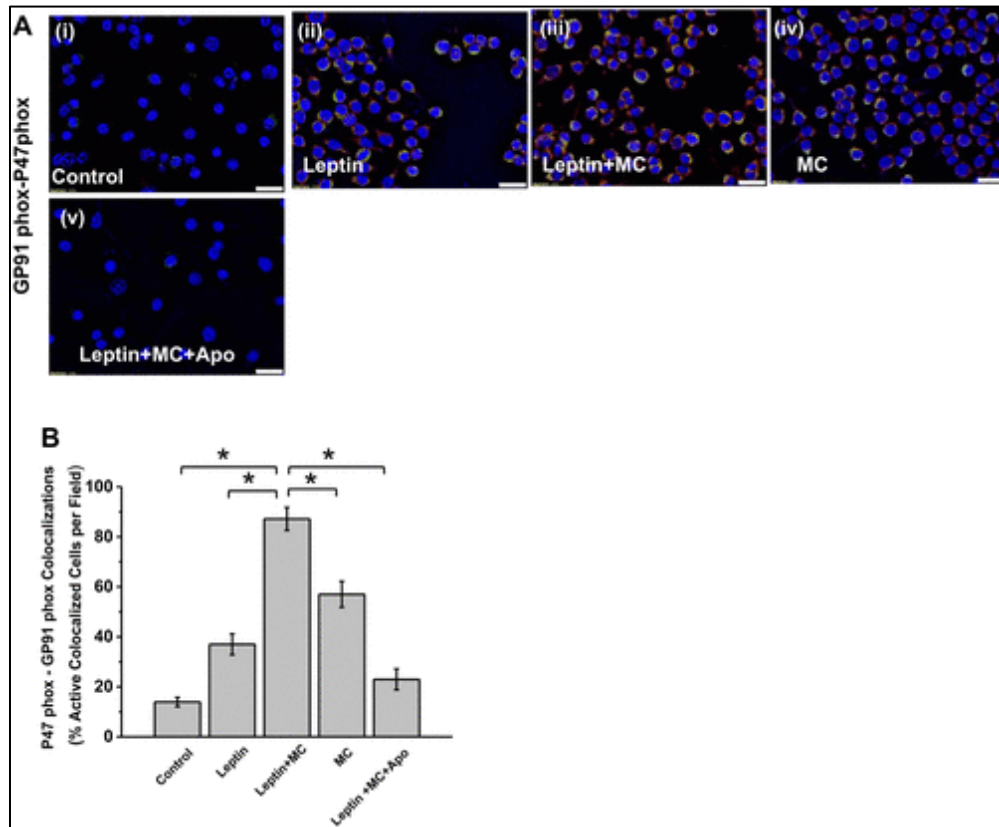


Figure 2.4. The protein phosphatase 2A inhibition activates NADPH oxidase 2-dependent oxidative stress in Kupffer cells. Leptin was used to mimic a nonalcoholic fatty liver disease (NAFLD) condition. Kupffer cells were exposed to 100 ng/mL leptin for 24 h. A: representative immunofluorescence images depicting P47 phox (red) and GP-91 phox (green) immunolabelling, counterstained with DAPI (blue), in control, leptin, microcystin (MC), leptin + MC, and leptin + MC + apocynin (Apo) rat Kupffer cells groups. Images were taken at $\times 60$ magnification. B: morphometric analysis of the number of cells

expressing a colocalization for P47 phox and GP91 phox. The y-axis shows colocalization events/100-cell unit (n = 3, analysis from 3 separate microscopic fields). *P < 0.05. Results were expressed as means ± SE.

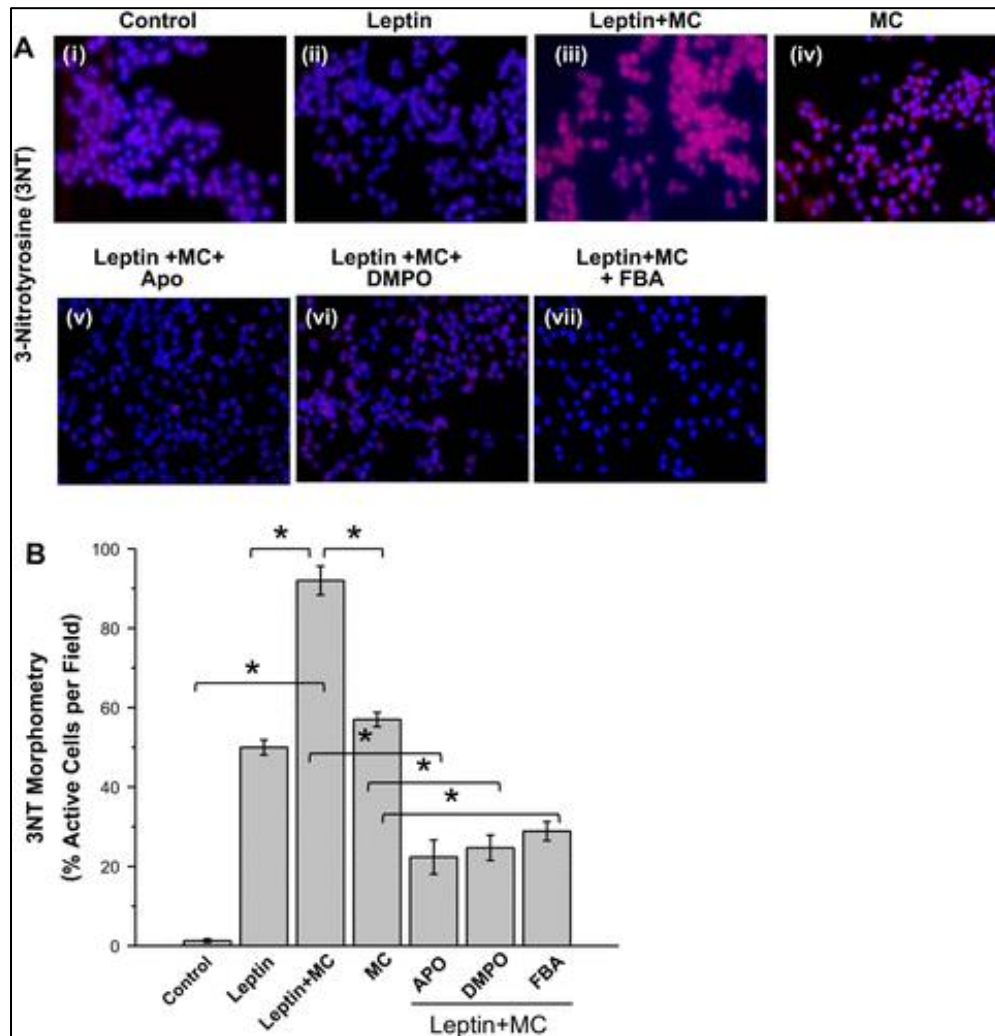


Figure 2.5. Protein phosphatase 2A inhibitor microcystin (MC) synergistically increases NADPH oxidase 2 (NOX2)-dependent tyrosine nitration in Kupffer cells. NOX2-dependent tyrosin nitration marker 3-nitrotyrosine (3NT) immunoreactivity in leptin-activated rat Kupffer cell line. A: representative immunofluorescence images depicting 3NT immunoreactivity in control, leptin, MC, leptin + MC, leptin + MC + apocynin (Apo), leptin + MC + DMPO, and leptin + MC + phenyl boronic acid (FBA) Kupffer cells groups. Images were taken at $\times 20$ magnification. B: morphometric analysis of the number of immunoreactive cells for 3NT in control and treated groups. The y-axis shows immunoreactive events/100-cell unit (n = 3, analysis from 3 separate microscopic fields). *P < 0.05. Results were expressed as means ± SE.

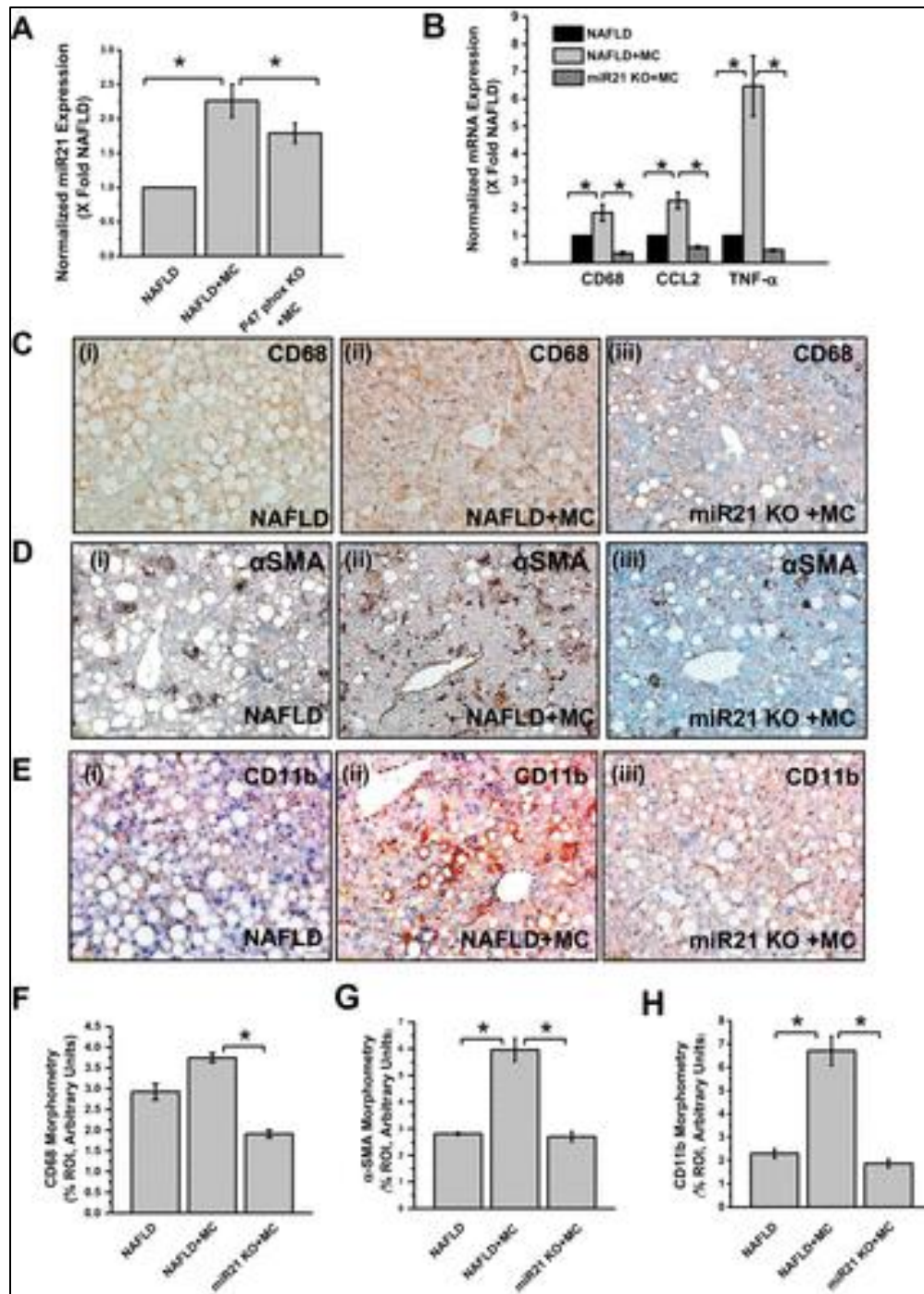


Figure 2.6. Exogenous protein phosphatase 2A inhibitor-induced oxidative stress triggers miR21-dependent NF- κ B pathway activation in nonalcoholic steatohepatitis. Histological features and morphometric analysis of CD68, α -smooth muscle actin (SMA), and CD11b expression in nonalcoholic fatty liver disease (NAFLD) and miR21 knockout (KO) mice. A: quantitative RT-PCR (qRT-PCR) analysis of miRNA expression of miR21 in NAFLD, NAFLD + microcystin (MC), and P47 KO + MC groups, expressed as fold change of NAFLD group. B: qRT-PCR analysis of mRNA expression of CD68, CCL2, and TNF- α , in NAFLD, NAFLD + MC, and miR21 KO groups. mRNA expression is represented as

fold change of NAFLD. Representative immunohistochemical images depicting CD68 (C), α -SMA (D), and CD11b (E) immunoreactivity in NAFLD, NAFLD + MC, and miR21 KO groups. Morphometric analysis of CD68 (F), α -SMA (G), and CD11b (H) immunolabelling in the various treated groups. The y-axis shows the percentage of positive immunoreactive area/region of interest (ROI) (n = 3, analysis from 3 separate microscopic fields). *P < 0.05. Results were expressed as means \pm SE.

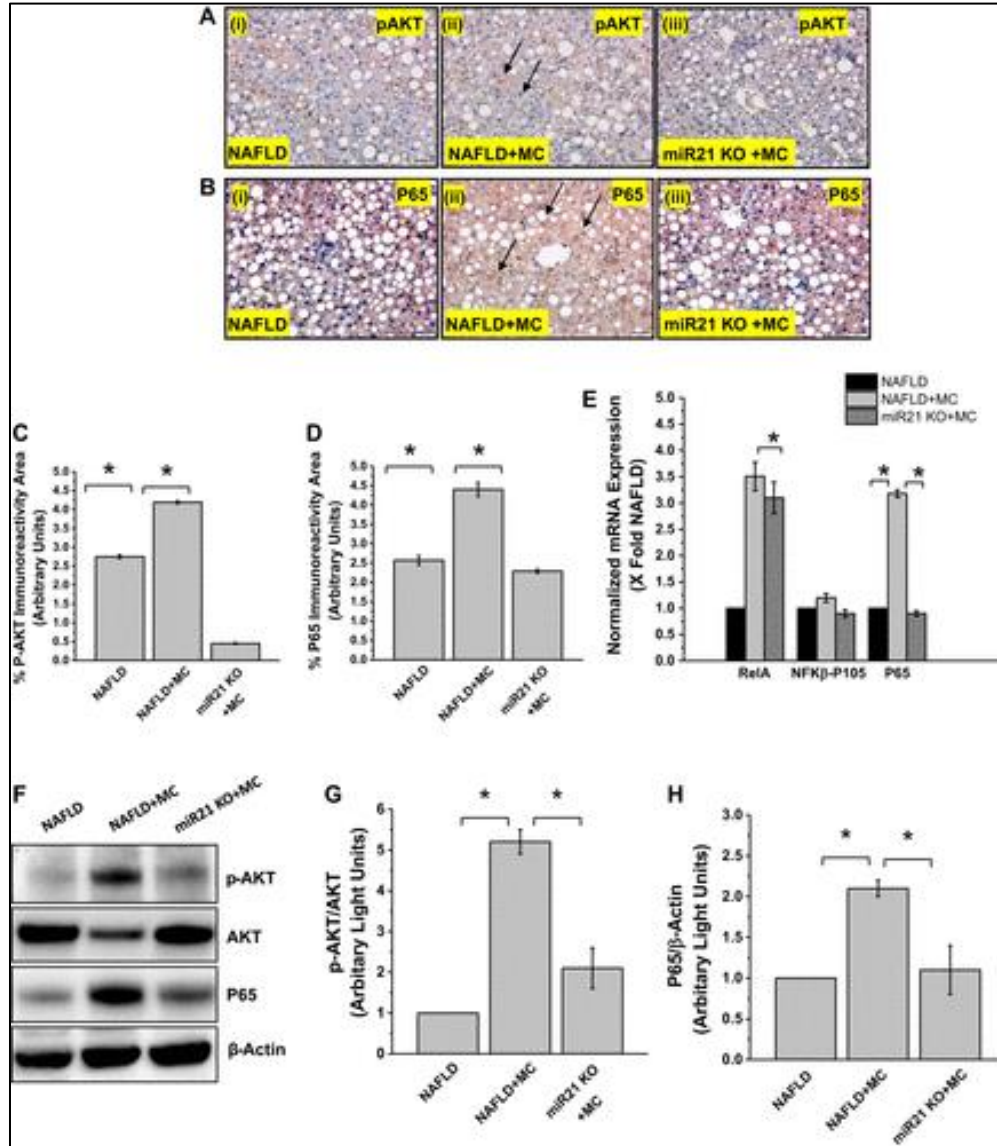


Figure 2.7. Exogenous protein phosphatase 2A inhibitor-induced miR21 upregulation acted downstream by modulating the p-AKT-NF- κ B signaling pathway. A and B: representative immunohistochemical images depicting p-AKT and P65 immunoreactivity in nonalcoholic fatty liver disease (NAFLD), NAFLD + microcystin (MC), and miR21 knockout (KO) + MC groups. C and D: morphometric analysis of p-AKT and P65 immunolabelling in various treated groups; y-axis shows the percentage of positive immunoreactive area/region of interest (ROI) (n = 3, analysis from 3 separate microscopic fields). E: quantitative RT-PCR analysis of mRNA expression of RelA, NF- κ B-P105, and

P-65 in NAFLD, NAFLD + MC, and miR21 KO groups, expressed as fold change of NAFLD. F: Western blot analysis of β -actin, p-AKT, AKT, and P65 protein levels in the liver homogenates in NAFLD, NAFLD + MC, and miR21 KO groups. G: morphometric band analysis of p-AKT normalized against AKT. The y-axis depicts the p-AKT-to-AKT ratio. H: morphometric band analysis of P65 normalized against β -actin. The y-axis depicts the P65-to- β -actin ratio in the liver of NAFLD, NAFLD + MC, and miR21 KO groups, expressed as fold change of NAFLD. *P < 0.05. Results were expressed as means \pm SE.

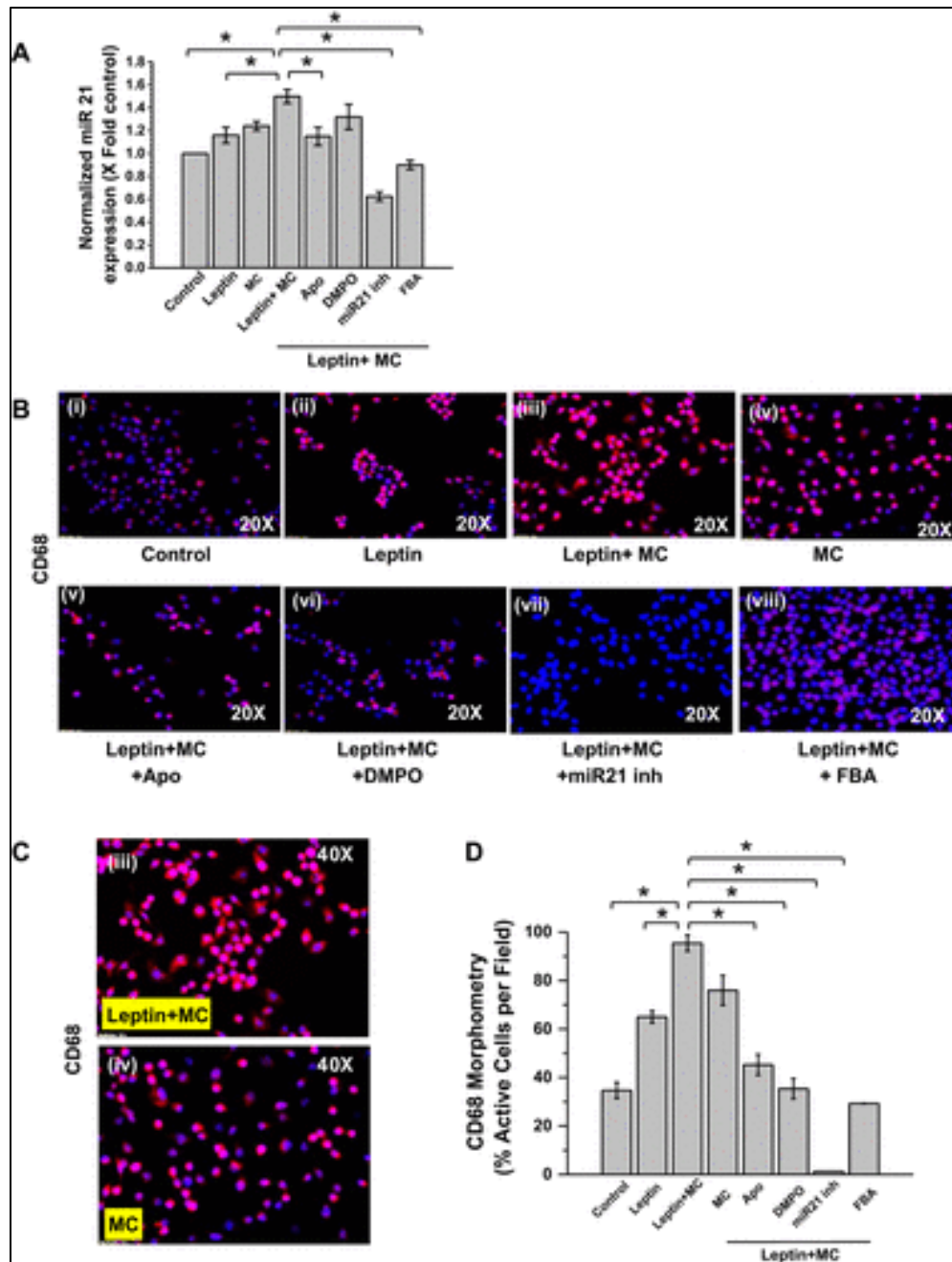


Figure 2.8. NADPH oxidase 2-miR21-NF- κ B signaling pathway in microcystin (MC)-exposed immortalized rat Kupffer cells. A: miR21 expression in control, leptin, MC, leptin + MC, leptin + MC + apocynin (Apo), leptin + MC + DMPO, leptin + MC + miR21 inhibitor (inh), and leptin + MC + phenyl boronic acid (FBA). miRNA expression is represented as fold change of control group. B: representative immunofluorescence images depicting CD68 (red), counterstained with DAPI (blue), in control and tested rat Kupffer cell groups. Images were taken at $\times 20$ magnification. C: immunofluorescence images depicting CD68 (red), counterstained with DAPI (blue), in leptin + MC and MC groups of rat Kupffer cells. Images were taken at $\times 40$ magnification. D: morphometric analysis of CD68 immunoreactivity; y-axis shows the percentage of activated Kupffer cells per region

of interest (n = 3, analysis from 3 separate microscopic fields). *P < 0.05. Results were expressed as means ± SE.

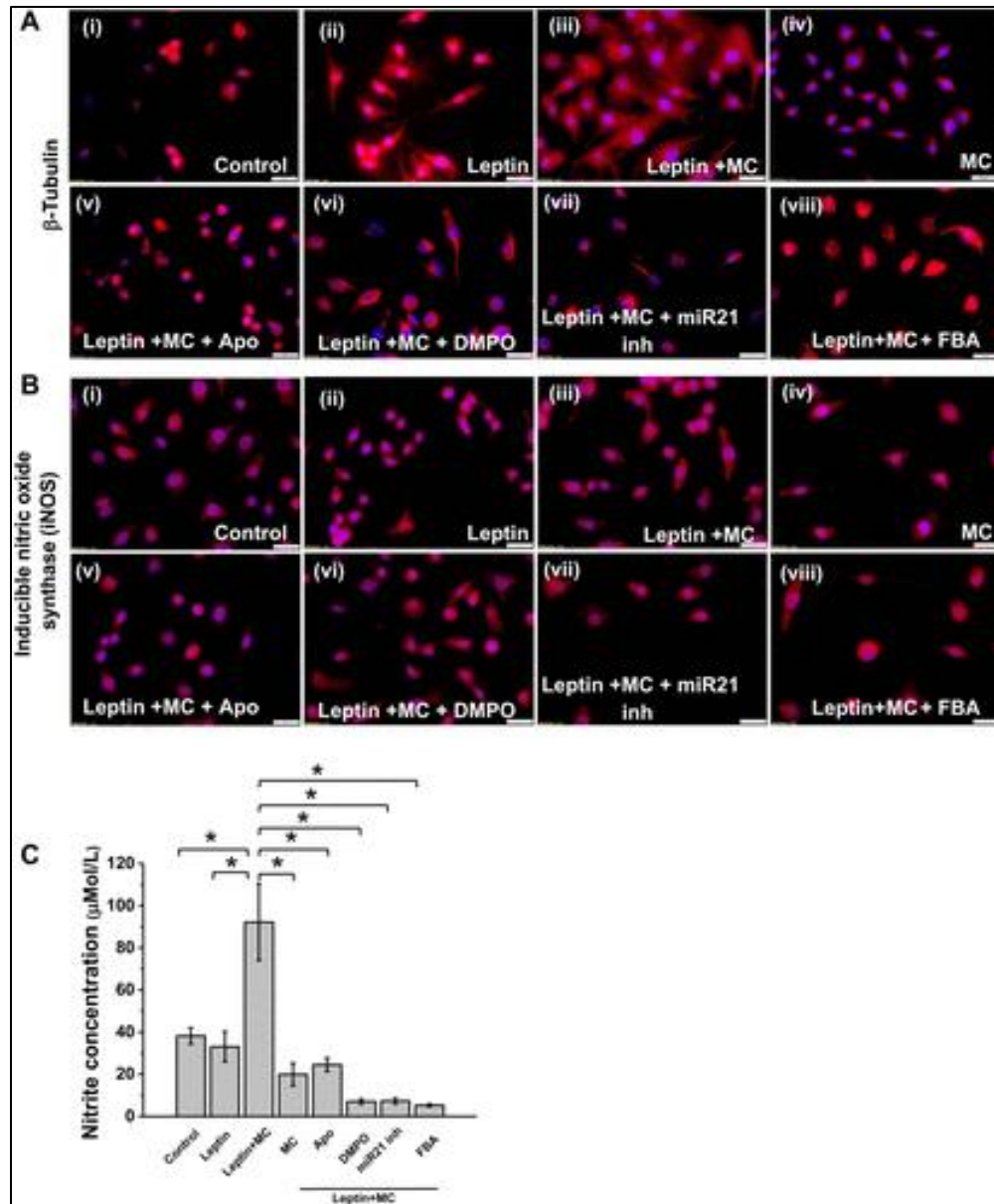


Figure 2.9. Exogenous protein phosphatase 2A inhibitor exposure increases M1 phenotype in Kupffer cells. Immunoreactivity of β -tubulin and inducible nitric oxide synthase (iNOS) and quantification of nitric oxide in leptin-activated rat Kupffer cell line. A and B: immunofluorescence images depicting β -tubulin and NOS2 (iNOS) (red), counterstained with DAPI (blue), in control, leptin, microcystin (MC), leptin + MC, leptin + MC + apocynin (Apo), leptin + MC + DMPO, leptin + MC + miR21 inhibitor (inh) and leptin + MC + phenyl boronic acid (FBA) groups of rat Kupffer cells. Images were taken at $\times 60$ magnification. C: nitric oxide release measured as total nitrite (μM) in variously treated leptin-activated Kupffer cells. *P < 0.05. Results were expressed as means \pm SE.

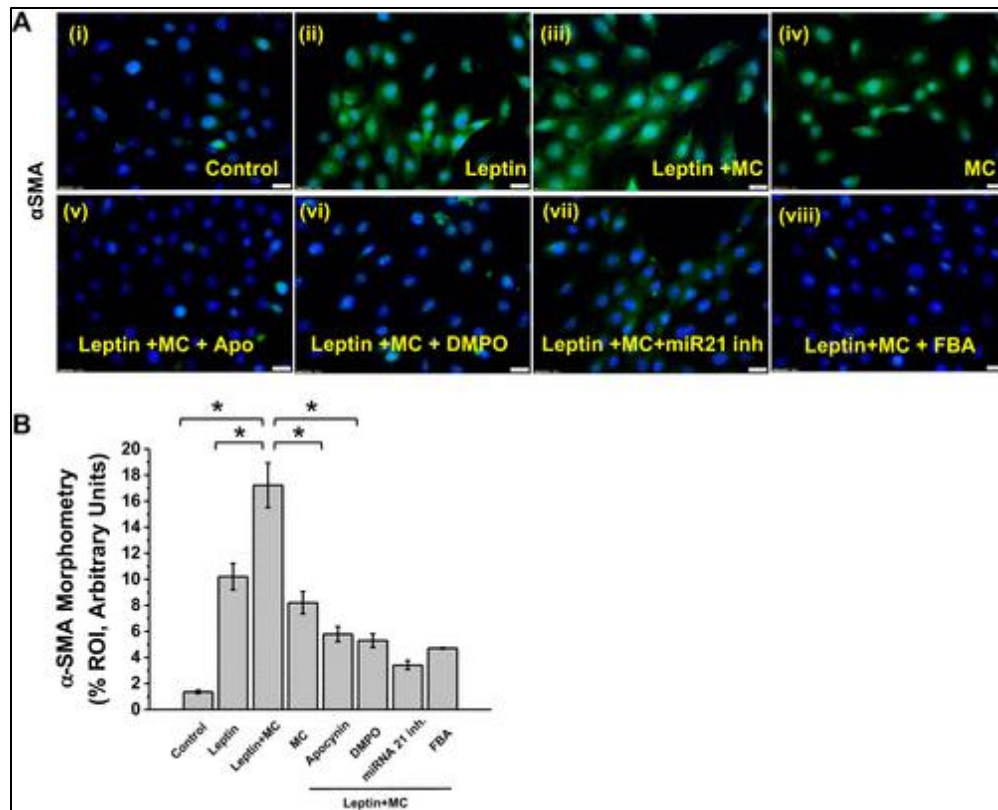


Figure 2.10. Exogenous protein phosphatase 2A inhibitor exposure activates hepatic stellate cells via NADPH oxidase 2-miR21 axis. A: immunofluorescence images depicting α -smooth muscle actin (SMA) (green), counterstained with DAPI (blue), in control, leptin, microcystin (MC), leptin + MC, leptin + MC + apocynin (Apo), leptin + MC + DMPO, leptin + MC + miR21 inhibitor (inh), and leptin + MC + phenyl boronic acid (FBA) groups of 8B rat hepatic stellate cells. Images were taken at $\times 40$ magnification. B: morphometric analysis of α -SMA immunoreactivity; y-axis shows the percentage of α -SMA-positive cells per region of interest (ROI) ($n = 3$, analysis from 3 separate microscopic fields). * $P < 0.05$. Results were expressed as means \pm SE.

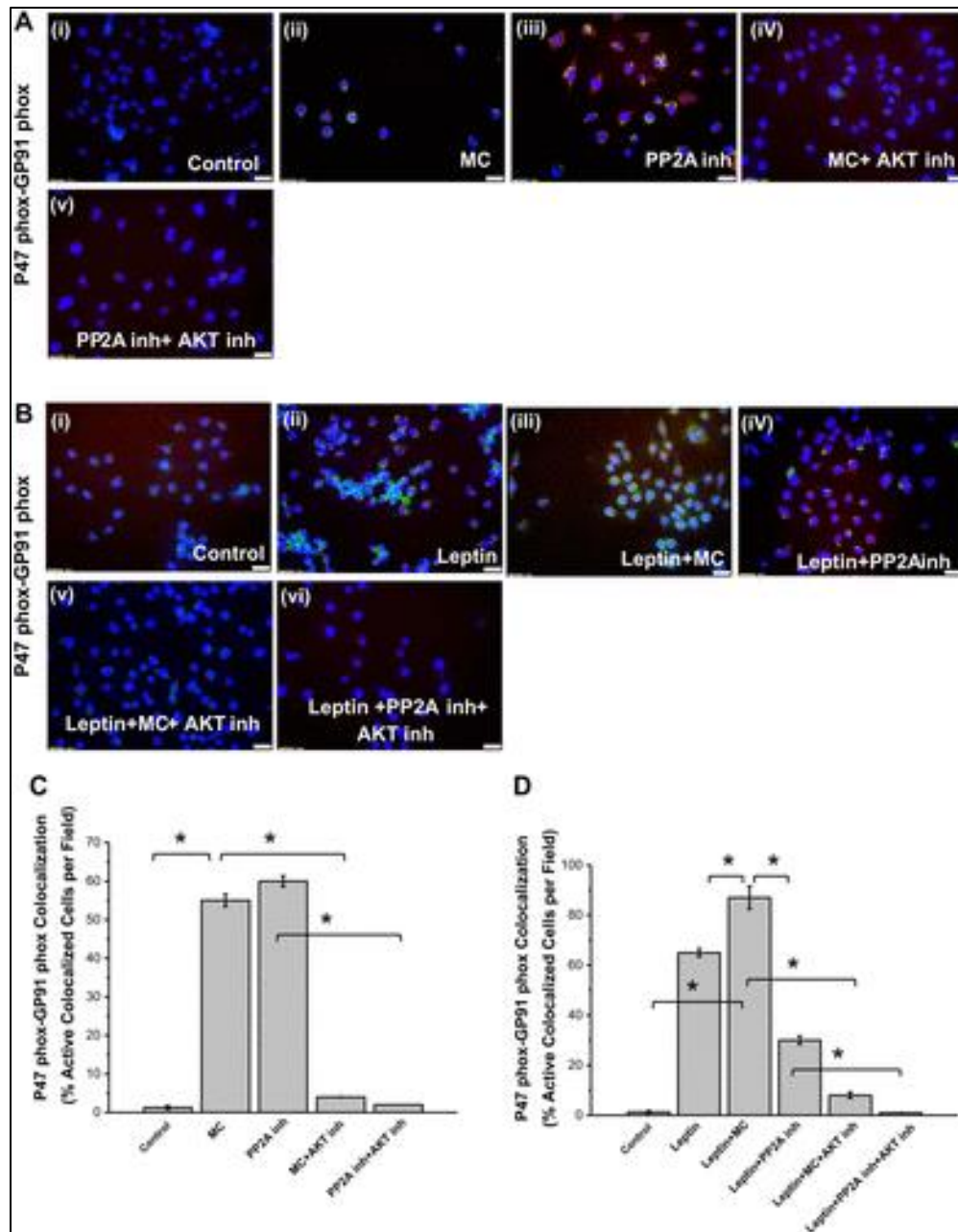


Figure 2.11. Exogenous protein phosphatase 2A (PP2A) inhibitor activates NADPH oxidase 2 via AKT pathway. Immunoreactivity and morphometric analysis of P47 phox and GP91 phox expression in leptin and microcystin (MC) -treated rat Kupffer cells. A: immunofluorescence images depicting P47 phox (red) and GP91 phox (green) colocalization, counterstained with DAPI (blue), in control, MC, PP2A inhibitor (inh), AKT inh + MC, and AKT inh + PP2A inh. B: immunofluorescence images depicting P47 phox (red) and GP91 phox (green) colocalization, counterstained with DAPI (blue), in control, leptin, leptin + MC, Leptin + PP2A inh, leptin + MC + AKT inh, and leptin + PP2A inh + AKT inh. C and D: quantitative analysis of the number of colocalized cells for P47 phox and GP91 phox in the various Kupffer cell line groups; y-axis shows

colocalization events/100-cell unit (n = 3, analysis from 3 separate microscopic fields).
 *P < 0.05. Results were expressed as means ± SE.

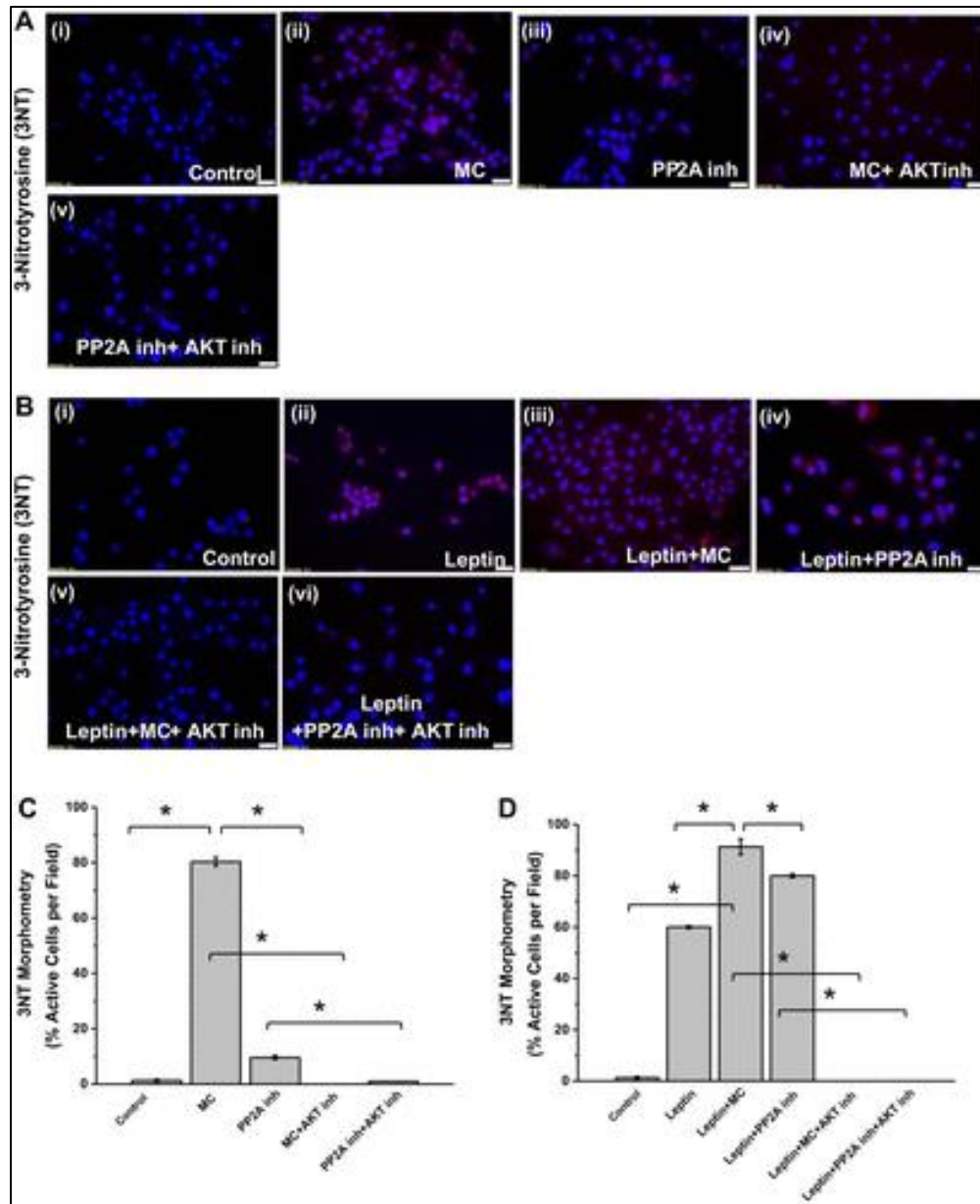


Figure 2.12. Exogenous protein phosphatase 2A (PP2A) inhibitor-activated NADPH oxidase 2 generates oxidative stress via AKT pathway. Immunoreactivity and morphometric analysis of 3-nitrotyrosine (3NT) expression in rat Kupffer cells. A: immunofluorescence images depicting 3NT immunoreactivity (red), counterstained with DAPI (blue), in control, microcystin (MC), PP2A inhibitor (inh), MC + AKT inh, and PP2A inh + AKTinh. B: immunofluorescence images depicting P47 phox (red) and GP91 phox (green) colocalization, counterstained with DAPI (blue), in control, leptin, leptin + MC, leptin + PP2A inh, leptin + MC + AKT inh, and leptin + PP2A inh + AKT inh. C and D: quantitative analysis of the number of immunoreactive cells for 3NT immunoreactivity

in various treated groups; y-axis shows colocalization events/100-cell unit (n = 3, analysis from 3 separate microscopic fields). *P < 0.05. Results were expressed as means ± SE.

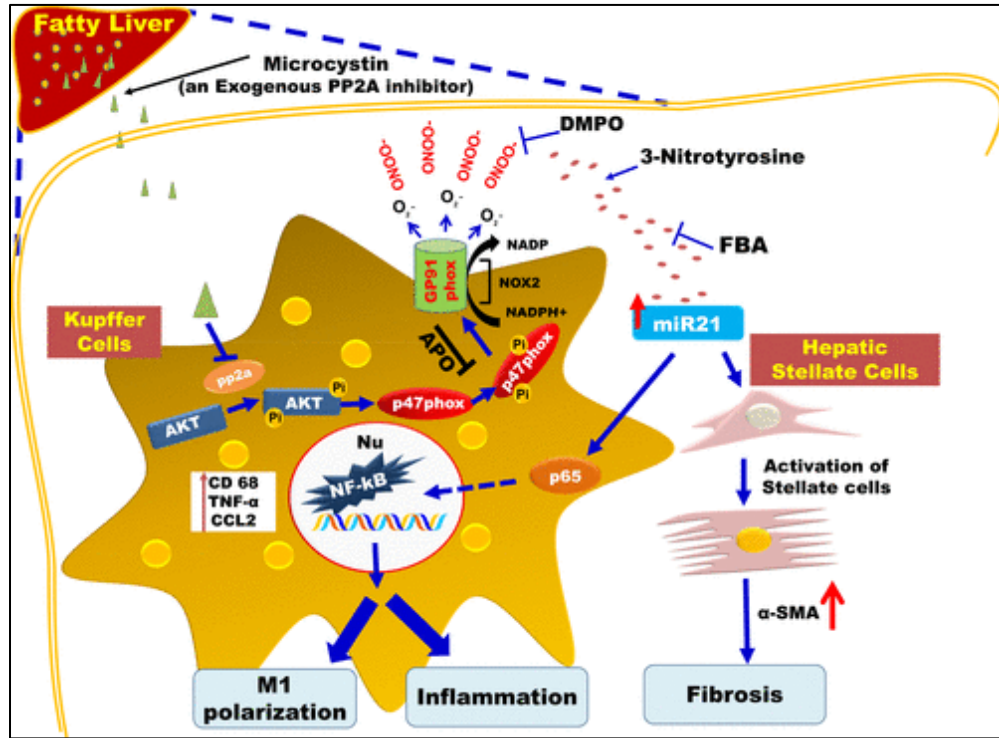


Figure 2.13. Mechanism of protein phosphatase 2A (PP2A) inhibition-induced nonalcoholic fatty liver disease (NAFLD) pathology. Graphical representation showing upregulation of miR21 via NADPH oxidase 2 (NOX2) activation by exogenous PP2A inhibitor (microcystin) in Kupffer cells, leading to transcriptional upregulation of inflammatory cytokines, M1 polarization, and fibrosis in NAFLD liver. α -SMA, α -smooth muscle actin; Apo, apocynin; FBA, phenyl boronic acid.

CHAPTER 3

EXOGENOUS PP2A INHIBITOR IN NAFLD CAN LEAD TO PYROPTOSIS AS WELL AS HEDGEHOG SIGNALING PATHWAY ACTIVATION VIA NOX2-DEPENDENT ACTIVATION OF MIR21²

² Albadrani M, Seth RK, Sarkar S, Kimono D, Mondal A, Bose D, Porter DE, Scott GI, Brooks B, Raychoudhury S, Nagarkatti M, Nagarkatti P, Jule Y, Diehl AM, Chatterjee S. Exogenous PP2A inhibitor in NAFLD can lead to pyroptosis as well as hedgehog signaling pathway activation via Nox2-dependent activation of Mir21. To be submitted.

Running title: Activation of Hedgehog Signaling Pathway and Pyroptosis Via NOX2 Pathway.

Key words: leptin; microcystin; miR21; NADPH; NAFLD; NOX-2; oxidative stress; PP2A inhibitor; siRNA; pyroptosis; hedgehog signaling pathway

Author for correspondence:

*Dr. Saurabh Chatterjee, Ph.D. Environmental Health and Disease Laboratory, Department of Environmental Health Sciences, University of South Carolina, Columbia 29208 USA. Email: schatt@mailbox.sc.edu; Tel: 803-777-8120; Fax: 803-777-3391.

Grant Support: This work has been supported by National Institutes of Health Awards 2-P20-GM-103641-06, 1-P01-ES-028942-01, and P01-AT-003961 to S. Chatterjee; 1-P01-ES-028942-01 to D. Porter and G. I. Scott; and P01-AT-003961, P20-GM-103641, R01-AT-006888, R01-ES-019313, R01-MH-094755, and Veterans Association Merit Award BX001357 to M. Nagarkatti and P. S. Nagarkatti.

Abstract:

Chronic Microcystin-LR exposure can cause serious liver injury. Liver injury can have multiple outcomes that can be studied in molecular pathology. One of them is a pyroptosis, which is a type of different types of cell death mechanisms. It is a result of releasing caspase 1 and its activation. Gasdermine D is a prevalent marker for pyroptosis. The second outcome is HH-signaling network's deregulation that may contribute to the pathogenesis and sequelae of liver damage resulting from metabolic syndrome. We in the previous study showed that MC-LR toxicity was be involved in the PP2A signaling

pathway and various cellular activities. The purpose of the present study was to investigate the impact of microcystin on hepatic pyroptosis as well as on hepatic fibrosis in vitro. Combined immunofluorescence imaging of transmembrane proteins E-Cadherin and GSDMD showed significant enhanced colocalization events in cells that is primed with leptin and exposed to MC as compared with the other groups especially the pharmacologically inhibited one. In addition, inhibitors which are added to leptin primed MC exposed stellate cell showed significant decreased in Gli1, PTCH1, IHH, SHH gene expression. Thus, increased pyroptosis as well as activate profibrotic hedgehog signaling pathway and activated stellate cells happened via NOX2 mediated ROS.

3.1 INTRODUCTION

Microcystin is known as a potent liver toxin that is available in pond waters that have the blue-green alga such as *Microcystis aeruginosa* [44]. The major determining factor of microcystin hepatotoxicity has the ability to accumulate in liver cells through mechanisms that facilitate its uptake [51]. OATP transporter family have been proven in research that they are responsible for the liver uptake as it shows that *Oatp1b2*-null mice has absence of the liver toxicity after being exposed to microcystin [46, 86]. The main mechanism of microcystin toxicity is by Protein phosphatase 2A (PP2A) inhibition [51]. We have shown that Microcystin is exacerbating NASH in NAFLD condition [87].

Nonalcoholic steatohepatitis (NASH) is a hepatic form of metabolic syndrome that is a result of the most widely known model of "two-hits" or "multiple-hits" hypothesis [12, 88]. It is started with long term liver fat accumulation, which is resulting in the primary hit. The main impact of asymptomatic primary hit is that it makes the liver more susceptible to

secondary hits that came as a result of exposure to an environmental toxin that causes additional stress, such as oxidative stress, as well as subsequent lipid peroxidation [6, 11, 89]. This will be followed by release of proinflammatory cytokines, and adipokines that cause the inflammation as well as fibrosis. Cellular death is associated with NASH conditions as a result of release of proinflammatory cytokines as well as the oxidative stress [90].

Eukaryotic cells are vulnerable to cell death in NASH condition where the loss of demarcation of cell margins and organelles can be seen microscopically happening in the intact tissue [90]. In eukaryotic cells, a wide range of cell death mechanisms has been shown by many researchers using molecular pathology markers. There are many mechanisms for cellular deaths such as apoptosis, necrosis, and pyroptosis [91]. One of these mechanisms is pyroptosis, which is a distinctive type of programmed cell death that is dependent on Caspase 1 activation, and it is characterized by release of pro-inflammatory cytokines such as of IL-1 β and IL-18, as well as cellular swell, burst and death [92].

There is a usual association between NASH pathophysiology and fibrosis particularly on its late stage as is shown by different research in molecular pathology of NAFLD [93-95]. Hepatic fibrosis is strongly associated with the aggregation of extracellular matrix (ECM) proteins in the liver parenchyma, primarily type I collagen, which is a characteristic in many chronic liver pathologies. This happens in liver as a response to wound-healing in chronic liver injury. The primary collagen-producing cells in the liver parenchyma were recognized as hepatic stellate cells (HSCs) [96]. We have already shown that Microcystin is causing activation of hepatic stellate cells (HSCs) [87]. This step is a crucial cellular event in a hepatic fibrosis [97]. It has been known that

Hedgehog signaling pathway can contribute considerably to liver fibrosis as well as in the process of activation of HSC [98].

The purpose of the present study was to investigate the impact of Microcystin as PP2 inhibitor to induce pyrrtosis as well as on hepatic fibrosis in vitro assessment.

3.2 MATERIALS AND METHODS

Materials:

Specific chemicals such as Microcystin-LR was purchased from Cayman (Ann Arbor, MI), and Leptin was purchased from BioVision (Milpitas, CA). Anti-E Cadherin primary antibody was purchased from Abcam (Cambridge, MA). Anti-Gasdermin D also was purchased from Santacruz Biotechnology (Dallas, TX). Fluorescence conjugated (Alexa fluor) secondary antibodies that used based on primary antibodies as well as ProLong Gold antifade mounting media with DAPI were bought from Thermo Fisher Scientific (Waltham, MA). miR21 inhibitor was bought from Qiagen (Valencia, CA). Phenyl Boronic Acid (FBA) and the spin trap 5,5 dimethyl-1- pyrroline N-oxide DMPO were bought from Alexis biochemical (San Diego, CA) All other chemicals not specified above were analytical grade and bought from Sigma Chemical Company.

Kupffer Cell Culture and Treatments

Immortalized rat Kupffer cell line (SV40) has been grown and cultured as described in the chapter 2. The cells were either kept without treatment (control) or treated with either leptin (100ng/ml), MC-LR (20 μ M), or leptin followed with MC-LR at the same doses. Certain cell groups have been incubated with pharmacological inhibitor first such as

Apocynin (100 μ M) , Phenyl Boronic Acid (FBA) (100 μ M) , (100 mM) the spin trap 5,5 dimethyl-1- pyrroline N-oxide DMPO , or (20 μ M) miR21 inhibitor. Then, followed by incubation with leptin, and microcystin at the same doses. All cells groups immediately after 24 hours incubation period were then plated on coverslips MatTek Corp, (Ashland, MA) for immunofluorescence staining according to our lab protocol that specified in chapter 2. Cells were incubated specifically with primary antibodies anti- Gasdermin D, and anti- E Cadherin, Then, cells groups followed by species-specific Alexa Fluor 633 and 488 in order to show the colocalization events. The stained cells attached on the coverslips were mounted on slides with ProLong Gold antifade reagent with DAPI (Life Technologies) and viewed under 60X oil magnification with an Olympus BX51 microscope.

Stellate Cells Culture and Treatments:

Immortalized rat hepatic stellate cell line (8B) kindly provided to us by Dr. Anna Mae Diehl (Duke-Gastroenterology), were cultured as described in the chapter 2. The cells were then treated the same way regarding to groups and treatment as Kupffer cells. Then immediately after treatments has completed, the cells were lysed in Trizol for mRNA extraction. mRNA levels of gene expression of Immortalized rat hepatic stellate cell line (8B) were measured using our standard laboratory protocol by using quantitative real-time reverse transcription-polymerase chain reaction (qRT-PCR). The primers used for Real-time PCR in 5' to 3' orientations are table 3.1.

Table 3.1. Primer sequences for the different target genes.

<i>Gene</i>	<i>Primer sequence</i>
Gli 1 (Rat)	Sense: AACTCCACGAGCACACAGG Antisense: GCTCAGGTTTCTCCTCTCTC
Shh (Rat)	Sense: CTGGCCAGATGTTTTCTGGT Antisense: TAAAGGGGTCAGCTTTTTTGG
IHH (Rat)	Sense: CCCTCGTCTTGGTGTAGAG Antisense: GAATCGCAGTCAGAGCTAGC
PTCH 1 (Rat)	Sense: CCTCTTGATGTGGCCCTTGT Antisense: GGCAGCCCTATCCTCATTCC

Statistical Analyses:

All cellular studies in vitro have been repeated at least three times ($n = 3$). The statistical analysis was carried out by unpaired t -test and ANOVA. For all analyses, $P < 0.05$ was considered statistically significant.

3.3 RESULTS

Microcystin induces Pyroptosis via NOX2-miR21 dependent pathway

Pyroptosis is a novel caspase-1 dependent lytic cell death process mediated by formation of inflammasome complex [99]. Previous studies suggest that NOX dependent

ROS and NF- κ B activation modulate inflammasome formation and subsequent pyroptosis [100]. Recently, pyroptosis defined as gasdermin D (GSDMD)-mediated programmed necrosis since GSDMD represent a substrate for both caspase-1 and caspase-11/4/5 which are mediators of pyroptosis [101]. Next, we investigated whether MC induced NOX2-miR21-Nf- κ B pathway activate GSDMD mediated pyroptosis in NASH. Dual immunofluorescence imaging of transmembrane protein E-Cadherin and GSDMD showed significant increased colocalization events in leptin primed cells exposed with MC as compared with vehicle control, leptin or MC treated cells (Fig.3.1, A,B). Interestingly, leptin primed cell co-treated with MC and Apo, DMPO, FBA and miR21 inhibitor showed significant decreased in E-Cadherin-GSDMD colocalization event (Fig.3.1,A,B). Results suggest that the increased localization of GSDMD to the membrane causes membrane permeability and GSDMD mediated cell death, thus increased pyroptosis.

Microcystin induced NOX2 and ROS activate profibrogenic hedgehog signaling in hepatic stellate cells

Next, we investigated whether MC induced NOX2-miR21 axis or NOX2 mediators activate stellate cells, pro-fibrogenic hedgehog signaling pathway and subsequent fibrosis. Leptin primed hepatic stellate cell were exposed with MC and co-exposed with Apo, DMPO, FBA and miR21 inhibitor to test the role of NOX2 mediators or miR21 in liver fibrosis. Results suggest that activation of stellate cells is mediated by MC induced NOX2 and oxidative stress instead NOX2-miR21 axis. Further, to correlate MC induced activation of profibrotic hedgehog signaling pathway, the mRNA expression of Gli1 gene (a hedgehog transcription factor), Patched 1 (PTCH1), Indian hedgehog (IHH) and Sonic hedgehog (SHH) were analyzed. The leptin primed stellate

cells exposed with MC showed significant increase in Gli1, PTCH1, IHH, SHH gene expression as compared to control, leptin or MC alone groups (Fig. 11B-E). However, Apo, DMPO, FBA or miR21 treatment to leptin primed MC exposed stellate cell showed significant decreased in Gli1, PTCH1, IHH, SHH gene expression (Fig.3.2,B-E). Results suggest that NOX2 mediated ROS activate profibrotic hedgehog signaling pathway and activate stellate cells.

3.4 DISCUSSION

The present study builds on our findings which we have reported in chapter 2. We investigated the mechanisms by which chronic exposure to MC-LR causes liver injury through activation of NOX-2 , profibrogenic hedgehog signaling and pyroptosis in hepatic stellate cells and Kupffer cells, in NAFLD.

We found that there was enhanced concentrations of Gli1, patched (PTCH1) and sonic hedgehog ligand SHH, which are significant mediators of the hedgehog signaling pathway which other research group had earlier shown to play a prominent part in liver fibrogenesis [102-104]. Interestingly, all these increases in the genes of the hedgehog signaling pathway following microcystin exposure that are associated with progressive phases of NAFLD were decreased when NOX2 inhibitors ,miR21 inhibitor, or FBA , were applied. However, we have seen in hepatic stellate cell (HSC) culture that MC enhanced the activation as well as profibrogenic proliferation of HSCs, which may have been through enhanced hedgehog signaling pathway via NOX2 dependent pathway.

One of the main regulators among others which are responsible for the growth of humans is the Hedgehog signaling pathway. Essentially, it regulates the progress of furrow by induction of at least two signals. The downstream of the hedgehog signaling can behave

as a long-range signaling molecule on anterior unvarying cells and prompts the expression of Hairy [105]. The pathway is being studied by the field of molecular biology, as it is of equal importance throughout the development of embryos. Namely, the Hedgehog signaling is a pathway which passes to the cells of the embryo the necessary information for proper cell differentiation. Different parts of the embryo concentrate different amounts of Hedgehog signaling proteins. Moreover, it is discovered that the malfunctioning of Hedgehog signaling is correlated with diseases such as basal cell carcinoma [106]. Furthermore, in recent researches, it is found that Hedgehog signaling plays also a hallmark role in regulating as well as controlling adult stem cells which have the potential for maintaining and regenerating human tissues [107]. In addition, numerous pharmaceutical companies have begun developing drugs which specifically aim in targeting the Hedgehog signaling pathway, as it is found involved in the development of certain types of cancer [108]. In NAFLD, the activity of the hepatic Hedgehog signaling pathway is connected to the extent of the severity of hepatic injury and with the levels of metabolic syndrome clinical parameters, which are expected to be predictive of advanced liver disease. Thus, the upregulation of the hedgehog signaling pathway can perhaps add to the pathogenesis and liver injury sequelae. On top of that, the increased activity of the pathway is directly connected with histological features of liver injury such as portal inflammation, hepatocyte ballooning and fibrosis. That supports further the association between Hedgehog signaling and the damage of the liver [109]. As is known in NASH, Hedgehog-stimulated hepatic stellate cells gain a pro-fibrogenic phenotype, as they transdifferentiated from epithelial-to-mesenchymal until becoming myofibroblasts. Moreover, after they transform into

myofibroblasts, they gain the ability to release pro-inflammatory and chemotactic cytokines [102-104].

Using a cell culture model of NAFLD that was induced by leptin, we show that MC treatment could assemble Gasdermin D (GSDMD) with transmembrane protein E-Cadherin. Leptin treatment primed cells that were co-treated with MC and pharmacological inhibitors such as Apo, DMPO, FBA and miR21 showed a substantial decline in this assembly events. Since caspase 1 can also cleave Gasdermine D because of pyroptosis, this results in the translocation of the membrane where they polymerize and form membrane pores where it can be assembled with E-Cadherin [110]. Another result is the release of pro-inflammatory cytokines through these membrane pores. This can be showed as a distinct mechanism of PP2A-induced NOX-2 activation.

In summary, we conclude that exposure to exogenous PP2A inhibitor such as microcystin can result in increased pyroptosis in Kupffer cells and activation of profibrogenic hedgehog signaling in hepatic stellate cells. We also conclude that these events are both linked to activation of NOX2-miRNA21 dependent pathway.

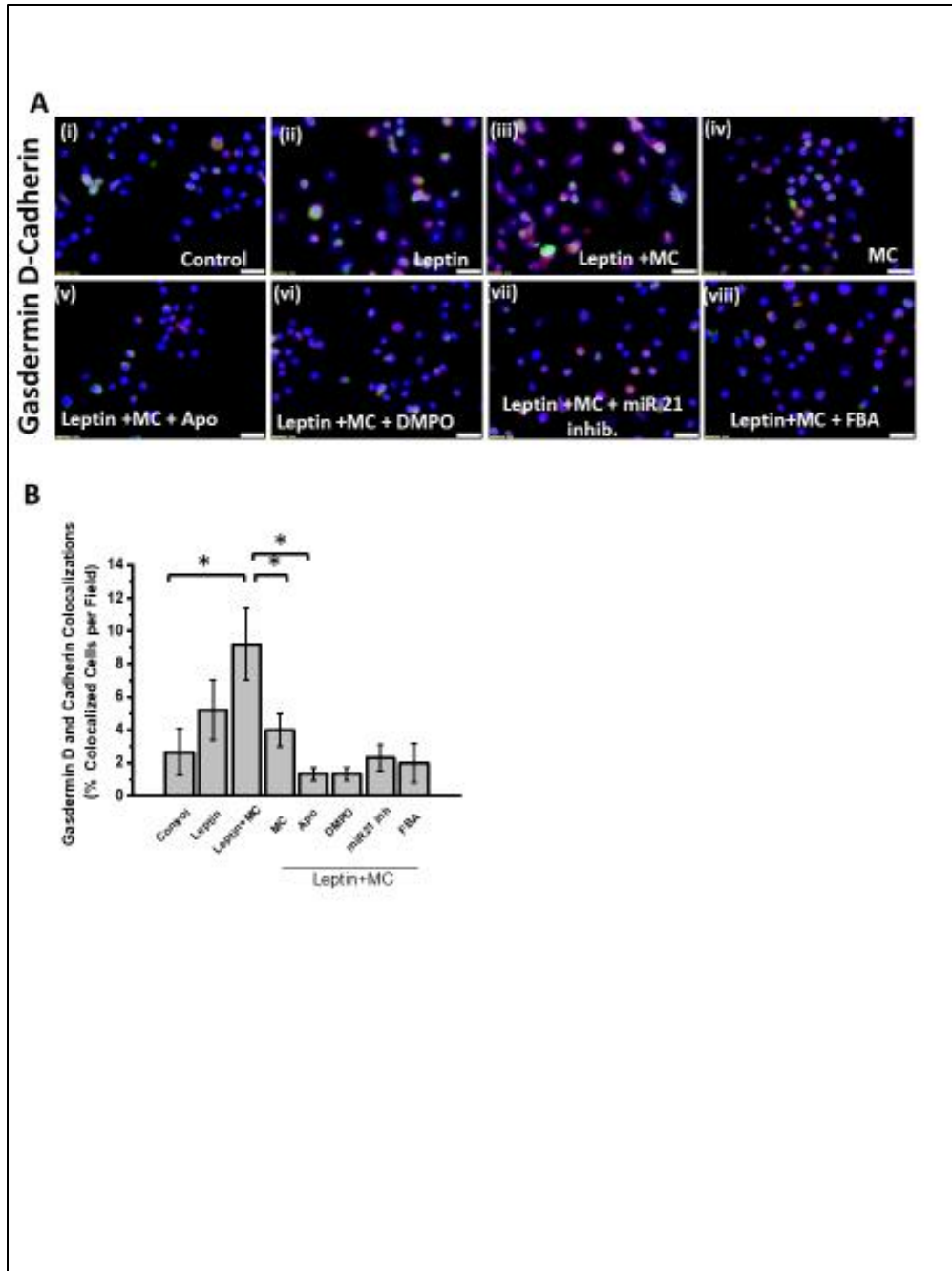


Figure 3.1. Exogenous PP2A inhibitor exposure induces pyroptosis in Kupffer cells. Immunoreactivity and morphometric analysis of Gasdermin D and E-cadherin expression in leptin-activated rat Kupffer cells. (A) Immunofluorescence images depicting Gasdermin D (GSDMD) (green) and Cadherin (red), colocalization (yellow), counterstained with DAPI (blue) in control, leptin, MC, leptin+MC, leptin+MC+apocynin, leptin+MC+DMPO, leptin+MC+miR21 inh. and leptin+MC+FBA groups of rat Kupffer cells. Images were taken at 60X magnification. (B) Quantification of the number of colocalized cells for Gasdermin D (GSDMD) and E-Cadherin

immunoreactivity, Y-axis shows colocalization events/100-cell unit (n=3, analysis from three separate microscopic fields). *p < 0.05. Results were expressed as mean ± SEM.

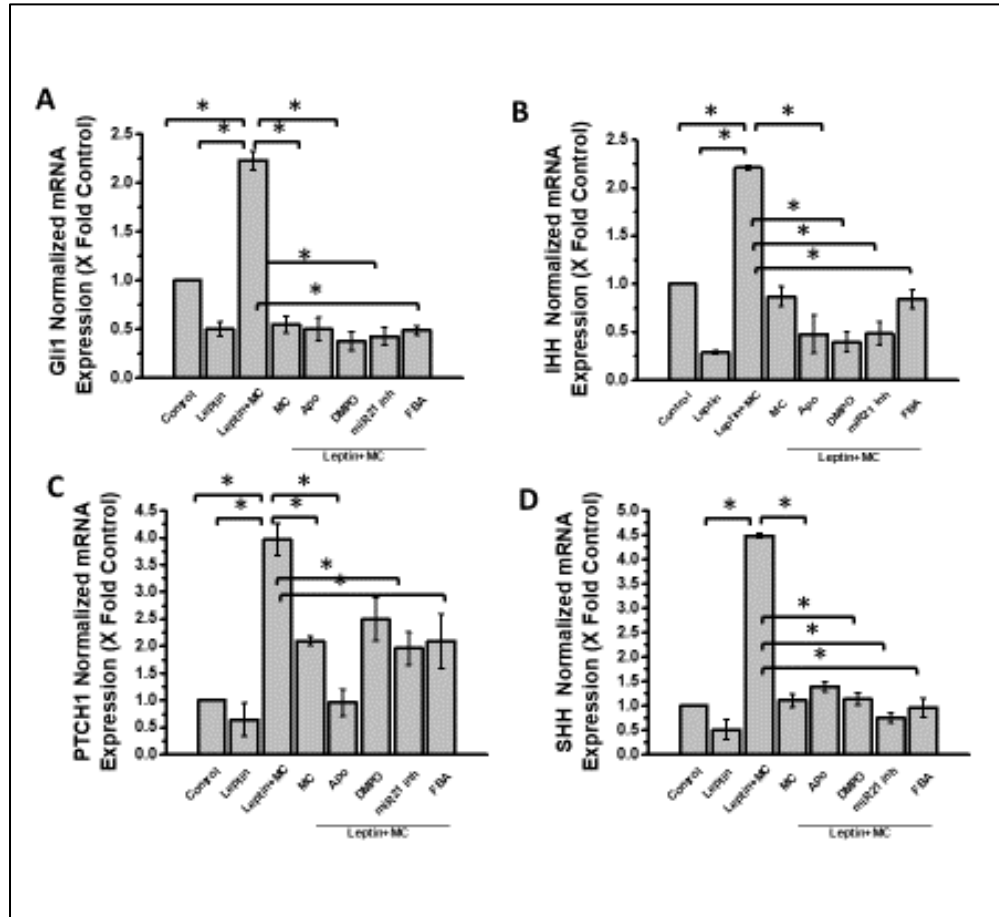


Figure 3.2. Exogenous PP2A inhibitor exposure activates profibrogenic hedgehog signaling in hepatic stellate cells via NOX2-miR21 axis. qRT-PCR analysis of mRNA expression of Gli1, PTCH1, IHH and SHH in leptin-activated rat hepatic stellate cells line. (A-D) qRT-PCR analysis of mRNA expression of Gli1, IHH, PTCH1, and SHH in various treated groups. *p < 0.05. Results were expressed as mean ± SEM.

CHAPTER 4

EARLY CHILDHOOD EXPOSURE AND PRIMING TO ALGAL TOXINS INDUCE MURINE ADULT HEPATIC INJURY FOLLOWING HIGH FAT DIET FEEDING VIA NLRP3 INFLAMMASOMES³

³ Albadrani M, Seth RK, Sarkar S, Kimono D, Mondal A, Bose D, Porter DE, Scott GI, Xiao S, Brooks B, Raychoudhury S, Nagarkatti M, Nagarkatti P, Chatterjee S. Early childhood exposure and priming to algal toxins induce murine adult hepatic injury following high fat diet feeding via NLRP3 inflammasomes. To be submitted.

Running title: Early Childhood Exposure to Mc Leads to Adult Hepatic Injury

Key words: microcystin; NLRP3; Livery injury; oxidative stress; PP2A inhibitor; Early Exposure

Author for correspondence:

*Dr. Saurabh Chatterjee, Ph.D. Environmental Health and Disease Laboratory, Department of Environmental Health Sciences, University of South Carolina, Columbia 29208 USA.
Email: schatt@mailbox.sc.edu; Tel: 803-777-8120; Fax: 803-777-3391.

Grant Support: This work has been supported by National Institutes of Health Awards 2-P20-GM-103641-06, 1-P01-ES-028942-01, and P01-AT-003961 to S. Chatterjee; 1-P01-ES-028942-01 to D. Porter and G. I. Scott; and P01-AT-003961, P20-GM-103641, R01-AT-006888, R01-ES-019313, R01-MH-094755, and Veterans Association Merit Award BX001357 to M. Nagarkatti and P. S. Nagarkatti.

Abstract:

Evidence is strong for early childhood exposure effects individuals with physical , biological , chemical , or psychological stimuli. Results from American Academy of Pediatrics show that infants and children are at risk for early exposure to microcystin. Notably, infants and children are known to consume more water relative to their body weight when compared to adults and thus are at increased risk of water borne exposures to environmental contaminants. The present report tests the hypothesis that early childhood exposure to microcystin (MC), a PP2A inhibitor and a principal component of harmful algal blooms activate Kupffer cells and hepatic stellate cells, which are considered to be

crucial mediators in hepatic fibrogenesis in an underlying condition of NAFLD. Mice exposed to subchronic doses of microcystin-LR (MC-LR) for two weeks immediately after the end of weaning and with a parallel high fat diet co-exposure showed classical symptoms of early NAFLD linked inflammation. Cytokines and chemokines such as CD68, IL1 β , MCP-1, and TNF- α , as well as α -SMA, hallmarks of NAFLD-linked inflammation were increased in the groups that were exposed to microcystin with high fat diet compared to the vehicle group. Also, NLRP3 KO mice showed significant decrease in the inflammation suggesting a decisive role of NLRP3 linked inflammasome activation and increased inflammation in these mice. The same trends were observed for liver injury biomarker IL-1 β , indicating a worsening outcome in liver health. Clinically, serum alanine aminotransferase (ALT) levels were significantly higher in the group that was primed to Microcystin followed by high fat feeding when compared to controls. The results suggest that toddlers and children might be at a greater risk of microcystin exposure and subsequent liver damage since data generated in mice models are highly translatable to humans. The results also bode well to strong clinical data that suggest increased incidences of NAFLD and NASH cases in children and juveniles in the US and around the developed world.

4.1 INTRODUCTION

Algae as well as cyanobacteria are detected in all types of aquatic environments. It has been published on a large number of studies that the presence of microcystins in surface waters that found worldwide [111]. Microcystins poses a strong risk to human health through drinking water. Drinking water has been reported to be contaminated by microcystin in many regions of harmful algal bloom [112-115]. For instance, there was an event of contamination of drinking water with *Microcystis* toxins in Caruarù, Brazil. This

was the first serious outbreak that was reported to cause symptoms of hepatotoxicity in humans as similar to what has been seen in laboratory studies. These data that came from dialysis center gave proof that microcystins are also potent inhibitors of Protein phosphatase 2A (PP2A) enzymes in humans [116, 117].

Early childhood exposure has the potential to have long-life effects on individuals exposed to physical, biological, chemical, or psychological stimuli. According to the American Academy of Pediatrics, infants and children are at elevated risk for early exposure to microcystin, a constituent of harmful algal blooms. Infants and children have been known to consume more water relative to their body weight when compared to adults and thus can incur higher risks to exposure from water-borne toxins such as microcystin. For example, the mean intake for water in infants and children are around 43 and 35 ml/kg/day, respectively. These values decrease when children are in their teen and adult ages, where they have the mean water intake of 18 and 19 ml/kg/day, respectively [118]. Also, children may be at the risk from exposure to coastal blooms from recreating near ponds and beach shores.

Several studies have also established that the tissues and organs of the body undergo fast development during fetal life as well as early infancy, during which any sort of toxic insult can have significant impacts [119, 120]. From progenitor cells stage, in fetus liver grows into a well-differentiated organ in which bile secretion can be started through 12 weeks gestation. It requires up to two years to reach full maturity after birth, in order to perform complete liver function [121].

We have reported in our studies that the activation of NLRP3-inflammasome in dysbiosis associated with NAFLD conditions following microcystin exposure [122]. NLRP3 inflammasome is a multiprotein complex that resides inside the cell structure [123]. It has different parts like the cytoplasmic receptor NLRP3 or also known as inflammasome sensor molecule, the adaptor protein caspase-recruitment domain ASC and the effector protein pro-caspase 1. Upon activation, their parts are assembled together yielding several pro-caspase sub-units close to each other. This pro-caspase 1 when close together within cytosolic multimolecular complexes, they cleave themselves in order to release the mature or active form, caspase 1. The activated caspase-1 further cleaves the , pro-IL-1 β as well as proIL-18 into their mature interleukin forms IL-1 β and IL-18 to be released into the system [92, 124-126].

In the present study, we used a juvenile mice model primed them with microcystin and fed them on high fat diet in order to investigate the role of early microcystin exposure in DIO model. We have chosen to investigate mechanistically whether early microcystin exposure triggered the NLRP3 inflammasome activation and intensified livery injury outcomes.

2.2 MATERIALS AND METHODS

Materials

All other chemicals needed for this study were of analytical grade and were purchased from Sigma Chemical Company unless indicated otherwise. From Cayman (Ann Arbor, MI), Microcystin-LR was purchased (Ann Arbor, MI). From The Jackson Laboratories (Bar Harbor, ME) ,wild-type and gene-specific knockout (KO) mice

including NLRP3 knock out mice were purchased. From Research Diets (New Brunswick, NJ), the animal diet specifically high-fat (60% KCal) (HFD) diet were purchased. From Abcam (Cambridge, MA), primary antibodies such as anti-CD68, anti- α -SMA, anti-3 nitrotyrosine (3NT), anti-IL-1 β , anti- GP91 phox, anti-P47phox, and anti- α SMA were purchased. Anti-NLRP3 and anti-ASC2 were purchased from Santacruz Biotechnology (Dallas, TX). From Abclonal (Woburn, MA), anti-IL18 antibody was purchased. From Vector Laboratories (Vectastain Elite ABC kit, Burlingame, CA), we purchased Species-specific biotinylated conjugated secondary antibody and streptavidin-horseradish peroxidase. From Thermo Fisher Scientific (Waltham, MA), fluorescence conjugated (Alexa fluor) secondary antibodies as well as ProLong Gold antifade mounting media with DAPI were bought. From IHC world (Woodstock, MD), NovaUltra Special Stain Kits were purchased. At AML laboratories (Baltimore, MD), paraffin embedding of the liver tissue sections on slides were performed.

Mouse model

Experimental Models Used:

Pathogen-free, Juvenile, male mice with C57BL/6J background (Jackson Laboratories, Bar Harbor, ME) will be used in the study. At the age of 4 weeks, they have been administered with vehicle (ethanol then dissolved in PBS), or microcystin-LR (MC-LR) (10 μ /kg, 5 dosages per week), through the intraperitoneal route for two weeks before starting in diet regime or euthanized . A group of injected mice were fed with a high-fat (60% KCal) (HFD) diet, (Research diets, New Brunswick, NJ) for 4 weeks and used as a model of diet-induced obesity (DIO+MC model) until the feeding is over and they are euthanized. Also, another group of mice were fed with a Chow diet (Lean MC model).

Also, mice with vehicle were fed the regular chow diet (Lean Control model). Another set of mice have not been injected with MC-RL were fed the HFD and used as (DIO model) in this study. An additional set of NLRP3 KO mice at the age of 4 weeks, they have been administered with microcystin-LR (MC-LR) at same dose. Then they had fed with HFD until the feeding is over and they were euthanized. All mice will be housed with 3-5 mice/cage at 23–24°C on a 12:12-h light-dark cycle with libitum access to food and water. The complete amount of mice in each group was evaluated on the basis of calculations that provided sufficient statistical power of 0.5. All animals have been treated in strict accordance with the NIH Guide for the Humane Care and Use of Laboratory Animals, and the experiments will be approved by the institutional review board at the University of South Carolina at Columbia. Mice had been euthanized at the completion of the diet regime or after priming and serum and liver tissue collected for further processing. Liver tissue sections from each mouse after euthanized were collected and fixed in 10% neutral buffered formalin.

Histopathology:

Sections of liver tissue from each mouse after were collected and fixed in 10% neutral buffered formalin. These Formalin-Fixed Paraffin-Embedded (FFPE) liver tissues were cut into 5-m thick sections. For histological examinations, liver sections slides were deparaffinized using standard protocol and stained with hematoxylin and eosin (H&E) and Picro-Sirius red using NovaUltra Special Stain Kits following manufacturer's protocol (IHC world, Woodstock, MD) and then observed under the light microscope using 20x objectives.

Serum ALT Measurements:

Serum alanine aminotransferase (ALT) levels were quantified and measured using an automated analyzer at the University of Georgia Clinical pathology core facility.

Immunohistochemistry:

Using standard protocol , formalin-fixed, paraffin-embedded liver tissue sections (5- μm thick) from all the mice groups were deparaffinized and subjected to antigen retrieval. The primary antibodies CD68, 3-nitrotyrosine , and TGF- β are used at recommended dilutions. The rest of the experiment was explained in details in chapter 2. Sections were finally observed under a 20X objective using an Olympus BX51 microscope (Olympus, America).

Immunofluorescence Microscopy:

Using standard protocol , formalin-fixed, paraffin-embedded liver tissue sections (5- μm thick) from all the mice groups were deparaffinized and subjected to antigen retrieval. The primary antibodies α -SMA, NLRP3,ASC2, IL-1 β , IL-18 are used at recommended dilutions. Species-specific anti-IgG secondary antibodies conjugated with Alexa Fluor 488 and Alexa Fluor 633 (Invitrogen, California, USA) ,were used against the appropriate primary antibodies. The rest of the experiment was explained in details in chapter 2. Sections were finally observed under a 40X objective using an Olympus BX51 microscope (Olympus, America).

Quantitative Real-Time Polymerase Chain Reaction:

Gene expression for mRNA levels from juvenile mice liver tissue were measured by quantitative real-time reverse transcription-polymerase chain reaction (qRT-PCR) by following our routine laboratory protocol. The primers used for RT-PCR in 5' to 3' orientations are provided in Table 4.1.

Table 4.1. Primer sequences for the different target genes.

<i>Gene</i>	<i>Primer sequence</i>
CD68 (Mouse)	Forward: GCTACATGGCGGTGGAGTACAA Reverse: ATGATGAGAGGCAGCAAGATGG
MCP-1 (Mouse)	Forward: CACAGTTGCCGGCTGGAGCAT Reverse: GTAGCAGCAGGTGAGTGGGGC
TNF- α (Mouse)	Sense: CAACGCCCTCCTGGCCAACG Antisense: TCGGGGCAGCCTTGTCCTT
IL-1 β (Mouse)	Sense: CCTCGGCCAAGACAGGTCGC Antisense: TGCCCATCAGAGGCAAGGAGGA
TGF- β (Mouse)	Sense: CTCACCGCGACTCCTGCTGC Antisense: TCGGAGAGCGGGAACCCTCG
α -SMA (Mouse)	Sense: GGAGAAGCCCAGCCAGTCGC Antisense: ACCATTGTCGCACACCAGGGC
NLRP3 (Mouse)	Sense: GGTGACCTTGTGTGTGCTTG Antisense: ATGTCCTGAGCCATGGAAGC
ASC-2	Sense: GGACAGTACCAGGCAGTTCG

(Mouse)	Antisense: TTCTTGCAGGTCAGGTTCCA
IL-18	Sense: ACACCACAAAACCTCAGCCA
(Mouse)	Antisense: AGGGACTIONTGAACCAGAGCC

Statistical Analyses:

All mice experiments were repeated three times with at least 3 mice per group ($n = 3$; data from each group of 3 mice were pooled). Data were represented as mean \pm S.E. The graphs were plotted using GraphPad Software, Inc. The statistical analysis was carried out by unpaired t-test and ANOVA. For all analyses, $P < 0.05$ was considered statistically significant.

4.3 RESULTS

Early priming with microcystin will induces liver injury

To determine the effects of early priming exposure of MC-LR in mice immediately after weaning on liver parenchyma, liver histopathology as well as inflammatory markers were analyzed. The early primed MC-LR mice showed an increase in liver injury pathophysiology, as shown by increased infiltrating immune cells (early inflammation) when compared with lean mice that only exposed to vehicles (Fig. 4.1 A). Moreover, in order to investigate if early priming with MC-LR can induce activation for both Kupffer cells and hepatic stellate cells, immunoreactivities of Kupffer cell activation marker CD68, as well as hepatic stellate cell activation marker α -SMA, were analyzed in liver tissue slices. Results showed that there was a significant increase in CD68 immunoreactivity in

early primed mice with MC-LR as compared with Lean group of mice that primed with vehicle ($P < 0.001$) (Fig. 4.1, C, and F). These findings have been further confirmed at the mRNA levels of CD68 as well as the inflammatory markers. CD68 mRNA expression in mice that primed with MC has increased significantly when compared with Lean mice ($P = 0.008$) (Fig. 3.1, H). Moreover, in order to test that the activation of Kupffer cells took part in a proinflammatory phenotype, mRNA expression of proinflammatory cytokines such as monocyte-chemoattractant protein-1 (MCP-1), Interleukin 1 beta (IL-1 β), and tumor necrosis factor- α (TNF- α) were evaluated. The result showed that there was a significant increase in CCL2, IL-1 β and TNF- α mRNA expression in mice that primed with MC as compared with lean mice ($P < 0.001$, $P=0.005$, and $P < 0.001$, respectively) (Fig. 3.1, H). α -SMA immunoreactivity, a characteristic of stellate cell activation, then was significantly increased as well in early primed mice with MC-LR groups when compared with Lean mice group ($P < 0.001$) (Fig. 3.1, D and G). α -SMA mRNA expressions in mice that primed with MC-LR have increased significantly when compared with lean mice ($P < 0.001$) (Fig. 3.1, H). Furthermore, liver tissues also were analyzed next for fibrosis status by assessing picosirius red staining. The early primed MC mice liver showed significantly increased picosirius red staining reactivity as compared with Lean mice ($P < 0.001$) (Fig. 3.1, B and E). The above results thus suggested that an early MC exposure will induce early inflammation during the process of increased proinflammatory responses via MCP1, IL-1 β and TNF- α .

Early exposure to microcystin followed by HFD will exacerbate liver injury

We, as will other authors, have shown that toxins from the environmental exposure are acting as a second hit to intensify the progression of NAFLD from stage to advanced

one [6, 8]. We have also published that exogenous inhibitors of PP2A such as microcystin can worsen the pathophysiology of NAFLD [87]. To investigate the role of early exposure to MC-LR in induction of liver injury in DIO model, we used a low, chronic dose of MC-LR in mice immediately after weaning to induce liver injury, followed by feeding them HFD (DIO + MC). Results showed that DIO+MC group that shows the typical features of liver injury include increased infiltrating immune cells (inflammation), and hepatocytes ballooning when compared to with DIO control mice alone, lean mice exposed to MC, or lean mice (Fig. 4.2, A). Early exposure to microcystin also significantly elevated Serum ALT level in DIO+MC mice as compared to lean, lean mice exposed to MC and DIO only mice ($P<0.05$) (Fig. 4.2, M) . Moreover, analysis of picrosirius staining in the early exposure to microcystin followed by HFD (DIO+MC) mice group showed increased reactivity as compared to lean, lean mice exposed to MC and DIO only mice ($P<0.05$) (Fig. 4.2, B and F). CD68 immunoreactivity as well as mRNA levels is significantly increased in early exposure to microcystin followed by HFD mice group as compared to lean, lean mice exposed to MC and DIO only mice ($P<0.05$) (Fig. 4.2, C,G and J). This is indicative of Kupffer cell activation in early exposure to microcystin followed by HFD mice group as evidenced by significant increase in CD68. Mice early exposed to MC also showed increase mRNA expression of proinflammatory cytokines TNF- α , IL-1 β , and MCP1 as compared to the other groups ($P<0.05$) (Fig. 4.2, J). The above findings therefore indicated that proinflammatory responses via IL-1 β , MCP1 and TNF- α are induced by early MC exposure in DIO mice. To study the effect of early microcystin exposure in NAFLD in stellate cell proliferation, immunohistochemistry, and mRNA expression of stellate cell activation marker α -SMA were studied. TGF- β also is studied similarly as α -SMA because

it has been shown in different researches to be key for fibrogenesis in liver injury outcomes [57, 127]. α -SMA as well as TGF- β immunoreactivity and their mRNA expression levels were significantly increased in the early exposure to microcystin followed by HFD (DIO+MC) mice groups when compared with DIO mice, the lean + MC mice group or lean (P < 0.001) (Fig. 3.2, D,E,H,I ,K and L).

Early exposure to microcystin followed by HFD will induce hepatic oxidative stress

Oxidative stress is one of the most important pathogenic mechanisms associated with Liver injury [128, 129] . Evidence based research confirms that 3-Nitrotyrosine formation in vivo as well as in vitro occurs under various pathological conditions particularly in liver. 3-Nitrotyrosine (3-NT) is known to be a marker of peroxynitrite-mediated oxidative damage in the diseased liver [130, 131]. Results showed that the immunoreactivity of 3-nitrotyrosine as analyzed by immunohistochemistry in early exposure to microcystin followed by HFD (DIO+MC) mice groups was significantly increased compared to DIO mice, the lean + MC mice group or lean (Figure 4.3A and B)(P<0.05). This indicates that early exposure to microcystin has a clear role in the development of tyrosine radicals and tyrosine residue nitration in the high fat diet with early microcystin exposure group.

Liver injury after early microcystin exposure is associated with inflammasome activation

There are many studies indicating the role of NLRP3 inflammasome activation in different liver injuries as a major contributor to hepatocyte damage, activation of immune cells and hepatic inflammation [132-135] . Our group also has shown that microcystin can

mediate peroxynitrite species via NOX2 in inflammasome activation at intestinal inflammatory pathology [122]. To investigate whether early exposure to microcystin can result in inflammasome activation in the liver tissue, we measured mRNA expressions of the NLRP3 as well as ASC2 inflammasome sub-units. We also conducted colocalization events of both subunits for ASC2 and NLRP3 to demonstrate efficient assembly of the inflammasome complex. Results showed that there was an increase in mRNA expression levels for NLRP3 as well as ASC2 inflammasome subunits in the early exposed to microcystin with HFD mice (DIO+MC) compared to with DIO control mice alone, lean mice exposed to MC, or lean mice (Figure 4.4,A,B,C, and D) ($P<0.05$). However, Caspase1 mediated IL-1 β as well as IL-18 release is completely associated with NLRP3 inflammasome activation in Kupffer cells [92, 136]. To investigate whether early exposure to microcystin can result in release IL-1 β and IL-18 as a pro-inflammatory cytokines depends on inflammasome activation, we measured mRNA expression that were assessed by qRT-PCR and their immunoreactivity, which were assessed by immunofluorescence microscopy. Results showed that there was an increase in mRNA expression levels for IL-1 β and IL-18 genes in mice that have early exposure to microcystin followed with HFD (DIO+MC) as compared to with DIO control mice alone, lean mice exposed to MC, or lean mice (Figure 4.5, D and E) ($P<0.05$). Results also showed increased immunoreactivity of IL-1 β and IL-18 in early exposed to MC with HFD (DIO + MC) mice groups as compared with DIO control mice alone, lean mice exposed to MC, or lean mice (Figure 4.5, A,B and C) ($P<0.05$). Furthermore, to investigate the role NLRP3 inflammasome activation and subsequent liver injury outcomes going forward, we used NLRP3 gene-deleted mice (NLRP3 KO) early exposed to microcystin and fed them with a HFD. The

immunohistochemistry of 3NT, a marker of peroxynitrite-induced oxidative stress, as well as Kupffer cell activation marker CD68 were performed. Results showed that there was a significant increased immunoreactivity of 3NT in early exposed to MC with HFD (DIO + MC) mice when compared with DIO mice alone, whereas there was a significant reduction in NLRP3 KO mice groups that early exposed to MC ($P = 0.013$) (Fig.4.6, A and G). Results also showed increased immunoreactivity of CD68 in early exposed to MC with HFD (DIO + MC) mice groups as compared with DIO alone, whereas there was a significant decrease in NLRP3 KO mice groups that early exposed to MC ($P < 0.001$) (Fig.4.6, B and H). The mRNA expression of proinflammatory cytokines CD68, MCP1, and TNF- α showed a significant increase in early exposed to MC with HFD (DIO + MC) mice groups, whereas a decrease in NLRP3 KO mice groups that early exposed to MC was observed ($P < 0.001$) (Fig. 4.6, M). Moreover, the immunoreactivity of a cytokine known for its role in fibrosis (TGF β) using immunohistochemistry staining as well as the immunoreactivity of stellate cell activation marker (α -SMA) using immunofluorescence staining were performed. Results showed that there was a significant increased immunoreactivity of TGF- β as well as α -SMA in early exposed to MC with HFD (DIO + MC) mice when compared with DIO mice alone, whereas there was a significant reduction in NLRP3 KO mice groups that early exposed to MC ($P < 0.001$) (Fig.4.6, C,D,I and J). Similarly, the mRNA expression of TGF- β and α -SMA genes showed a significant increase in early exposed to MC with HFD (DIO + MC) mice groups, whereas a decrease in NLRP3 KO mice groups that early exposed to MC was observed ($P < 0.001$) (Fig.4.6, N). Caspase1 mediated IL-1 β as well as IL-18 release also is evaluated. Results also showed increased immunoreactivity of IL-1 β and IL-18 in early exposed to MC with HFD (DIO + MC) mice

groups as compared with DIO mice alone, whereas there was a significant reduction in NLRP3 KO mice groups that early exposed to MC ($P < 0.001$) (Fig.4.6, E,F,K and L). The mRNA expression of IL-1 β and IL-18 genes showed a significant increase in early exposed to MC with HFD (DIO + MC) mice groups, whereas a decrease in NLRP3 KO mice groups that early exposed to MC was observed ($P < 0.001$) (Fig.4.6, O). Together this data suggested that early microcystin exposure activated Kupffer as well as stellate cells, increased inflammation, and were NLRP3 inflammasome assembly dependent.

4.4 DISCUSSION

The present study reports the role of early microcystin exposure in exacerbating liver injury outcomes. Moreover, this study suggests the role of assembling the NLRP3 inflammasome complex in the progressing of liver injury. The findings reported in this study indicate that early MC-LR exposure induced increased inflammation, increased stellate cell activation, and early fibrosis starting. In addition, results showed that mice primed with subchronic doses of microcystin for two weeks immediately after their weaning followed by a high fat diet has increased serum ALT levels in comparison to the other groups. These are collectively considered classical signs for early NAFLD link inflammation. Using these mice models that are highly translatable to humans in generating the above data is suggesting that children and infants may be at risk of exposure to microcystin and subsequent hepatic injury, particularly if they are obese. These findings are connected to pediatric epidemiology data, as the NAFLD prevalence is increasing among children that are overweight in comparison to children who are not. This can have huge implications for them, causing NAFLD cases to advance to NASH. Our findings also assume relevance in clinical settings research using reports from Center for Disease

Control and Prevention, as it has been published that there are positive associations between obesity and progressions of chronic liver pathologies such as NASH.

It has been shown by using the pharmacological inhibitor for NLRP3 activation in a mouse model of NASH, that liver injury including liver inflammation and fibrosis processes have been reduced [137]. The same findings have been shown by using knockout mouse models. There are also many triggers such as lipotoxic lipids, like free fatty acid, and diacylglycerols for hepatic NLRP3 inflammasome activation in NASH [138]. Moreover, the conceptual “two hit” or “multi hit” paradigm can be applied here by using environmental contaminants such as early microcystin exposure in DIO mice models for activation of NLRP3 inflammasome. In our study, in order to understand the role of early exposure to the microcystin in liver injury at diet induced obesity mice , we studied the activation of NLRP3 inflammasome using proteins as well as mRNA expression for genes. NLRP3 inflammasome, if activated, will result in activation of pro-caspase1 and pro-IL-1 β . That in turn will be converted to IL-1 β , which is known to have a key role in NASH development within NAFLD spectrum [133]. Our findings of increased NLRP3 and ASC2 assembly using dual staining for colocalization proved the process of inflammasome activation following priming with microcystin in DIO models. Subsequent to inflammasome activation there are increases in markers of Kupffer cells activation (CD68) as well as stellate cell activation (α -SMA) while at the same time there were observed decreases of all the above markers in NLRP3 KO mice. IL1B as well as IL18 are also shown to be increased in their expression in mice primed with microcystin in DIO models , while their level of expressions is attenuated in NLRP3 KO mice.

It has been shown by our group that oxidative stress mediated by peroxynitrite generation plays a central role in activating Kupffer cells during early steatohepatic process in NASH [6]. We and others also have shown earlier that peroxynitrite generation in NAFLD creates a stable nitrated residue of tyrosine called 3-nitrotyrosine (3NT) protein [6, 54]. This protein is established as a biomarker for oxidative stress in liver injuries [130, 139]. Moreover, we published data that provided mechanistic cues in microcystin exposure that induced NASH pathology, wherein Kupffer cells could be the key cell site for the generation of NOX2-dependent ROS. In our study here, we found an increase at level of 3-NT in mice primed with microcystin in DIO models while also finding a decrease of this ROS marker in NLRP3 KO mice. This can give us a good evidence for the role of NLRP3 activation in ROS generation .

Our results showed significant increase in expression levels of α -SMA and TGF- β in mice primed with microcystin in DIO models , while their level of expressions is reduced in NLRP3 KO mice. The fibrosis also was analyzed by showing significant increased morphometry of picro sirius red in liver tissues slides of mice primed with microcystin in DIO models. This indicates that early exposure to microcystin can cause early fibrosis , which is considered a characteristic for early NAFLD-linked inflammation.

In summary, our results clearly assumed that early exposure to microcystin causes liver injury outcomes in high fat diet-induced obesity and is dependent on NLRP3 inflammasome activation. Drinking water or swimming in water sheds that have microcystin levels higher than EPA permissible limits particularly in childhood stage, might result in adult hepatic injury. Moreover, it can result in the development of metabolic syndrome including NASH if the individual has tendencies for obesity.

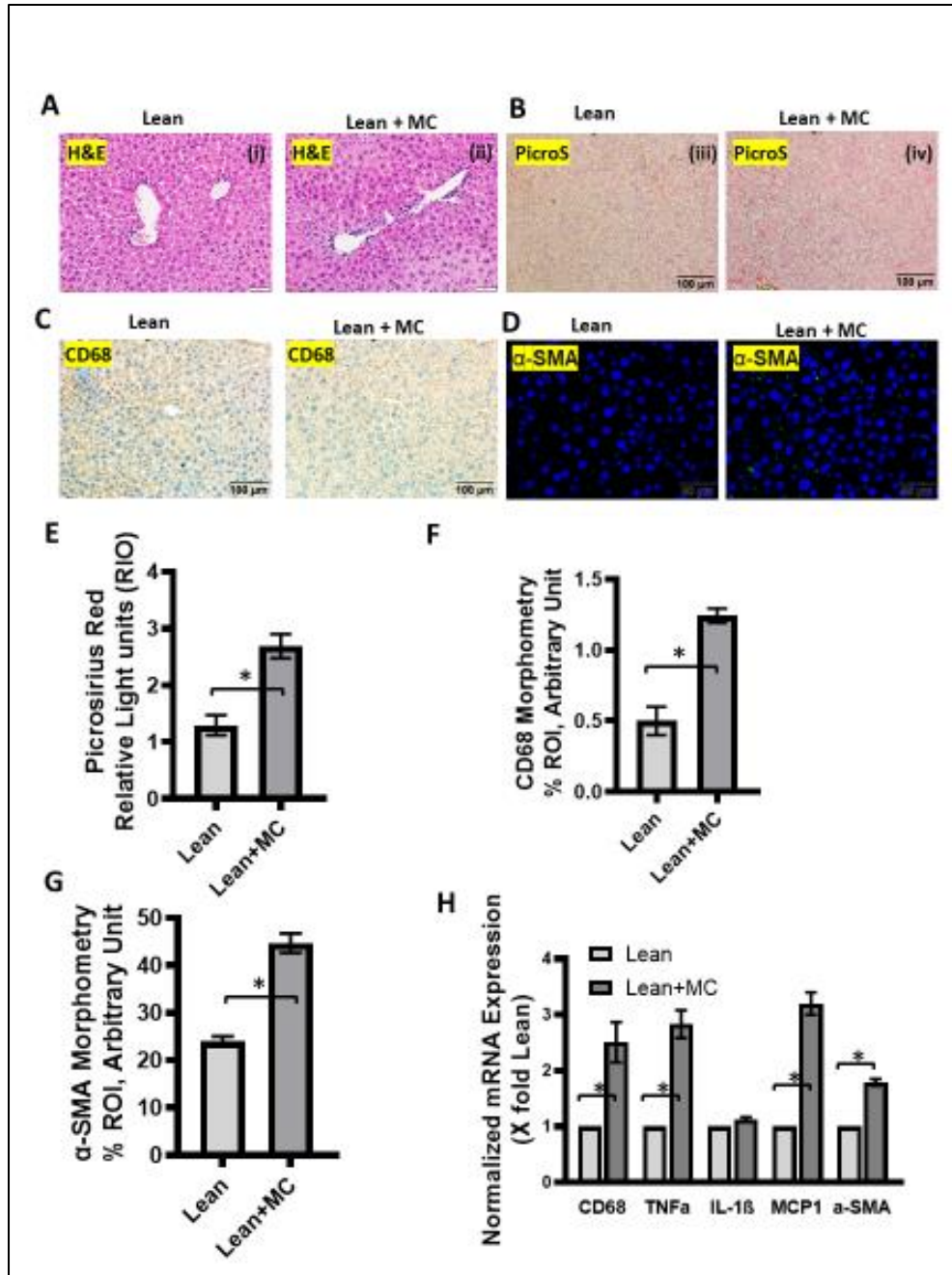
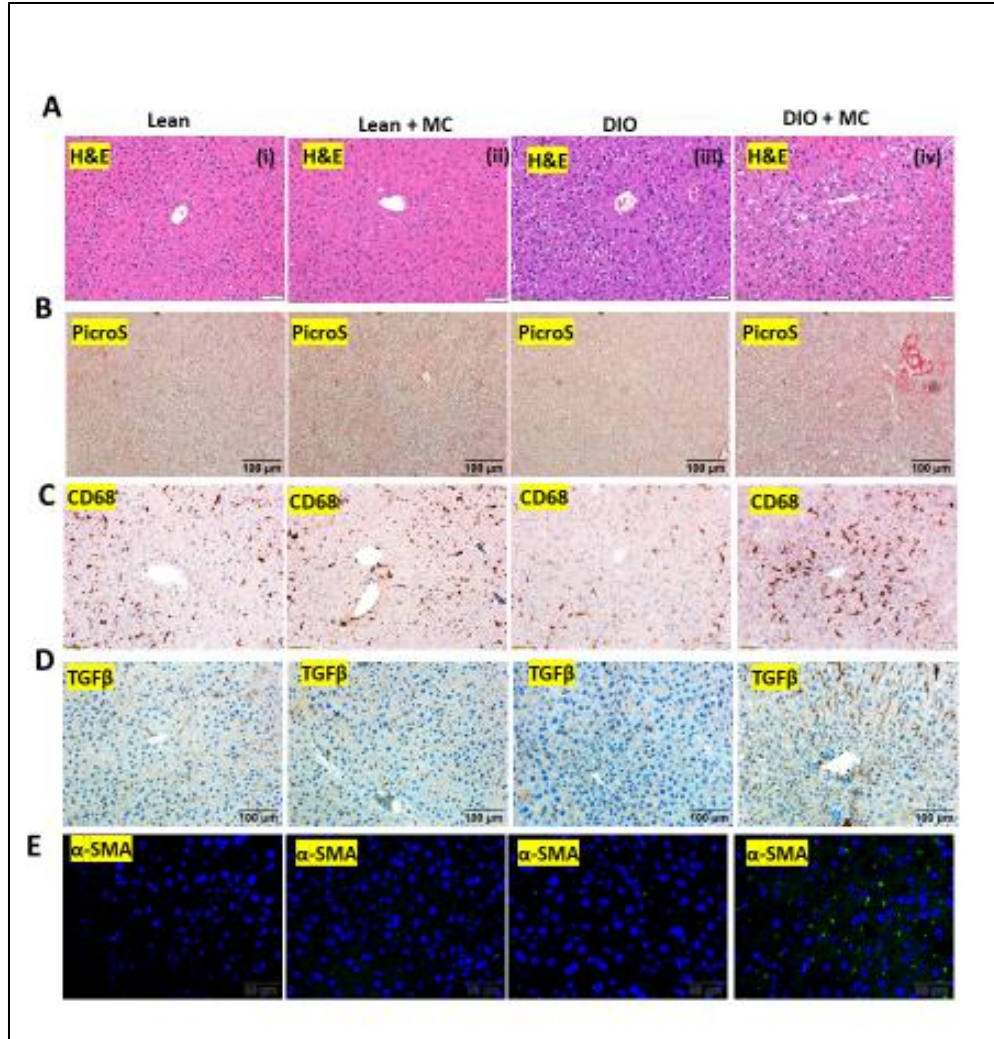
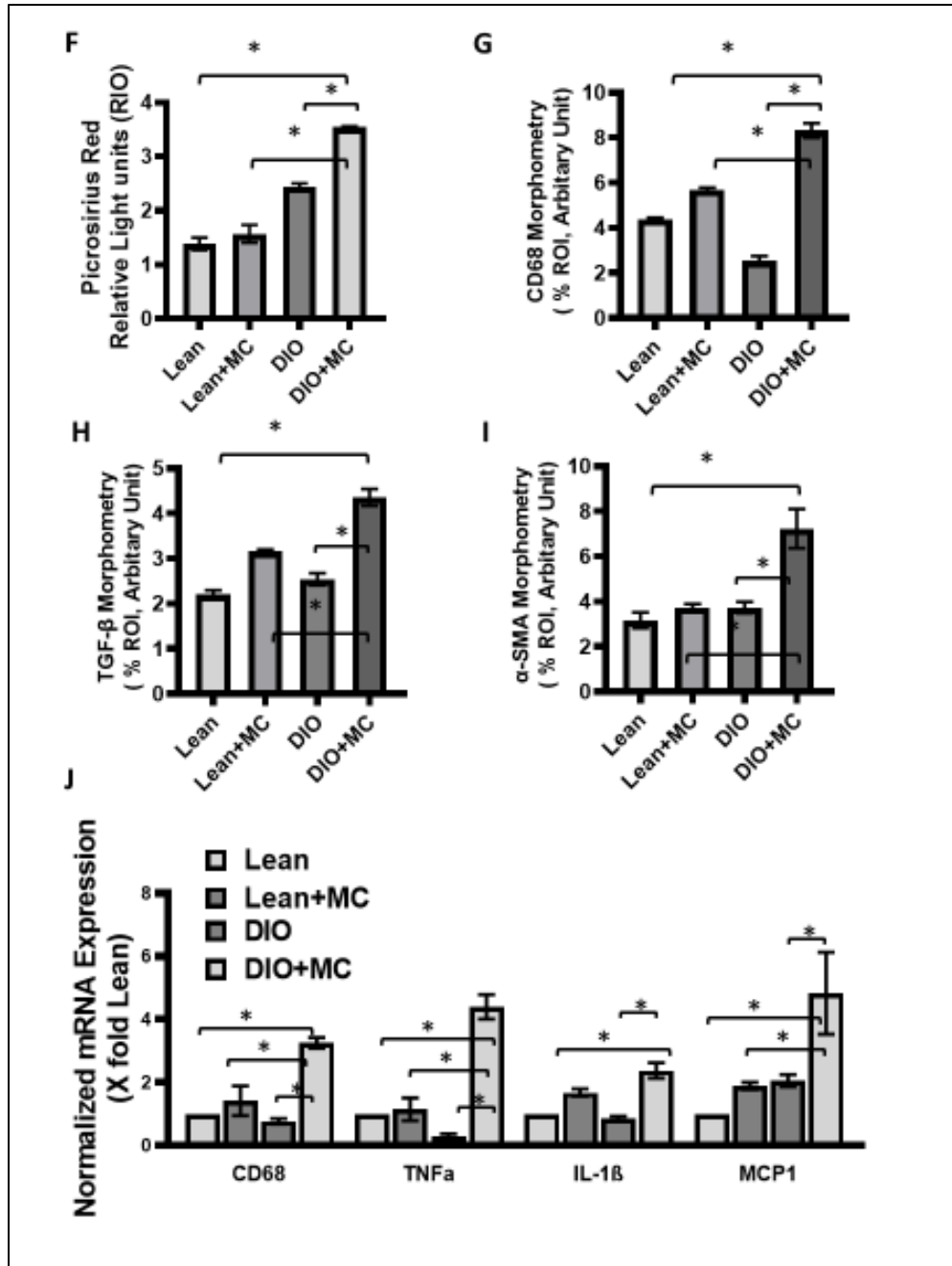


Figure 4.1. Early priming with microcystin for two weeks in juvenile mice liver induces liver injury. A: representative histological images of liver sections stained with hematoxylin-eosin (H&E), from lean mouse control and early primed with microcystin, MC (n = 3). B: representative histological images of the same groups of mice stained with picrosirius red (PicroS). C: Representative immunohistochemistry images of liver sections of the same groups of mice immunostained with CD68. Images were taken at $\times 20$ magnification. D: Representative immunofluorescence images of liver sections of the same groups of mice immunostained with α -SMA (green) counterstained with DAPI (blue). Images were taken at $\times 40$ magnification. Morphometric analysis of PicroS (E)

CD68 (F), and α -SMA (G) in lean mouse control and early primed with microcystin ,MC groups (n = 3/group). Morphometric analysis was expressed in percentage of positive immunoreactive area per regions of interest (ROIs) (3 ROIs/liver section). H: Quantitative RT-PCR analysis of mRNA expression of CD68, TNF- α , MCP1, IL-1 β , and α -SMA in lean, lean + MC livers. The mRNA expressions were normalized with 18s and presented as fold change of lean group. *P < 0.05. Results were expressed as means \pm SE.





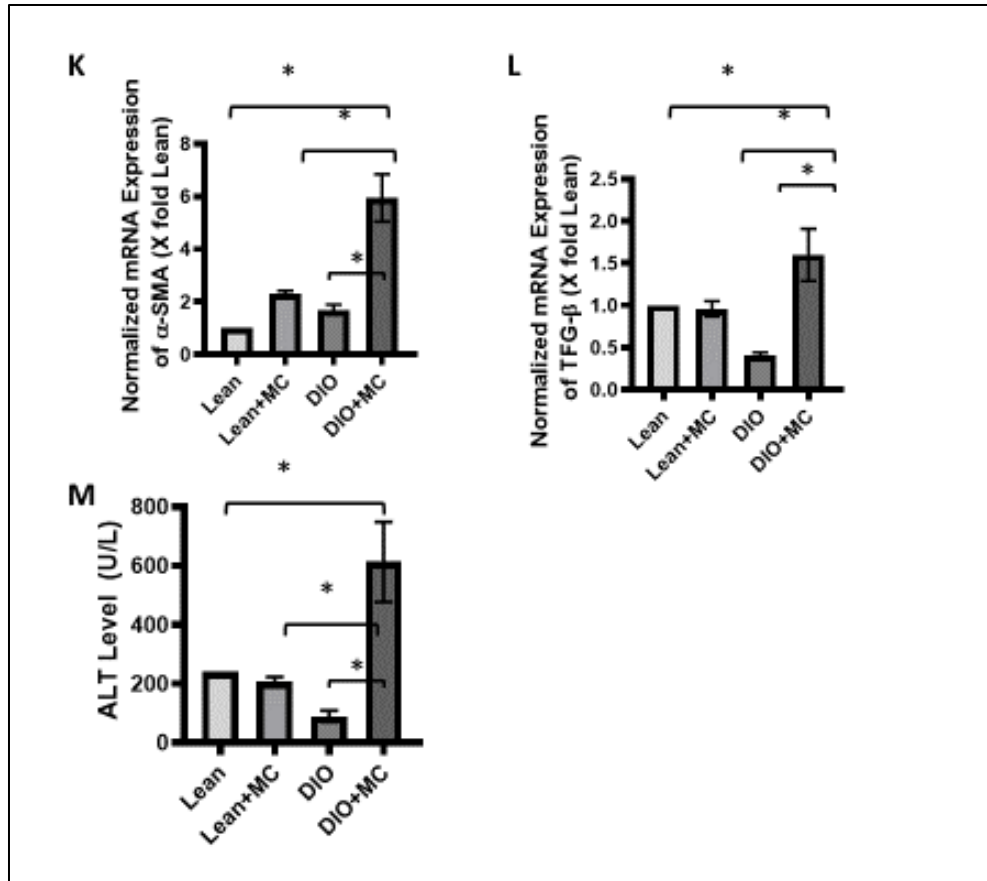


Figure 4.2. Early exposure to microcystin followed by HFD will exacerbate liver injury . A: representative histological images of liver sections stained with hematoxylin-eosin (H&E), from lean mouse control, early exposed to microcystin (MC),DIO and DIO+MC (n = 3). B: representative histological images of the same groups of mice stained with picosirius red (PicroS). Representative immunohistochemistry images of liver sections of the same groups of mice immunostained with CD68 (C), and TGF- β (D). Images were taken at $\times 20$ magnification. E: Representative immunofluorescence images of liver sections of the same groups of mice immunostained with α -SMA (green) counterstained with DAPI (blue). Images were taken at $\times 40$ magnification. Morphometric analysis of PicroS (F) CD68 (G),TGF β (H) and α -SMA (G) in lean mouse control and exposed to microcystin (MC),DIO,DIO+MC groups (n = 3/group). Morphometric analysis was expressed in percentage of positive immunoreactive area per regions of interest (ROIs) (3 ROIs/liver section). Quantitative RT-PCR analysis of mRNA expression of (J) CD68, TNF- α , MCP1, IL-1 β , (K) TGF- β , and α -SMA (L) in lean, lean + MC, DIO, and DIO+MC livers. The mRNA expressions were normalized with 18s and presented as fold change of lean group. M: quantification of serum alanine aminotransferase (ALT) level and comparison between lean mouse control and exposed to microcystin (MC),DIO,DIO+MC groups (n = 3/group). *P < 0.05. Results were expressed as means \pm SE.

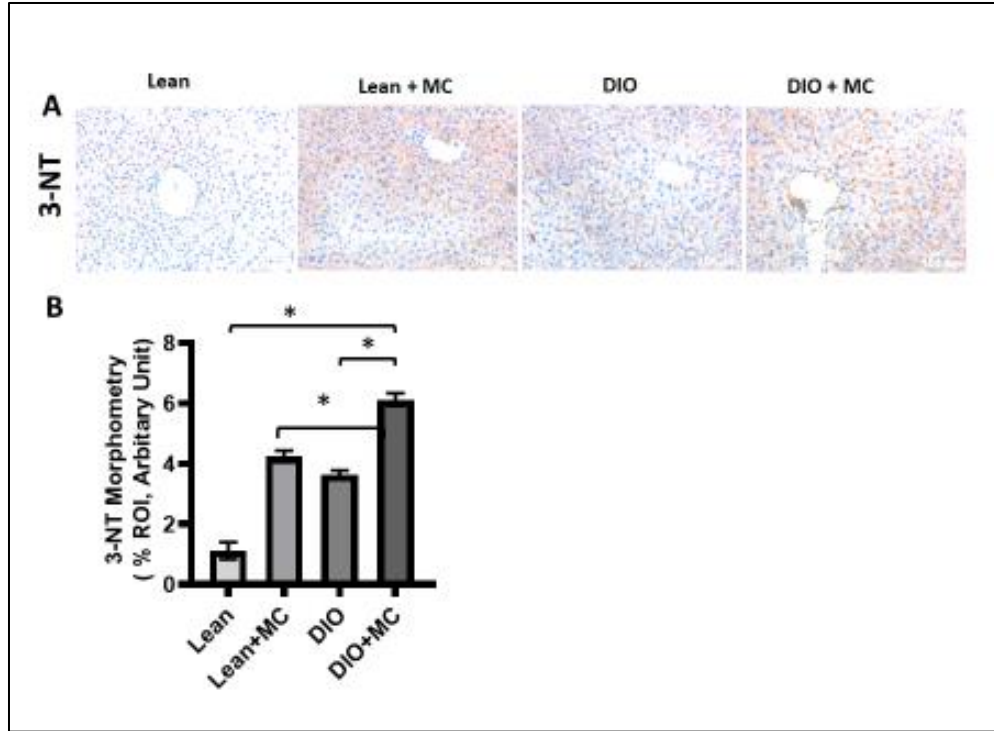


Figure 4.3. Early exposure to microcystin followed by HFD will induce hepatic oxidative stress. A: representative immunohistochemistry images of liver sections immunostained with 3-NT, from lean mouse control, early exposed to microcystin (MC), DIO and DIO+MC (n = 3). Images were taken at $\times 20$ magnification. B: Morphometric analysis of 3-NT in lean mouse control and exposed to microcystin (MC), DIO, DIO+MC groups (n = 3/group). Morphometric analysis was expressed in percentage of positive immunoreactive area per regions of interest (ROIs) (3 ROIs/liver section). * $P < 0.05$. Results were expressed as means \pm SE.

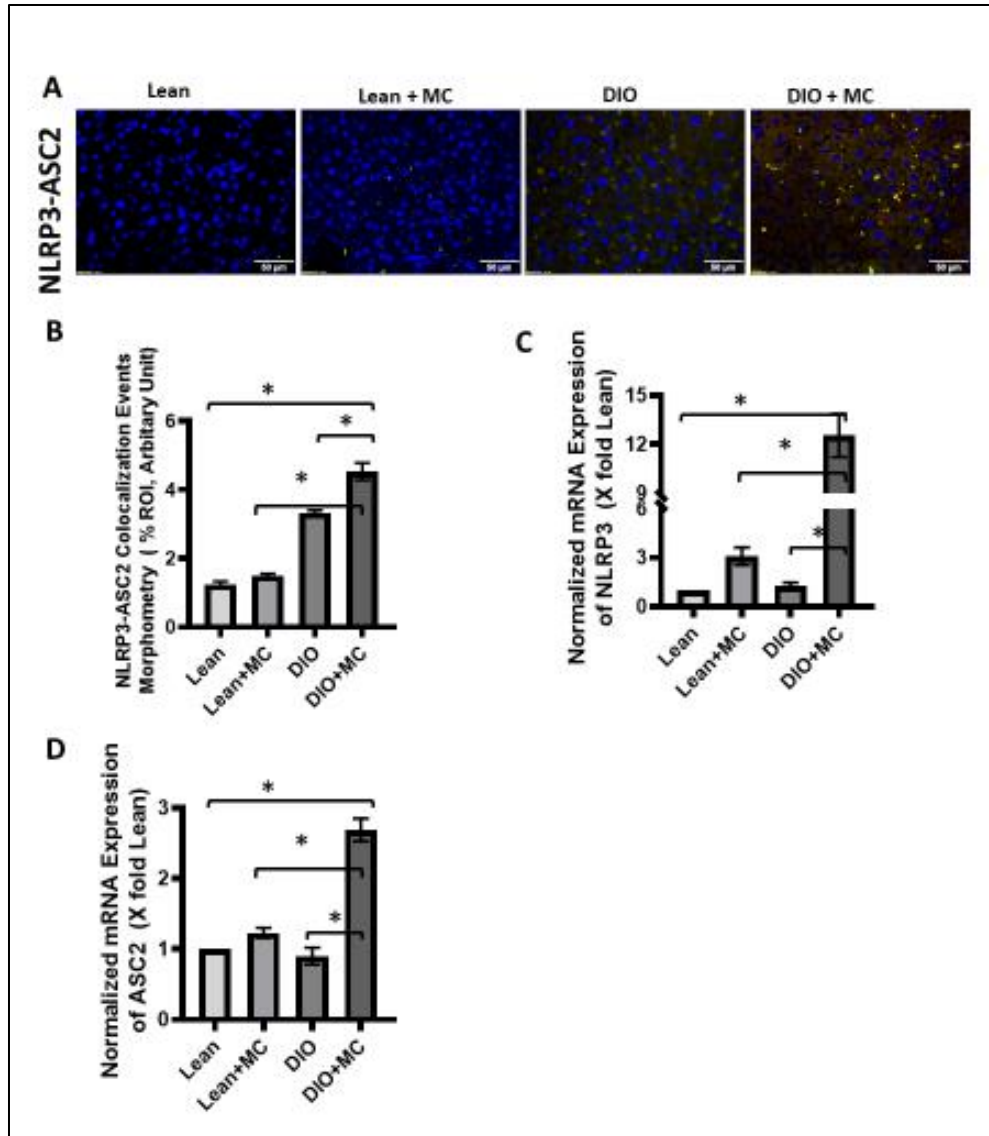


Figure 4.4. Early exposure to microcystin followed by HFD induces NLRP3 inflammasome activation. A: representative images of NLRP3 (red) and ASC2 (green) immunofluorescence counterstained with DAPI (blue) in lean mouse control and exposed to microcystin (MC), DIO, DIO+MC groups (n = 3/group). Images were taken at $\times 40$ magnification. B: morphometric analysis of NLRP3 and ASC2 colocalization expressed in percentage of positive colocalized immunoreactive area per region of interest (ROI) (3 ROIs/liver section, n = 3 each group). Quantitative RT-PCR analysis of mRNA expression of NLRP3 (C) and ASC2 (D) in lean, lean + MC, DIO, and DIO+MC livers. The mRNA expressions were normalized with 18s and presented as fold change of lean group. *P < 0.05. Results were expressed as means \pm SE.

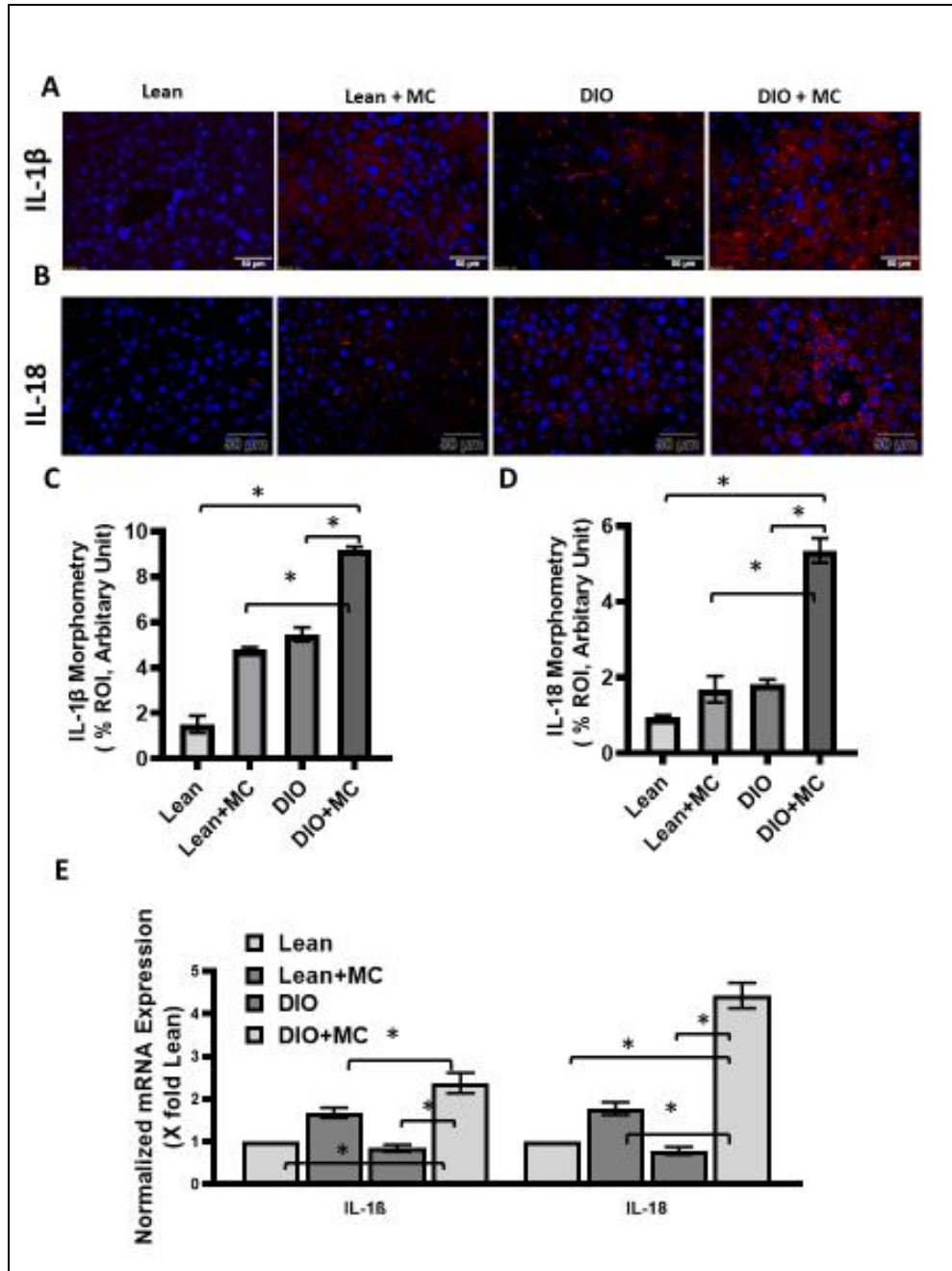
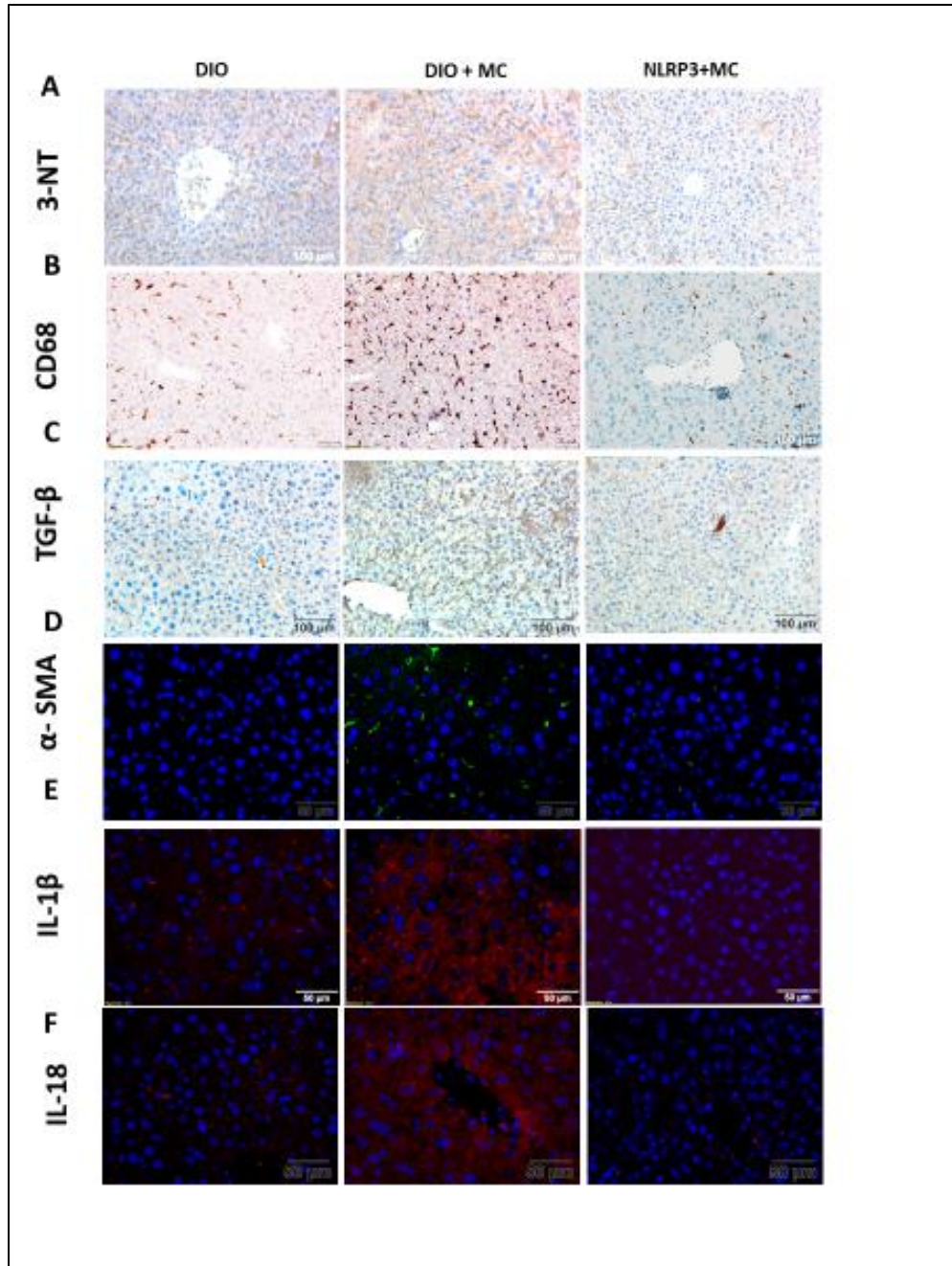
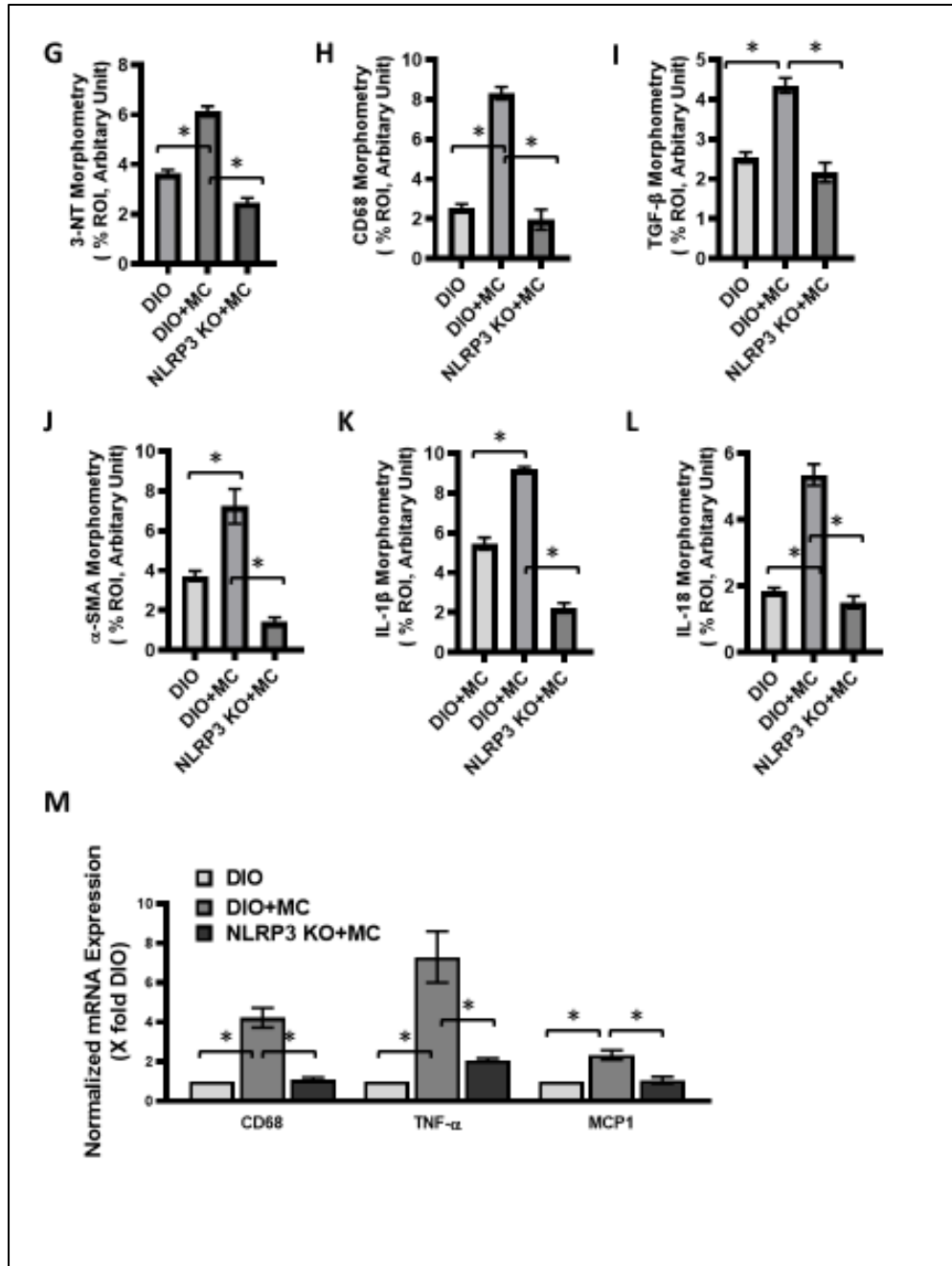


Figure 4.5. Early exposure to microcystin followed by HFD releases IL-1 β and IL-18. representative images of IL-1 β (red) (A), and IL-18 (red) (B) immunofluorescence counterstained with DAPI (blue) in lean mouse control and exposed to microcystin (MC),DIO,DIO+MC groups (n = 3/group). Images were taken at $\times 40$ magnification. Morphometric analysis of IL-1 β (C) and IL-18 (D) in lean mouse control and exposed to microcystin (MC),DIO,DIO+MC groups (n = 3/group). Morphometric analysis was expressed in percentage of positive immunoreactive area per regions of interest (ROIs) (3 ROIs/liver section). E: Quantitative RT-PCR analysis of mRNA expression of IL-1 β and IL-18 in lean, lean + MC, DIO, and DIO+MC livers. The mRNA expressions were

normalized with 18s and presented as fold change of lean group. *P < 0.05. Results were expressed as means \pm SE.





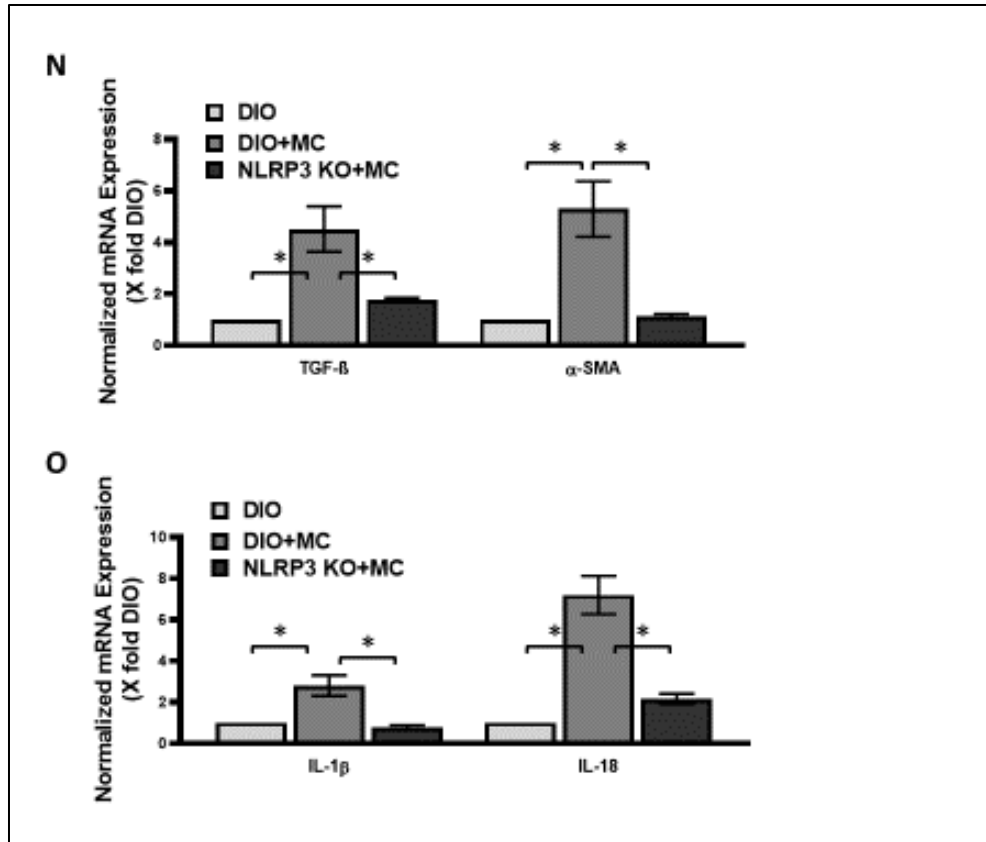


Figure 4.6. The activation of Kupffer cells, hepatic stellate cells, and an inflammatory surge in early microcystin (MC) exposure are mediated by NLRP3 inflammasome activation. Immunohistochemistry images of liver sections immunostained with 3-NT (A), CD68 (B), and TGF- β (C) from DIO, DIO+MC, and NLRP3 KO mice treated with MC (n = 3). Images were taken at 20X magnification. representative images of α -SMA (Green) (D), IL-1 β (red) (E), and IL-18 (red) (F) immunofluorescence counterstained with DAPI (blue) in DIO, DIO+MC, and NLRP3 KO mice treated with MC (n = 3/group). Images were taken at \times 40 magnification. Morphometric analysis of 3-NT (G), CD68 (H), and TGF- β (I) IL-1 β (J) and IL-18 (K) in DIO, DIO+MC, and NLRP3 KO mice treated with MC (n = 3/group). Morphometric analysis was expressed in percentage of positive immunoreactive area per regions of interest (ROIs) (3 ROIs/liver section). Quantitative RT-PCR analysis of mRNA expression of CD68, MCP1, TNF- α (L), TGF- β , α -SMA (M), IL-1 β and IL-18 (N) in DIO, DIO+MC, and NLRP3 KO mice treated with MC livers. The mRNA expressions were normalized with 18s and presented as fold change of DIO group. *P < 0.05. Results were expressed as means \pm SE.

CHAPTER 5

CONCLUSION

Obesity is a condition which arises due to the influence of multiple factors. According to Brehm and D'Alessio, some of these factors are external in the environmental predisposition while the others arise internally from the genetic structure [140]. There is a higher level of significance associated with the influence of genetic factors in the nature and development of an individual. However, recent trends also indicate that other factors in an individual such as their social behavior, including education levels, food, and dietary patterns, as well as the level of physical activity, all influence the prevalence of obesity. Each of these factors influences the prevalence and development of obesity because they predispose an individual to conditions that influence and support their development and progress. Obesity as a genetic underlay also depends on these factors to manifest and actively develop because, in their absence, it is impossible to develop such a set of background attributes.

Education levels influence an individual's understanding of aspects such as diet and nutrition. Reduced levels of education mean that households lack the proper form of access to information and knowledge that would allow them to develop and sustain a healthy lifestyle [141]. The food market also defines the types of nutritional components which households access. The rise in the fast food market supports and leads to a higher level of obesity due to its level of sugars and fats. The market also makes it harder to access healthy alternatives. Further, eating patterns are a major factor in the prevalence of obesity [140].

Practices such as binge eating, late eating, and attributes of frequency all have an influence on the presence and influence of obesity in an individual or a family setting. Ultimately, physical activity defines the level of exercise in an individual and influences how they use their food uptake.

Jiang et al. (2016) indicate that obesity has a direct correlation with the presence and level of hypertension in an individual [142]. Essentially, obesity arises when an individual is unable to use up their extra food intake through energy expenditure. Therefore, the energy accumulates as fat and glycogen reserves in various parts of the body. An increase in weight due to the deposits and the specific areas where these deposits arise influence the circulatory system. Obesity arises due to associated conditions such as arteriosclerosis where fat and mineral components accumulate in blood vessels. An extra amount of weight also puts additional pressure on the blood vessels to supply blood deeper into the tissues. There is a larger amount of energy expenditure that is necessary to support that higher level of activity in the tissues, which is the reason there is need for more flow of blood into the tissues.

Further, there is a correlation between obesity and inflammatory, metabolic disorders. Some of these conditions arise due to genetic conditions or other factors surrounding an individual. A common example of these conditions is a non-alcoholic fatty liver disease which arises due to the abnormal deposition of fats in the liver [143]. The liver performs a role in detoxification and component breakdown through the process of oxidation. However, when there is an extra amount of deposition in the liver, there is a resultant effect of oxidative stress which leads to inflammation, injury, and dysfunction within the hepatic cells in the liver. The progression of non-alcoholic fatty liver disease

creates an adverse effect because most of its progress is asymptomatic. Therefore, the condition can arise and progress to a point where there is extensive hardening and scarring of tissues before it is possible to detect. Therefore, its effects are devastating to the affected subject.

Previous studies have shown that pollutants from the environment behave in the liver as a "second/multiple hit" in order to augment NAFLD pathophysiology [6, 8]. For example, our group has shown that chronic low doses exposure to Bromo-dichloromethane (BDCM), which is known to be a prevalent by-product of water disinfection, can induce liver injury in preexisting NAFLD condition causing non-alcoholic steatohepatitis (NASH) via oxidative stress mediated by CYP2E1 in obese mice [6]. This idea has been translated into epidemiological study where using the U.S. Data from NHANES 1999–2006 as cross-sectional study has revealed higher concentrations of the alanine aminotransferase (ALT), which is an enzyme that is used as a common marker of liver injury in people exposed to greater concentrations than average concentrations of trihalomethane brominated in their blood with prevalence odds ratios (ORs) equal to 1.35 times for its level (95% CI: 1.02, 1.79) [144]. In both the United States and other countries, total trihalomethanes concentrations exceeding the benchmark exposure threshold as well as obesity prevalence continue to be reported [144].

In the present study, I examined the different basic molecular mechanisms of hepatic injury in NASH that is induced by microcystin exposure. Inhibition of PP2A both via endogenous and exogenous routes can be a cause of liver injuries including in adult as well as juvenile age groups. An important public health issue is an increase in obesity prevalence as well as an increased prevalence of NAFLD among them. In NAFLD

progression to advanced NASH stage, the concept of two-hit and the multi-hit theory plays an important role, in which an environmental agent apart from obesity is a significant cause of liver injury. We found in our study that microcystin is activated Kupffer cells as well as hepatic stellate cells, that release the proinflammatory mediators involved in progression of NAFLD to NASH. Different studies have shown that environmental toxicants exposure, which act as second hits, can regulate NOX2 activation in NAFLD condition. In our study we found in Kupffer cells that microcystin exposure will increase the activation of NOX2 and tyrosine nitration. This has been shown in vitro by visualizing the significant increase in GP91 phox-p47 phox colocalization events in Kupffer cells that have been exposed to leptin with MC as compared with other cell groups. In vivo also, we have been shown the significant increase in the colocalization events of GP91 phox-p47 phox in NAFLD mice that have been exposed to microcystin as compared to other groups. Moreover, several publications have shown that microRNA 21 (miR21) in NAFLD and NAFLD-associated kidney inflammation is upregulated there. If upregulated, miR21 also has been shown to regulate the NAFLD fibrogenesis via SMAD pathway. In our study, we have shown that microcystin can activate the miR21 in progressive NASH. We found in NAFLD mice that were exposed to microcystin that there is a significant increase in miR21 level of expression among them as compared to other groups. Interestingly, *P47 phox* KO mice that were exposed to microcystin showed a significant decline in miR21 expression level as compared to NAFLD mice that were exposed to microcystin. In addition, we found that miR21 KO as well as *P47 phox* KO mice that were exposed to microcystin showed a significant decrease in immunoreactivity of CD68, CD11b, and α -SMA. These are known biomarkers for Kupffer cells as well as

hepatic stellate cells. This indicates that microcystin exposure can activate the NOX2-induced miR21 which plays an important role in the activation of Kupffer cells and stellate cells. Mechanistically, immortalized Kupffer cells as well as stellate cells treated with pharmacological inhibitors such as apocynin ,nitron spin trap DMPO, or phenyl boronic acid (FBA) with microcystin and leptin exposure showed a decrease in miR21 levels , activation of both Kupffer and stellate cell , and a decrease in inflammatory cytokines release. Moreover, using the same pharmacological inhibition in cells primed with leptin and co-exposed to microcystin showed attenuation in Gli 1, PTCG1, IHH , SHH gene expression, hallmarks for hedgehog signaling activation in NAFLD.

We have also proved in our research that M1 phenotype increases in Kupffer cells via the same pathway by showing adaptation to an elongated morphology, activation of iNOS and release of nitric oxide. Further we showed that blocking of the AKT pathway using AKT inhibitor decreased the ability of PP2A-inhibitor such as microcystin in induction of NOX2 activation and miR21 upregulation.

In the juvenile mice study, we primed them with microcystin-LR (MC-LR) for two weeks after the end of weaning followed by high fat diet for four weeks . This study aimed to be translatable to what has been seen in clinical data. This is because it has been reported by American Academy of Pediatrics that there is a risk of early exposure to microcystin in infants as well as children. In our study, we have shown that early exposure to microcystin can increase proinflammatory cytokines and chemokines in diet induced obesity model as compared to other groups. Early exposure to microcystin can also increases the serum alanine aminotransferase (ALT) as compared to the other groups. Interestingly, we have shown the significant increase in the colocalization events of NLRP3-ASC2 in DIO mice

model that was primed with microcystin as compared to other groups. Moreover, in *NLRP3* KO mice that were exposed to microcystin showed a significant decrease in the proinflammatory cytokines and chemokines levels as compared to DIO mice that were primed with microcystin. In summary, we can conclude that early exposure to microcystin followed by HFD can exacerbate liver injury outcomes via NLRP3 pathway.

REFERENCES

1. Sakaguchi, S., et al., *Progression of alcoholic and non-alcoholic steatohepatitis: common metabolic aspects of innate immune system and oxidative stress*. Drug Metab Pharmacokinet, 2011. **26**(1): p. 30-46.
2. Marra, F. and S. Lotersztajn, *Pathophysiology of NASH: perspectives for a targeted treatment*. Curr Pharm Des, 2013. **19**(29): p. 5250-69.
3. Lonardo, A., et al., *Nonalcoholic fatty liver disease: Evolving paradigms*. World J Gastroenterol, 2017. **23**(36): p. 6571-6592.
4. Brunt, E.M. and D.G. Tiniakos, *Histopathology of nonalcoholic fatty liver disease*. World J Gastroenterol, 2010. **16**(42): p. 5286-96.
5. Takahashi, Y. and T. Fukusato, *Histopathology of nonalcoholic fatty liver disease/nonalcoholic steatohepatitis*. World J Gastroenterol, 2014. **20**(42): p. 15539-48.
6. Seth, R.K., et al., *Environmental toxin-linked nonalcoholic steatohepatitis and hepatic metabolic reprogramming in obese mice*. Toxicol Sci, 2013. **134**(2): p. 291-303.
7. Younossi, Z.M., *Non-alcoholic fatty liver disease - A global public health perspective*. J Hepatol, 2019. **70**(3): p. 531-544.
8. Nagata, K., H. Suzuki, and S. Sakaguchi, *Common pathogenic mechanism in development progression of liver injury caused by non-alcoholic or alcoholic steatohepatitis*. J Toxicol Sci, 2007. **32**(5): p. 453-68.
9. Buzzetti, E., M. Pinzani, and E.A. Tsochatzis, *The multiple-hit pathogenesis of non-alcoholic fatty liver disease (NAFLD)*. Metabolism, 2016. **65**(8): p. 1038-48.
10. Yu, J., et al., *The Pathogenesis of Nonalcoholic Fatty Liver Disease: Interplay between Diet, Gut Microbiota, and Genetic Background*. Gastroenterol Res Pract, 2016. **2016**: p. 2862173.
11. Jou, J., S.S. Choi, and A.M. Diehl, *Mechanisms of disease progression in nonalcoholic fatty liver disease*. Semin Liver Dis, 2008. **28**(4): p. 370-9.
12. Tilg, H. and A.R. Moschen, *Evolution of inflammation in nonalcoholic fatty liver disease: the multiple parallel hits hypothesis*. Hepatology, 2010. **52**(5): p. 1836-46.
13. Musso, G., M. Cassader, and R. Gambino, *Non-alcoholic steatohepatitis: emerging molecular targets and therapeutic strategies*. Nat Rev Drug Discov, 2016. **15**(4): p. 249-74.
14. Bellentani, S., et al., *Epidemiology of non-alcoholic fatty liver disease*. Dig Dis, 2010. **28**(1): p. 155-61.
15. Johnson, A.M. and J.M. Olefsky, *The origins and drivers of insulin resistance*. Cell, 2013. **152**(4): p. 673-84.
16. Polyzos, S.A., et al., *The potential adverse role of leptin resistance in nonalcoholic fatty liver disease: a hypothesis based on critical review of the literature*. J Clin Gastroenterol, 2011. **45**(1): p. 50-4.
17. Tsochatzis, E., G.V. Papatheodoridis, and A.J. Archimandritis, *The evolving role of leptin and adiponectin in chronic liver diseases*. Am J Gastroenterol, 2006. **101**(11): p. 2629-40.

18. Seth, R.K., et al., *CYP2E1-dependent and leptin-mediated hepatic CD57 expression on CD8+ T cells aid progression of environment-linked nonalcoholic steatohepatitis*. Toxicol Appl Pharmacol, 2014. **274**(1): p. 42-54.
19. Kelesidis, T., et al., *Narrative review: the role of leptin in human physiology: emerging clinical applications*. Ann Intern Med, 2010. **152**(2): p. 93-100.
20. Ogden, C.L., et al., *Prevalence of Obesity Among Adults and Youth: United States, 2011-2014*. NCHS Data Brief, 2015(219): p. 1-8.
21. Raddatz, D. and G. Ramadori, *Carbohydrate metabolism and the liver: actual aspects from physiology and disease*. Z Gastroenterol, 2007. **45**(1): p. 51-62.
22. Ponziani, F.R., et al., *Physiology and pathophysiology of liver lipid metabolism*. Expert Rev Gastroenterol Hepatol, 2015. **9**(8): p. 1055-67.
23. Bilzer, M., F. Roggel, and A.L. Gerbes, *Role of Kupffer cells in host defense and liver disease*. Liver Int, 2006. **26**(10): p. 1175-86.
24. Safadi, R. and S.L. Friedman, *Hepatic fibrosis--role of hepatic stellate cell activation*. MedGenMed, 2002. **4**(3): p. 27.
25. Tsuchida, T. and S.L. Friedman, *Mechanisms of hepatic stellate cell activation*. Nat Rev Gastroenterol Hepatol, 2017. **14**(7): p. 397-411.
26. Tosello-Tramont, A.C., et al., *Kupffer cells trigger nonalcoholic steatohepatitis development in diet-induced mouse model through tumor necrosis factor-alpha production*. J Biol Chem, 2012. **287**(48): p. 40161-72.
27. Lanthier, N., *Targeting Kupffer cells in non-alcoholic fatty liver disease/non-alcoholic steatohepatitis: Why and how?* World J Hepatol, 2015. **7**(19): p. 2184-8.
28. Benedict, M. and X. Zhang, *Non-alcoholic fatty liver disease: An expanded review*. World J Hepatol, 2017. **9**(16): p. 715-732.
29. Seth, R.K., et al., *TRPV4 activation of endothelial nitric oxide synthase resists nonalcoholic fatty liver disease by blocking CYP2E1-mediated redox toxicity*. Free Radic Biol Med, 2017. **102**: p. 260-273.
30. Spiekermann, S., et al., *Electron spin resonance characterization of vascular xanthine and NAD(P)H oxidase activity in patients with coronary artery disease: relation to endothelium-dependent vasodilation*. Circulation, 2003. **107**(10): p. 1383-9.
31. Weltman, M.D., et al., *Hepatic cytochrome P450 2E1 is increased in patients with nonalcoholic steatohepatitis*. Hepatology, 1998. **27**(1): p. 128-33.
32. De Minicis, S., R. Bataller, and D.A. Brenner, *NADPH oxidase in the liver: defensive, offensive, or fibrogenic?* Gastroenterology, 2006. **131**(1): p. 272-5.
33. Yao, H., et al., *Redox regulation of lung inflammation: role of NADPH oxidase and NF-kappaB signalling*. Biochem Soc Trans, 2007. **35**(Pt 5): p. 1151-5.
34. Polimeni, L., et al., *Oxidative stress: New insights on the association of non-alcoholic fatty liver disease and atherosclerosis*. World J Hepatol, 2015. **7**(10): p. 1325-36.
35. Schriks, M., et al., *Toxicological relevance of emerging contaminants for drinking water quality*. Water Res, 2010. **44**(2): p. 461-76.
36. Dittmann, E. and C. Wiegand, *Cyanobacterial toxins--occurrence, biosynthesis and impact on human affairs*. Mol Nutr Food Res, 2006. **50**(1): p. 7-17.
37. Reynhout, S. and V. Janssens, *Physiologic functions of PP2A: Lessons from genetically modified mice*. Biochim Biophys Acta Mol Cell Res, 2019. **1866**(1): p. 31-50.
38. Lone, Y., R.K. Koiri, and M. Bhide, *An overview of the toxic effect of potential human carcinogen Microcystin-LR on testis*. Toxicol Rep, 2015. **2**: p. 289-296.
39. Svircev, Z., et al., *Toxicology of microcystins with reference to cases of human intoxications and epidemiological investigations of exposures to cyanobacteria and cyanotoxins*. Arch Toxicol, 2017. **91**(2): p. 621-650.
40. Codd, G.A., et al., *Cyanobacterial toxins, exposure routes and human health*. European Journal of Phycology, 1999. **34**(4): p. 405-415.

41. Benson, J.M., et al., *The toxicity of microcystin LR in mice following 7 days of inhalation exposure*. *Toxicol*, 2005. **45**(6): p. 691-8.
42. Zhou, M., W.W. Tu, and J. Xu, *Mechanisms of microcystin-LR-induced cytoskeletal disruption in animal cells*. *Toxicol*, 2015. **101**: p. 92-100.
43. Duy, T.N., et al., *Toxicology and risk assessment of freshwater cyanobacterial (blue-green algal) toxins in water*. *Rev Environ Contam Toxicol*, 2000. **163**: p. 113-85.
44. Oh, H.M., et al., *Microcystin production by Microcystis aeruginosa in a phosphorus-limited chemostat*. *Appl Environ Microbiol*, 2000. **66**(1): p. 176-9.
45. Masten S, C.B., *Cylindrospermopsin- Review of Toxicological Literature*. Toxicological Summary For Cylindrospermopsin. CASRN 143545-90-8, 2000.
46. Klaassen, C.D. and H. Lu, *Xenobiotic transporters: ascribing function from gene knockout and mutation studies*. *Toxicol Sci*, 2008. **101**(2): p. 186-96.
47. Trauner, M. and J.L. Boyer, *Bile salt transporters: molecular characterization, function, and regulation*. *Physiol Rev*, 2003. **83**(2): p. 633-71.
48. Fischer, W.J., et al., *Organic anion transporting polypeptides expressed in liver and brain mediate uptake of microcystin*. *Toxicol Appl Pharmacol*, 2005. **203**(3): p. 257-63.
49. Puerto, M., et al., *Comparison of the toxicity induced by microcystin-RR and microcystin-YR in differentiated and undifferentiated Caco-2 cells*. *Toxicol*, 2009. **54**(2): p. 161-9.
50. Maynes, J.T., et al., *Crystal structures of protein phosphatase-1 bound to motuporin and dihydromicrocystin-LA: elucidation of the mechanism of enzyme inhibition by cyanobacterial toxins*. *J Mol Biol*, 2006. **356**(1): p. 111-20.
51. Campos, A. and V. Vasconcelos, *Molecular mechanisms of microcystin toxicity in animal cells*. *Int J Mol Sci*, 2010. **11**(1): p. 268-87.
52. Brandes, R.P., N. Weissmann, and K. Schroder, *Nox family NADPH oxidases: Molecular mechanisms of activation*. *Free Radic Biol Med*, 2014. **76**: p. 208-26.
53. You, Y.H., et al., *Role of Nox2 in diabetic kidney disease*. *Am J Physiol Renal Physiol*, 2013. **304**(7): p. F840-8.
54. Chatterjee, S., et al., *Leptin is key to peroxynitrite-mediated oxidative stress and Kupffer cell activation in experimental non-alcoholic steatohepatitis*. *J Hepatol*, 2013. **58**(4): p. 778-84.
55. Panday, A., et al., *NADPH oxidases: an overview from structure to innate immunity-associated pathologies*. *Cell Mol Immunol*, 2015. **12**(1): p. 5-23.
56. Rastogi, R., et al., *NOX Activation by Subunit Interaction and Underlying Mechanisms in Disease*. *Front Cell Neurosci*, 2016. **10**: p. 301.
57. Dattaroy, D., et al., *Micro-RNA 21 inhibition of SMAD7 enhances fibrogenesis via leptin-mediated NADPH oxidase in experimental and human nonalcoholic steatohepatitis*. *Am J Physiol Gastrointest Liver Physiol*, 2015. **308**(4): p. G298-312.
58. Lakner, A.M., H.L. Bonkovsky, and L.W. Schrum, *microRNAs: fad or future of liver disease*. *World J Gastroenterol*, 2011. **17**(20): p. 2536-42.
59. Zhang, Z., et al., *3,3'-Diindolylmethane ameliorates experimental hepatic fibrosis via inhibiting miR-21 expression*. *Br J Pharmacol*, 2013. **170**(3): p. 649-60.
60. Noetel, A., et al., *microRNA are Central Players in Anti- and Profibrotic Gene Regulation during Liver Fibrosis*. *Front Physiol*, 2012. **3**: p. 49.
61. Arciello, M., et al., *Environmental pollution: a tangible risk for NAFLD pathogenesis*. *Int J Mol Sci*, 2013. **14**(11): p. 22052-66.
62. Sauve, S. and M. Desrosiers, *A review of what is an emerging contaminant*. *Chem Cent J*, 2014. **8**(1): p. 15.
63. Dawson, R.M., *The toxicology of microcystins*. *Toxicol*, 1998. **36**(7): p. 953-62.
64. Amado, L.L. and J.M. Monserrat, *Oxidative stress generation by microcystins in aquatic animals: why and how*. *Environ Int*, 2010. **36**(2): p. 226-35.





65. Huang, H., et al., *Microcystin-LR Induced Apoptosis in Rat Sertoli Cells via the Mitochondrial Caspase-Dependent Pathway: Role of Reactive Oxygen Species*. *Front Physiol*, 2016. **7**: p. 397.
66. Woolbright, B.L., et al., *Microcystin-LR induced liver injury in mice and in primary human hepatocytes is caused by oncotic necrosis*. *Toxicol*, 2017. **125**: p. 99-109.
67. Zheng, C., et al., *Serum microcystin levels positively linked with risk of hepatocellular carcinoma: A case-control study in southwest China*. *Hepatology*, 2017. **66**(5): p. 1519-1528.
68. Xian, L., et al., *Liver-specific deletion of Ppp2calpha enhances glucose metabolism and insulin sensitivity*. *Aging (Albany NY)*, 2015. **7**(4): p. 223-32.
69. Frijhoff, J., et al., *Clinical Relevance of Biomarkers of Oxidative Stress*. *Antioxid Redox Signal*, 2015. **23**(14): p. 1144-70.
70. Penman AD, K.G., Daniels KK, *MicroRNA expression as an indicator of tissue toxicity, in In: Gupta RC (ed) Biomarkers in toxicology*. 2014. p. 1003–1018.
71. Wang, F., C. Chen, and D. Wang, *Circulating microRNAs in cardiovascular diseases: from biomarkers to therapeutic targets*. *Front Med*, 2014. **8**(4): p. 404-18.
72. Alhasson, F., et al., *High circulatory leptin mediated NOX-2-peroxynitrite-miR21 axis activate mesangial cells and promotes renal inflammatory pathology in nonalcoholic fatty liver disease*. *Redox Biol*, 2018. **17**: p. 1-15.
73. Pourhoseini, S., et al., *Upregulation of miR21 and repression of Grhl3 by leptin mediates sinusoidal endothelial injury in experimental nonalcoholic steatohepatitis*. *PLoS One*, 2015. **10**(2): p. e0116780.
74. Gilhodes, J.C., et al., *Quantification of Pulmonary Fibrosis in a Bleomycin Mouse Model Using Automated Histological Image Analysis*. *PLoS One*, 2017. **12**(1): p. e0170561.
75. Bohinc, B.N. and A.M. Diehl, *Mechanisms of disease progression in NASH: new paradigms*. *Clin Liver Dis*, 2012. **16**(3): p. 549-65.
76. Barrett, J.P., et al., *NOX2 deficiency alters macrophage phenotype through an IL-10/STAT3 dependent mechanism: implications for traumatic brain injury*. *J Neuroinflammation*, 2017. **14**(1): p. 65.
77. Tan, H.Y., et al., *The Reactive Oxygen Species in Macrophage Polarization: Reflecting Its Dual Role in Progression and Treatment of Human Diseases*. *Oxid Med Cell Longev*, 2016. **2016**: p. 2795090.
78. Sarsour, E.H., et al., *Redox control of the cell cycle in health and disease*. *Antioxid Redox Signal*, 2009. **11**(12): p. 2985-3011.
79. Yan, S., et al., *Inhibition of NADPH oxidase protects against metastasis of human lung cancer by decreasing microRNA-21*. *Anticancer Drugs*, 2015. **26**(4): p. 388-98.
80. Grunhut, J., et al., *Macrophages in Nonalcoholic Steatohepatitis: Friend or Foe?* *Eur Med J Hepatol*, 2018. **6**(1): p. 100-109.
81. Kadl, A., et al., *Identification of a novel macrophage phenotype that develops in response to atherogenic phospholipids via Nrf2*. *Circ Res*, 2010. **107**(6): p. 737-46.
82. Mustafa, S.B. and M.S. Olson, *Expression of nitric-oxide synthase in rat Kupffer cells is regulated by cAMP*. *J Biol Chem*, 1998. **273**(9): p. 5073-80.
83. Koliwad, S.K., et al., *DGAT1-dependent triacylglycerol storage by macrophages protects mice from diet-induced insulin resistance and inflammation*. *J Clin Invest*, 2010. **120**(3): p. 756-67.
84. Yamaguchi, K., et al., *Inhibiting triglyceride synthesis improves hepatic steatosis but exacerbates liver damage and fibrosis in obese mice with nonalcoholic steatohepatitis*. *Hepatology*, 2007. **45**(6): p. 1366-74.
85. Shimizu, S., et al., *Protein-tyrosine phosphatase 1B as new activator for hepatic lipogenesis via sterol regulatory element-binding protein-1 gene expression*. *J Biol Chem*, 2003. **278**(44): p. 43095-101.

86. Lu, H., et al., *Characterization of organic anion transporting polypeptide 1b2-null mice: essential role in hepatic uptake/toxicity of phalloidin and microcystin-LR*. *Toxicol Sci*, 2008. **103**(1): p. 35-45.
87. Albadrani, M., et al., *Exogenous PP2A inhibitor exacerbates the progression of nonalcoholic fatty liver disease via NOX2-dependent activation of miR21*. *Am J Physiol Gastrointest Liver Physiol*, 2019. **317**(4): p. G408-G428.
88. Day, C.P. and O.F. James, *Steatohepatitis: a tale of two "hits"?* *Gastroenterology*, 1998. **114**(4): p. 842-5.
89. Torres, D.M., C.D. Williams, and S.A. Harrison, *Features, diagnosis, and treatment of nonalcoholic fatty liver disease*. *Clin Gastroenterol Hepatol*, 2012. **10**(8): p. 837-58.
90. Kanda, T., et al., *Apoptosis and non-alcoholic fatty liver diseases*. *World J Gastroenterol*, 2018. **24**(25): p. 2661-2672.
91. Lemasters, J.J., *Molecular Mechanisms of Cell Death*, in *Molecular Pathology*. 2018, Elsevier. p. 1-24.
92. Fink, S.L. and B.T. Cookson, *Apoptosis, pyroptosis, and necrosis: mechanistic description of dead and dying eukaryotic cells*. *Infect Immun*, 2005. **73**(4): p. 1907-16.
93. Singh, S., et al., *Fibrosis progression in nonalcoholic fatty liver vs nonalcoholic steatohepatitis: a systematic review and meta-analysis of paired-biopsy studies*. *Clin Gastroenterol Hepatol*, 2015. **13**(4): p. 643-54 e1-9; quiz e39-40.
94. Schuppan, D. and J.M. Schattenberg, *Non-alcoholic steatohepatitis: pathogenesis and novel therapeutic approaches*. *J Gastroenterol Hepatol*, 2013. **28 Suppl 1**: p. 68-76.
95. Yilmaz, Y. and Z.M. Younossi, *Obesity-associated nonalcoholic fatty liver disease*. *Clin Liver Dis*, 2014. **18**(1): p. 19-31.
96. Paik, Y.H., et al., *Role of NADPH oxidases in liver fibrosis*. *Antioxid Redox Signal*, 2014. **20**(17): p. 2854-72.
97. Hou, W. and W.K. Syn, *Role of Metabolism in Hepatic Stellate Cell Activation and Fibrogenesis*. *Front Cell Dev Biol*, 2018. **6**: p. 150.
98. Yang, J.J., H. Tao, and J. Li, *Hedgehog signaling pathway as key player in liver fibrosis: new insights and perspectives*. *Expert Opin Ther Targets*, 2014. **18**(9): p. 1011-21.
99. Basiorka, A.A., et al., *The NLRP3 inflammasome functions as a driver of the myelodysplastic syndrome phenotype*. *Blood*, 2016. **128**(25): p. 2960-2975.
100. Simard, J.C., et al., *S100A8 and S100A9 induce cytokine expression and regulate the NLRP3 inflammasome via ROS-dependent activation of NF-kappaB(1.)*. *PLoS One*, 2013. **8**(8): p. e72138.
101. Shi, J., W. Gao, and F. Shao, *Pyroptosis: Gasdermin-Mediated Programmed Necrotic Cell Death*. *Trends Biochem Sci*, 2017. **42**(4): p. 245-254.
102. Verdelho Machado, M. and A.M. Diehl, *Role of Hedgehog Signaling Pathway in NASH*. *Int J Mol Sci*, 2016. **17**(6).
103. Syn, W.K., et al., *Hedgehog-mediated epithelial-to-mesenchymal transition and fibrogenic repair in nonalcoholic fatty liver disease*. *Gastroenterology*, 2009. **137**(4): p. 1478-1488 e8.
104. Fleig, S.V., et al., *Hepatic accumulation of Hedgehog-reactive progenitors increases with severity of fatty liver damage in mice*. *Lab Invest*, 2007. **87**(12): p. 1227-39.
105. Chanut, F. and U. Heberlein, *Role of decapentaplegic in initiation and progression of the morphogenetic furrow in the developing Drosophila retina*. *Development*, 1997. **124**(2): p. 559-67.
106. Hausmann, G., C. von Mering, and K. Basler, *The hedgehog signaling pathway: where did it come from?* *PLoS Biol*, 2009. **7**(6): p. e1000146.
107. Pasca di Magliano, M. and M. Hebrok, *Hedgehog signalling in cancer formation and maintenance*. *Nat Rev Cancer*, 2003. **3**(12): p. 903-11.

108. Katoh, Y. and M. Katoh, *Hedgehog signaling, epithelial-to-mesenchymal transition and miRNA (review)*. Int J Mol Med, 2008. **22**(3): p. 271-5.
109. Guy, C.D., et al., *Hedgehog pathway activation parallels histologic severity of injury and fibrosis in human nonalcoholic fatty liver disease*. Hepatology, 2012. **55**(6): p. 1711-21.
110. Liu, X., et al., *Inflammasome-activated gasdermin D causes pyroptosis by forming membrane pores*. Nature, 2016. **535**(7610): p. 153-8.
111. Funari, E. and E. Testai, *Human health risk assessment related to cyanotoxins exposure*. Crit Rev Toxicol, 2008. **38**(2): p. 97-125.
112. Kotak, B.G., et al., *VARIABILITY OF THE HEPATOTOXIN MICROCYSTIN-LR IN HYPEREUTROPHIC DRINKING WATER LAKES 1*. 1995. **31**(2): p. 248-263.
113. Hoffmann, L., *Geographic distribution of freshwater blue-green algae*, in *Biogeography of Freshwater Algae*. 1996, Springer. p. 33-40.
114. Mohamed, Z.A.J.T., *Toxic cyanobacteria and cyanotoxins in public hot springs in Saudi Arabia*. 2008. **51**(1): p. 17-27.
115. Lun, Z., Y. Hai, and C.J.B.E.S. Kun, *Relationship between microcystin in drinking water and colorectal cancer*. 2002. **15**(2): p. 166-171.
116. Carmichael, W.W., et al., *Human fatalities from cyanobacteria: chemical and biological evidence for cyanotoxins*. Environ Health Perspect, 2001. **109**(7): p. 663-8.
117. Jochimsen, E.M., et al., *Liver failure and death after exposure to microcystins at a hemodialysis center in Brazil*. N Engl J Med, 1998. **338**(13): p. 873-8.
118. Selevan, S.G., C.A. Kimmel, and P. Mendola, *Identifying critical windows of exposure for children's health*. Environ Health Perspect, 2000. **108 Suppl 3**: p. 451-5.
119. Osmond, C. and D.J. Barker, *Fetal, infant, and childhood growth are predictors of coronary heart disease, diabetes, and hypertension in adult men and women*. Environ Health Perspect, 2000. **108 Suppl 3**: p. 545-53.
120. Andra, S.S., et al., *Reconstructing pre-natal and early childhood exposure to multi-class organic chemicals using teeth: Towards a retrospective temporal exposome*. Environ Int, 2015. **83**: p. 137-45.
121. Beath, S.V., *Hepatic function and physiology in the newborn*. Semin Neonatol, 2003. **8**(5): p. 337-46.
122. Sarkar, S., et al., *Environmental microcystin targets the microbiome and increases the risk of intestinal inflammatory pathology via NOX2 in underlying murine model of Nonalcoholic Fatty Liver Disease*. Sci Rep, 2019. **9**(1): p. 8742.
123. Swanson, K.V., M. Deng, and J.P.-Y.J.N.R.I. Ting, *The NLRP3 inflammasome: molecular activation and regulation to therapeutics*. 2019: p. 1.
124. Agostini, L., et al., *NALP3 forms an IL-1beta-processing inflammasome with increased activity in Muckle-Wells autoinflammatory disorder*. Immunity, 2004. **20**(3): p. 319-25.
125. Kanneganti, T.D., et al., *Critical role for Cryopyrin/Nalp3 in activation of caspase-1 in response to viral infection and double-stranded RNA*. J Biol Chem, 2006. **281**(48): p. 36560-8.
126. Mariathasan, S., et al., *Cryopyrin activates the inflammasome in response to toxins and ATP*. Nature, 2006. **440**(7081): p. 228-32.
127. Dooley, S. and P. ten Dijke, *TGF-beta in progression of liver disease*. Cell Tissue Res, 2012. **347**(1): p. 245-56.
128. Zhang, C., et al., *Molecular Mechanisms Involved in Oxidative Stress-Associated Liver Injury Induced by Chinese Herbal Medicine: An Experimental Evidence-Based Literature Review and Network Pharmacology Study*. Int J Mol Sci, 2018. **19**(9).
129. Mortezaee, K. and N. Khanlarkhani, *Melatonin application in targeting oxidative-induced liver injuries: A review*. J Cell Physiol, 2018. **233**(5): p. 4015-4032.

130. Ahsan, H., *3-Nitrotyrosine: A biomarker of nitrogen free radical species modified proteins in systemic autoimmunogenic conditions*. Hum Immunol, 2013. **74**(10): p. 1392-9.
131. Dattaroy, D., et al., *Sparstolonin B attenuates early liver inflammation in experimental NASH by modulating TLR4 trafficking in lipid rafts via NADPH oxidase activation*. Am J Physiol Gastrointest Liver Physiol, 2016. **310**(7): p. G510-25.
132. Szabo, G. and J. Petrasek, *Inflammasome activation and function in liver disease*. Nat Rev Gastroenterol Hepatol, 2015. **12**(7): p. 387-400.
133. Wan, X., et al., *Role of NLRP3 Inflammasome in the Progression of NAFLD to NASH*. Can J Gastroenterol Hepatol, 2016. **2016**: p. 6489012.
134. Wree, A., et al., *NLRP3 inflammasome activation is required for fibrosis development in NAFLD*. J Mol Med (Berl), 2014. **92**(10): p. 1069-82.
135. Yang, S.J. and Y. Lim, *Resveratrol ameliorates hepatic metaflammation and inhibits NLRP3 inflammasome activation*. Metabolism, 2014. **63**(5): p. 693-701.
136. Kelk, P., et al., *Caspase 1 involvement in human monocyte lysis induced by Actinobacillus actinomycetemcomitans leukotoxin*. Infect Immun, 2003. **71**(8): p. 4448-55.
137. Yang, G., H.E. Lee, and J.Y. Lee, *A pharmacological inhibitor of NLRP3 inflammasome prevents non-alcoholic fatty liver disease in a mouse model induced by high fat diet*. Scientific Reports, 2016. **6**(1): p. 24399.
138. Thomas, H., *A critical role for the NLRP3 inflammasome in NASH*. Nature Reviews Gastroenterology & Hepatology, 2017. **14**: p. 197.
139. Abdelmegeed, M.A. and B.J. Song, *Functional roles of protein nitration in acute and chronic liver diseases*. Oxid Med Cell Longev, 2014. **2014**: p. 149627.
140. Brehm, B.J. and D.A. D'Alessio, *Environmental Factors Influencing Obesity*, in *Endotext*, K.R. Feingold, et al., Editors. 2000: South Dartmouth (MA).
141. Yildirim, S. and E. Uskun, *Risk factors affecting obesity development in high school students: a community based case-control study*. Turk Pediatri Ars, 2018. **53**(3): p. 155-162.
142. Jiang, S.Z., et al., *Obesity and hypertension*. Exp Ther Med, 2016. **12**(4): p. 2395-2399.
143. Saltiel, A.R. and J.M. Olefsky, *Inflammatory mechanisms linking obesity and metabolic disease*. J Clin Invest, 2017. **127**(1): p. 1-4.
144. Burch, J.B., et al., *Trihalomethane exposure and biomonitoring for the liver injury indicator, alanine aminotransferase, in the United States population (NHANES 1999-2006)*. Sci Total Environ, 2015. **521-522**: p. 226-34.

APPENDIX A: COPYRIGHT PERMISSION FOR CHAPTER 2

		Account Info	Help	
	<p>Title: Exogenous PP2A inhibitor exacerbates the progression of nonalcoholic fatty liver disease via NOX2-dependent activation of miR21</p> <p>Author: Muayad Albadrani, Ratanesh K. Seth, Sutapa Sarkar, et al</p> <p>Publication: Am J Physiol-Gastrointestinal and Liver Physiology</p> <p>Publisher: The American Physiological Society</p> <p>Date: Oct 1, 2019</p> <p>Copyright © 2019, The American Physiological Society</p>	<p>Logged in as: Muayad Albadrani Account #: 3001524585</p> <p style="text-align: center;">LOGOUT</p>		
Order Completed				
Thank you for your order.				
This Agreement between Muayad Albadrani ("You") and The American Physiological Society ("The American Physiological Society") consists of your order details and the terms and conditions provided by The American Physiological Society and Copyright Clearance Center.				
Licensed Content Reference confirmation email for license number				
Licensed Content License date	Sep, 26 2019			
Licensed Content Publisher	The American Physiological Society			
Licensed Content Publication	Am J Physiol-Gastrointestinal and Liver Physiology			
Licensed Content Title	Exogenous PP2A inhibitor exacerbates the progression of nonalcoholic fatty liver disease via NOX2-dependent activation of miR21			
Licensed Content Author	Muayad Albadrani, Ratanesh K. Seth, Sutapa Sarkar, et al			
Licensed Content Date	Oct 1, 2019			
Licensed Content Volume	317			
Licensed Content Issue	4			
Type of Use	Thesis/Dissertation			
Requestor type	author of original work			
Format	print and electronic			
Portion	full article			
Will you be translating?	no			
World Rights	no			
Order reference number				
Title	Microcystins Exposure and liver Injury Outcomes in NAFLD			
Institution name	University of South Carolina			
Expected presentation	Oct 2019			